APPLICATION OF HEURISTIC OPTIMIZATION TO GROUNDWATER MANAGEMENT

Loren Shawn Matott
September 20, 2006

A dissertation submitted to the
Faculty of the Graduate School of
The State University of New York at Buffalo
in partial fulfillment of the requirements for the
degree of

Doctor of Philosophy

Department of Civil, Structural, and Environmental Engineering

ACKNOWLEDGEMENTS

The research described herein would not exist without the contributions of numerous people. My advisor, Alan J. Rabideau, has been a continuing source of guidance and inspiration throughout the course of my graduate studies. The members of my faculty committee (John Van Benschoten, Scott Weber, Igor Jankovic, and Matthew Becker) have also provided useful instruction and insightful comments. My fellow colleagues in Trailer C, most notably James Criag, Karl Bandilla, Zhengzheng Jiang, Samuela Franchescini, Raghu Suribhatla, and Kyle Fredrick, have also been very generous with their friendship and good humor. This work was performed in part at SUNY-Buffalo's Center for Computational Research (CCR), whose staff (particularly Matt Jones and Jon Bednasz) provided superb and timely technical guidance.

Outside of University at Buffalo faculty, students, and staff, the following researchers provided valuable assistance: Kathleen Fowler (Clarkson University), Shannon Bartelt-Hunt (University of Nebraska, Omaha Campus), Mary Hill (USGS), Eileen Poeter (Colorado School of Mines), and Steven Kraemer (EPA).

Financial support for the research was provided by the National Science Foundation Integrative Graduate Education and Training (NSF IGERT) program in Geographic Information Science, award #DGE-9870668. The research was also supported by Grant # R82-7961 from the U.S. Environmental Protection Agency's (EPA) Science to Achieve Results (STAR) program and Grant # BES 0202077 from the National Science Foundation.

Where noted, portions of this work have been published (or submitted for publication) in peer-reviewed journals and such material is reproduced here with kind permission. Special thanks go to the anonymous reviewers of the original, revised (and sometimes re-revised) draft manuscripts of these published materials.

Ann Marie, my wife and constant companion, displayed endless amounts of patience and love during my entire graduate school experience, for which I am forever grateful. Finally, this document is dedicated to my mother, Lynne Matott, who taught me, through her example, the value of scholarship and perseverance.

TABLE OF CONTENTS

LIST OF TABLES

LIST OF FIGURES

ABSTRACT

Subsurface flow and contaminant transport models are often used in solving groundwater management problems. Automated optimization involving such models is becoming commonplace, and researchers are increasingly encountering problems for which standard gradient-based search algorithms are inadequate. Such cases have motivated an interest in the use of more robust, but computationally expensive, heuristic algorithms.

The research reported in this dissertation advances the state-of-practice of heuristic optimization in groundwater management by applying a variety of heuristic methods to three groundwater management problems: (1) optimization of pump-and-treat containment systems, (2) optimization of multi-layered sorptive barrier systems, and (3) calibration of reactive transport models involving nitrate contamination. These studies were facilitated by the development of a new open source software package for model-independent multi-algorithm optimization, which includes special tools for calibration and model ranking and selection.

Overall, the optimization studies make several important research contributions by (1) suggesting methods and guidelines for the effective selection and use of heuristic algorithms, (2) investigating techniques for reducing the computational demand associated with heuristic algorithms, (3) providing general insight into the behavior of the selected problems, (4) utilizing modeling techniques, remediation constraints, and/or parameter representations not previously applied to the selected problems, and (5) introducing a novel optimization software package to the research community.

1 INTRODUCTION

Computer models of groundwater and contaminant transport are often key components in the investigation of groundwater management problems. More and more, such models are subjected to automated calibration, a specific type of optimization problem that quantifies and minimizes the level of uncertainty associated with model parameters and predictions. Furthermore, flow and transport models are increasingly being used in a general simulation-optimization framework; where the optimal design of a remedial system is determined by coupling a computer model with an optimization search algorithm.

As suggested by Barry et al. (2002) and Mayer et al. (2002), rapid advances in the computational power of desktop computers have spurred the consideration of ever-more complex and computationally expensive simulations of groundwater flow and contaminant transport. Sophisticated computational techniques, requiring one or more levels of iteration, are typically employed to solve the governing equations for a given model. Optimization of such models adds additional levels of complexity and can require vast increases in computation time, due to the large number of required model evaluations. For example, the calibration exercise presented in Bell and Binning (2004) required more than 2,000 times the computation of a single model evaluation. Furthermore, the pump-and-treat optimizations of Maskey at al. (2002) required up to 1,500 model evaluations, with each evaluation requiring execution of two programs (MODFLOW and MODPATH). In light of such added computational expense, an

important component of current research is the development and identification of efficient, yet robust, search algorithms.

Traditional approaches to optimization have relied on gradient-based search algorithms, which are derived from formal mathematical analysis and are contingent upon several basic assumptions about the nature of the problem. To the extent that these assumptions are correct, gradient-based algorithms can be highly efficient and effective, identifying optimal parameter values using a minimal amount of computation. For problems that fail to satisfy the assumptions inherent in gradient-based approaches, heuristic algorithms offer a more robust, but less efficient, alternative. Heuristic techniques do not have mathematically rigorous formulae, and instead incorporate elements of randomness and follow empirical guidelines developed without regard to the character of the underlying problem.

The inadequacy of traditional search methods for solving a variety of problems involving flow and transport modeling is becoming widely recognized [e.g. Ahlfeld and Sprong (1998), Mayer et al. (2002) and Smalley et al. (2000)] and researchers have begun adopting various heuristic methods [e.g. Bell and Binning (2004), Solomatine et al. (1999), and Dougherty et al. (1991)]. However, the selection and use of these methods has proceeded in a more or less ad hoc fashion. For example, the choice of heuristic has often been arbitrary and based on a given investigators particular preference. Furthermore, the adjustment of algorithm-specific parameters to values that best suit a given problem (a process known as algorithm tuning) has not been considered in any sort of rigorous

fashion. Additionally, due to inherent inefficiencies, heuristic algorithms often require large numbers of potentially expensive model evaluations. This computational burden has limited the general applicability of heuristics and has discouraged rigorous and routine analysis of algorithm behavior. Finally, whereas automated model calibration has been aided by the availability of several public-domain model-independent gradient-based calibration packages (e.g. PEST and UCODE), an equivalent code supporting multi-algorithm general-purpose optimization is presently unavailable.

The work performed for this dissertation has addressed the aforementioned deficiencies in the current state-of-practice of heuristic optimization in groundwater management. The research was organized into a sequence of studies applying a variety of heuristic techniques to three important groundwater management problems: (1) optimization of pump-and-treat system design, (2) optimization of sorptive landfill liner design, and (2) calibration of subsurface nitrogen transport models.

The pump-and-treat and landfill liner design problems were motivated by federally regulated activities (i.e. site remediation and solid waste disposal) that require enormous financial expenditures. For example, NRC (1994) estimated the national cost of cleaning up hazardous waste sites (where pump-and-treat systems are commonly employed) to be around $750 billion. Likewise, Koerner (1994) projected the nationwide cost of solid waste disposal to be $43 billion, and estimated that 70% of such waste would end up in some type of lined facility. Given the high costs associated with pump-and-treat and landfill liner systems,

insight into the optimal design of such systems can be expected to yield substantial practical benefit.

Federally mandated TMDL (total maximum daily load) requirements have generated an increased interest in the detailed transport modeling of Nitrogen, one of the most commonly identified pollutants in the TMDL program (USEPA, 1999). To improve the TMDL program and to assist states with the daunting task of implementing nearly 42,000 TMDL analyses, USEPA (2002) identified twenty research needs that could be effectively addressed by the scientific community. One of these needs is improvement in TMDL uncertainty analysis and the calibration component of this dissertation was designed, in part, to help advance the TMDL research agenda.

Each of the three studies involved extensive numerical experimentation on a set of hypothetical model problems. These carefully formulated problems utilized field observed data and/or data derived from available literature, and, wherever possible, were based on published benchmark problems. The studies shared a number of common features, including (1) knowledge of the 'true' solution, discovered via exhaustive search or, in the case of calibration, known a-priori due to the use of synthetic observation data, (2) where applicable, heuristic algorithms were benchmarked against gradient-based approaches, and (3) to complete the studies in a reasonable timeframe, the numerical experiments relied heavily on parallel processing.

In terms of research contributions, each study provided general insight into the particular problem considered, and considered methods and formulations

not previously applied to the selected problem. Furthermore, study results have been synthesized into a set of general guidelines for the selection, tuning, and assessment of heuristic algorithms. Portions of each study also explored methods of reducing the computation associated with heuristic algorithms. These guidelines and computational improvements establish an important basis for future research into groundwater management applications that involve the use of heuristic methods.

A public-domain multi-algorithm optimization software code (named OSTRICH) was developed to facilitate the previously listed studies. The package is model-independent and can be integrated with a wide variety of conventional flow and transport modeling codes. Furthermore, the package contains several calibration-specific components, including a special-purpose calibration search algorithm and a variety of post-calibration statistical and diagnostic measures. It is anticipated that the availability of OSTRICH will contribute to the continued exploration of sophisticated optimization problems involving complex flow and transport models. Early evidence of this contribution is provided by published studies in which OSTRICH and a related package named ISOFIT have been used [e.g. Rabideau et al. (2005a), Bartelt-Hunt et al. (2005), and Rabideau et al. (2005b)].

2 OBJECTIVES

The primary research hypothesis for this work is that, within the groundwater management community, the usefulness of heuristic optimization can be improved by appropriate attention to algorithm selection and implementation, and by the adoption of recent computational advances. This hypothesis was formally investigated through a series of studies that are fully detailed in Chapters 4-6 of this manuscript. The general research organization and objectives for these studies, taken as a whole, are briefly outlined below. Section 2.1 frames the research in terms of optimization research objectives, while Section 2.2 organizes the research around the investigation of groundwater management applications.

2.1 Optimization Research Objectives

In terms of heuristic optimization, each study was organized around the development of methods for robust algorithm selection and implementation, and the integration of computational advances, with a particular focus on reducing computation time. In this regard, four specific optimization methods were examined: (1) swarm intelligence algorithms, (2) formal algorithm tuning, (3) parallel computing, and (4) model-based surrogate methods.

2.1.1 Swarm intelligence algorithms

Many heuristic algorithms are population-based in that they utilize a collection of solution sets that are revised and evaluated at each algorithm step. A current trend in heuristic optimization research is the development of algorithms in which population elements maintain some form of limited memory,

a concept known as *swarm intelligence*. Examples of swarm intelligence algorithms include particle swarm optimization (Kennedy and Eberhart, 1995), ant colony optimization (Dorigo and Stutzle, 2004), and tribes (Clerc, 2003). At the start of this research, a review of existing literature revealed that swarm intelligence algorithms had not yet been applied to problems involving groundwater flow and/or transport modeling. *Therefore, it was hypothesized that swarm intelligence algorithms could be more effective than classical heuristic methods (e.g. the genetic and simulated annealing algorithms) at solving such problems.* For this research hypothesis, the corresponding research objective was to introduce swarm intelligence algorithms to the groundwater management community and compare the performance of such algorithms to more established optimization methods.

2.1.2 Algorithm tuning

Recent studies in the heuristic optimization literature have highlighted the importance of tuning algorithm parameters so as to enhance optimization performance. While a variety of procedures have been suggested for this purpose [e.g. Coy et al. (2001), Parsons and Johnson (1997), Hinterding et al. (1997), Kivijarvi et al. (2003), and Talbi (2002)], none were previously incorporated into optimization studies involving flow and transport modeling. *Therefore, it was hypothesized that automated tuning of heuristic algorithms would lead to more robust optimization of problems based on flow and/or transport models.* As such, a corresponding research objective was to examine

methods for the automated tuning of heuristic algorithms, as applied to realistic groundwater management problems.

2.1.3 Parallel computing

Within the last decade, the state-of-practice in parallel computing has shifted from a shared- to distributed-memory architecture [Gropp et al. (1999) and Foster (1995)]. In a distributed computing environment, population-based heuristic algorithms may be characterized as ”embarrassingly parallel” because evaluation of a given population set may be distributed across processors with a minimum of inter-processor coordination. Therefore, one goal of this research was to quantify the speedup afforded by parallel implementations of population-based algorithms.

2.1.4 Model-based surrogate methods

Automated model calibration (also known as parameter estimation and inverse modeling) is a specific type of optimization problem that has been extensively studied in relation to groundwater flow modeling. In this regard, recent research has stressed the consideration of alternative conceptual models. To minimize uncertainty, these models are first calibrated and then subjected to a model ranking procedure that seeks to select the “best” conceptual model. Application of such multi-model uncertainty analysis techniques to reactive transport models has not been previously investigated, primarily because of the high computational costs that are incurred.

A possible technique for addressing the computational burden of automated reactive-transport calibration is the use of surrogate models (Booker

et al., 1999). As calibration proceeds, simpler surrogate models are evaluated in lieu of the more complex model, reducing the required number of complex model evaluations. *This research hypothesized that, in addition to reducing the computational burden of automated calibration, model-based surrogate methods could also be used to simultaneously perform the tasks of model ranking and selection.* Therefore, the final optimization-based objective of this research was to develop and test a novel model-based surrogate calibration method that is capable of simultaneous model ranking, selection, and calibration.

2.2 Applications Research Objectives

Objectives related to applications research focused on three problems involving the simulation of groundwater flow and/or subsurface contaminant transport: (1) pump-and-treat optimization, (2) multi-layer sorptive barrier design, and (3) calibration of subsurface reactive transport models. The selected problems provided an experimental framework for testing the optimization research objectives discussed in Section 2.1. Additionally, each study was designed to address a number of application-based research objectives, as described below.

2.2.1 Pump-and-treat optimization

Engineering objectives for pump-and-treat optimization are to determine the number, locations, and rates of extraction and injection wells such that plume containment is realized at the lowest cost. Previous simulation-optimization studies of pump-and-treat systems have utilized either finite-difference or finite-element flow-models, and have considered particle tracks and/or simulated head

values to determine whether remedial goals are satisfied. To advance this state-of-practice, research objectives were to (1) assess the applicability of an alternative flow modeling technique, the analytic element method (AEM), in a pump-and-treat optimization context, and (2) introduce and assess an alternative plume containment indicator that utilizes AEM flux output. *Research hypotheses related to these objectives were that (1) the AEM could be effectively employed in a pump-and-treat optimization context, and (2) using AEM flux output as a plume containment constraint could lead to improved reliability.*

2.2.2 Multi-layer sorptive barrier design

Engineering objectives for multi-layer sorptive barrier design are to determine the appropriate number, ordering, and material-composition of a sequence of layers so that contaminant transport through such layers is minimized at the lowest financial cost. Optimal sorptive barrier design using automated simulation-optimization techniques is a recent development and research objectives were to (1) assess the performance of several heuristic algorithms, as applied to such problems, (2) explore techniques for integrating design constraints into the barrier cost function, and (3) examine relationships between algorithm performance and barrier problem formulation.

2.2.3 Subsurface transport model calibration

Modeling subsurface nitrogen transport is of considerable interest to the bioremediation and water quality communities, where it is alternately viewed as a remediation aid and a groundwater contaminant. In general, subsurface reactive transport (SRT) is influenced by a complex set of hydrologic and biogeochemical

processes. To be used effectively in a regulatory or research context, SRT models must adequately represent these processes while being computationally tractable. Furthermore, model uncertainty must be rigorously quantified. In this regard, two extremes must be avoided: (1) very complex models with many highly uncertain parameters, and (2) highly simplified models that calibrate well but "lump" and/or omit important processes.

When determining an appropriate balance between computation, complexity and uncertainty, modelers have generally relied on ad-hoc model development and trial-and-error and/or literature-derived assignment of uncertain model parameter values. Regulators are increasingly stressing the importance of more rigorous procedures, including automated model calibration and formal consideration of multiple models. The computational burden of these uncertainty analysis techniques was addressed in this research via the surrogate model approach (outlined in Section 2.1.4) and via the use of massively parallel computing infrastructure. These computational developments facilitated the assessment of several application-based research objectives, which were to: (1) characterize the degree of non-linearity associated with subsurface reactive transport calibration, (2) compare the performance of heuristic and gradient-based algorithms, as applied to such problems, and (3) examine techniques for determining the appropriate level of model complexity, given the types of data that are typically collected from the field.

2.3 Organization of the Research and Thesis Document

The research objectives were realized in four stages, starting with the development of the OSTRICH optimization software package, described in Chapter 3. The OSTRICH code formed the basis for subsequent studies in heuristic optimization, namely the studies of pump-and-treat optimization (Chapter 4), multi-layer sorptive barrier design (Chapter 5), and the calibration of subsurface nitrogen transport models (Chapter 6). Finally, Chapter 7 provides a summary of all research results.

3 SOFTWARE DEVELOPMENT

The software development approach for the OSTRICH code focused on object-oriented design and parallel computing. All code was written in C/C++ and compiled for execution on both Linux and Windows platforms. The model-calibration component of OSTRICH was also ported to execute on the super-computing 'Grid', a geographically disparate and multi-institutional network of heterogeneous computing clusters. Access to Grid-based calibration is provided via a user-friendly and web-accessible graphical user interface developed using a combination of PHP, HTML and JavaScript. OSTRICH software has been released to the public domain via the University at Buffalo Groundwater Research Group website (www.groundwater.buffalo.edu), which provides access to the latest OSTRICH binaries (version 1.8) and a pdf version of the user-manual (Matott, 2006a).

3.1 Optimization

Optimization may be defined as the minimization (or maximization) of an objective function (e.g. cost), subject to a variety of constraints. Equation 3.1 provides a general mathematical formulation of constrained optimization (Vanderplaats, 2001):

$$\begin{aligned} &\text{minimize } f(\mathbf{X}) \\ &\text{subject to}: \mathbf{X}_{\mathrm{L}} < \mathbf{X} < \mathbf{X}_{\mathrm{U}} \\ &\qquad g_i(\mathbf{X}) < 0 \ , \ i = 1..m \\ &\qquad h_j(\mathbf{X}) = 0 \ , j = 1..l \end{aligned} \tag{3.1}$$

where $f(\mathbf{X})$ is the objective function, which depends on some vector of parameters ($\mathbf{X}$) whose values are constrained by upper ($\mathbf{X_U}$) and lower ($\mathbf{X_L}$)

bounds, and $g_i(\mathbf{X})$ and $h_j(\mathbf{X})$ are a set of m and l inequality and equality constraints, respectively.

Equation 3.2 describes two techniques (the additive and multiplicative penalty methods) for converting constrained optimization into more readily solvable unconstrained optimization problems:

$$\begin{aligned} &\text{minimize } F(\mathbf{X}) \\ &\text{where } : F(\mathbf{X}) = f(\mathbf{X})(1 + P(\mathbf{X})) \text{ (mult.method)} \\ &\qquad \text{or} \\ &\qquad F(\mathbf{X}) = f(\mathbf{X}) + P(\mathbf{X}) \qquad \text{(additive method)} \end{aligned} \tag{3.2}$$

where $F(\mathbf{X})$ is the penalty-adjusted objective function, and $P(\mathbf{X})$ is a penalty term that accounts for violations of one or more equality and inequality constraints. For this research, the optimization parameters ($\mathbf{X}$) consisted of inputs to a flow or transport model that was coupled with the optimization software (i.e. OSTRICH). Upon completing a run of the model using a given set of parameter values, the optimization software would compute $F(\mathbf{X})$, $f(\mathbf{X})$ and $P(\mathbf{X})$ based on the parameter values and/or any relevant model-simulated output.

3.2 Calibration

Model calibration is a specific type of optimization wherein the objective is to assign parameter values such that model uncertainty is minimized. A variety of mathematical formulations have been applied to the task of model calibration, including least squares, average weighted error, maximum-likelihood, and maximum entropy. One of the main differences between the various formulations is the manner in which residuals (i.e. differences between model-simulated and field-observed data) are accumulated.

In groundwater flow and transport modeling, the dominant automated calibration approach is weighted least squares, where the objective is to find the values of model parameters such that the resulting sum of squared error between field-measured and model-computed observations (as shown in Equation 3.3) is minimized:

$$\Phi = (\mathbf{Y}_{\mathbf{obs}} - \mathbf{Y}_{\mathbf{sim}})^T \mathbf{Q} (\mathbf{Y}_{\mathbf{obs}} - \mathbf{Y}_{\mathbf{sim}}) \tag{3.3}$$

Where Φ is the weighted sum of squared errors objective function, $\mathbf{Y}_{\mathbf{obs}}$ is a vector of *m* measured observation values, $\mathbf{Y}_{\mathbf{sim}}$ is a vector of *m* model simulated values, and **Q** is an *m* × *m* observation weight matrix.

Automated calibration using regression (e.g. Draper and Smith, 1998) is a well-established approach for groundwater flow modeling [e.g. Cooley and Naff (1990) and Hill (1998)], and recent research [e.g. Christensen and Cooley (1999), Yager (1998), and Rabideau et al. (2005a)] has begun utilizing a variety of post-regression diagnostic measures, such as measures of model non-linearity [e.g. Bates and Watts (1980) and Linssen (1975)] and influential observation measures [e.g. Belsley et al. (1980) and Cook and Weisberg (1982)]. Such post-regression measures are calculated and reported by the OSTRICH software following a successful calibration.

Due to their high complexity and associated computation time, automated calibration of subsurface reactive-transport models is relatively uncommon. Parameter values in such models are generally: (1) taken from available literature, (2) extrapolated from laboratory experiments, and/or (3) calibrated via trial-and-error. Notable exceptions include Barth and Hill (2005) who used the

UCODE software package, and Bell et al. (2002) and Bell and Binning (2004), who used an evolutionary algorithm.

3.3 Search Algorithms

The studies described in Chapters 4-6 considered up to five search algorithms: four heuristic algorithms (particle swarm optimization, two genetic algorithm variants, and simulated annealing), a conjugate gradient algorithm (Fletcher-Reeves), and a non-linear regression algorithm (Levenberg-Marquardt). Many other optimization algorithms have been developed, including: ant colony optimization (Dorigo and Stutzle, 2004), big bang - big crunch (Erol and Eksin, 2006), tribes (Clerc 2003), tabu search (Glover, 1986), implicit filtering (Gilmore and Kelley, 1995), branch-and-bound (Balas, 1968), artificial neural networks (Govindaraju and Rao, 2000), and outer approximation methods (Duran and Grossman, 1986). An investigation of the entire catalog of available algorithms was beyond the scope of the research and the chosen algorithms represent a manageable cross-section of established methods.

3.3.1 Fletcher-Reeves algorithm

The Fletcher-Reeves algorithm (Fletcher and Reeves, 1964) is representative of the general class of gradient-based methods. At each iteration of the algorithm, gradient information [$\nabla F(\mathbf{X})$] is used to compute a revised search direction (Vanderplaats, 2001):

$$\mathbf{S} = -\nabla F(\mathbf{X}) + \beta \mathbf{S}_{\mathbf{old}} \tag{3.4}$$

Where, **S** and $\mathbf{S}_{old}$ are the revised and previous search directions, respectively, and β is a scalar multiplier. As suggested by Press et al. (1995), β is computed using the Polak-Ribiere formulation:

$$\beta = \frac{\left(\nabla F(\mathbf{X}) + \nabla F(\mathbf{X}_{old})\right)^T \left(\nabla F(\mathbf{X})\right)}{\left(\nabla F(\mathbf{X}_{old})\right)^T \left(\nabla F(\mathbf{X}_{old})\right)} \tag{3.5}$$

where $\nabla F(\mathbf{X}_{old})$ is the gradient vector of the previous iteration. Following the standard simulation-optimization approach, the OSTRICH package evaluates the gradient vector numerically using a finite-difference approximation. This technique requires repeated executions of the underlying flow or transport model.

3.3.2 Levenberg-Marquardt algorithm

Levenberg-Marquardt regression (Levenberg, 1944, with extensions by Marquardt, 1963), is utilized by several popular automated calibration codes [e.g. PEST (Doherty, 2004) and UCODE (Poeter and Hill, 1998)]. Minimization of Equation 3.3 proceeds by performing a Taylor series expansion about $\mathbf{X}_{old}$, yielding a linearized approximation for $\mathbf{Y}_{sim}$:

$$\mathbf{Y}_{sim} \approx \mathbf{Y}_{old} + \mathbf{J}(\mathbf{X} - \mathbf{X}_{old}) \tag{3.6}$$

Where **J** is the Jacobian matrix, consisting of the partial derivatives of each simulated observation with respect to each parameter, and $\mathbf{Y}_{old}$ is the simulated observation vector from the previous iteration.

Based on this approximation, the following iterative update strategy for computing a revised parameter estimate is defined:

$$\mathbf{X} = \mathbf{X}_{old} + (\mathbf{J}^T\mathbf{Q}\mathbf{J} + \alpha\mathbf{I})^{-1}\mathbf{J}^T\mathbf{Q}(\mathbf{Y}_{obs} - \mathbf{Y}_{old}) \tag{3.7}$$

Where α is a control parameter and I is the identity matrix. Adjustment of the control parameter allows the method to smoothly transition from a steepest-descent approach far away from the optimal parameter set to a more efficient Taylor series approximation close to the optimal parameter set. Like the gradient computations of the Fletcher-Reeves algorithm, OSTRICH evaluates the Jacobian matrix numerically using finite-differences.

3.3.3 Genetic Algorithm (GA)

The GA (Goldberg, 1989) operates on a population of parameter sets and follows a Darwinian survival of the fittest process, where selection, crossover, mutation, and elitism operators are applied to successive generations of the population. In this manner, the GA gradually evolves the initial population into one that surrounds, and may contain, the globally optimal solution. As shown in Figure 3.1, the optimization process begins by randomly initializing the population. Then, an iterative process is followed in which successive generations of the algorithm are evolved. Population evolution begins with a preservation stage, in which the fittest members (the elites) are added, unaltered, to the gene pool of the next generation. Remaining population members compete for membership in a mating pool via the tournament selection operator. Members of the mating pool are then selected two-at-a-time to serve as parents for the next generation of the population. The crossover operator simulates the generation of a child population member, whose parameter values are assigned based on a mixing of parent parameter values. After subjecting child parameter values to random adjustment via the mutation operator, each child enters the

gene pool of the next generation. When the new gene pool is full, the fitness (objective function) of each child member is evaluated by executing the simulation model multiple times.

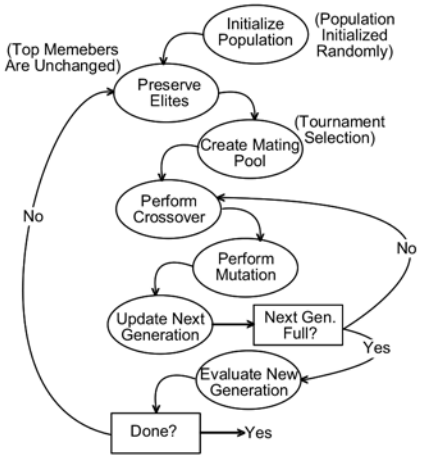

Figure 3.1: Genetic Algorithm Optimization Procedure

3.3.4 Particle Swarm Optimization (PSO)

Particle swarm optimization (Kennedy and Eberhart, 1995) was developed from attempts to simulate the flocking behavior of birds, fish and other animals. The PSO algorithm contains a population of parameter sets, known as the particle swarm. During iteration, particles move through the design space and revised locations are computed as follows (Beielstein et al., 2002):

$$v_j^{i+1} = \chi\left(w^i v_j^i + c_1 r_1^i \left(p_{l_j}^{\ i} - x_j^i\right) + c_2 r_2^i \left(p_{g_j}^{\ i} - x_j^i\right)\right) \quad j = 1..n$$
$$x_j^{i+1} = x_j^i + v_j^{i+1} \quad j = 1..n \tag{3.8}$$

where i is the iteration number, n is the number of parameters, x_j is the value and v_j the velocity of parameter j, χ is the constriction factor, w is the inertia weight, r_1 and r_2 are independent and uniformly distributed random numbers, c_1 is the cognitive parameter, the weight of a particles own experience, c_2 is the social parameter, the weight of the combined experience of the swarm, p_l is the

parameter value corresponding to the best solution ever personally visited by the given particle, and p_g is the parameter value corresponding to the best solution ever visited by any particle (the current global best). The components for updating a particle are the previous velocity, and the current local and global best. A given particle retains a fraction (w) of its velocity and the direction of movement is biased towards the global (p_g) and local (p_l) best, which are randomly weighted (via the r_1 and r_2 terms) and scaled by the cognitive (c_1) and social (c_2) parameters.

3.3.5 Simulated Annealing (SA) algorithm

The SA algorithm (Kirkpatrick et al., 1983) is based on analogy to the physical process of annealing; wherein a solid is heated to an extremely high energy state and then slowly cooled, enabling the material to achieve its lowest possible energy state. Simulated annealing emulates this cooling process by introducing a randomness control parameter (i.e. the temperature) that is reduced after each step of the optimization, such that a highly random initial search is slowly transitioned into a focused descent onto the global minimum. Within each SA iteration is an equilibration process that makes a series of transitional moves based on the Metropolis algorithm (Metropolis et al., 1953). An important characteristic of the Metropolis algorithm is that, depending on the value of the randomness control parameter, moves that increase the objective function may be made.

Figure 3.2 illustrates the simulated annealing algorithm utilized in this research. Following Vanderbilt and Louie (1984), the procedure begins with a

melting phase, in which the initial temperature is established by evaluating many different parameter sets. The algorithm proceeds by performing a sequence of Metropolis equilibrations and temperature reductions until convergence is achieved.

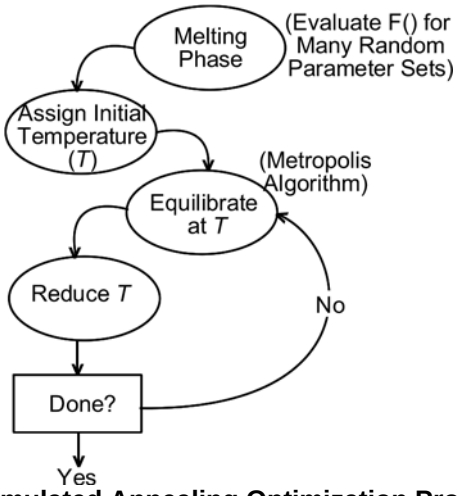

Figure 3.2: Simulated Annealing Optimization Procedure

3.3.6 Parallel Algorithms

Research objectives related to algorithm parallelization were addressed by implementing parallel versions of the genetic algorithm and the particle swarm optimization algorithm. These population-based algorithms were coded to run in parallel on distributed, cluster-based processors using the industry-standard Message Passing Interface (MPI) (Gropp et al., 1999) library. In the parallel version of each algorithm, a supervisor processor begins each step by broadcasting a revised population set to a group of subordinate processors. Each subordinate processor computes the objective function (via model execution) of one or more population members and sends the results back to the supervisor. The supervisor completes the procedure by performing bookkeeping and algorithm-specific operations (i.e. particle advection (PSO) or selection,

crossover, and mutation (GA)). The entire process begins again with the next iteration.

3.4 Multi-Model Ranking and Selection

Researchers are beginning to embrace multi-model approaches to subsurface reactive transport (SRT) modeling, in which more than one model is considered for a given application. For example, Dai and Samper (2004) advocate a stepwise calibration strategy in which sequentially more complex SRT models are calibrated and compared. Such procedures mirror recent efforts by Poeter and Anderson (2005), who applied information theoretic measures to statistically rank a set of calibrated groundwater flow models. Information theoretic metrics suitable for comparing multiple SRT formulations include variations of Akaike's *Information Criterion* (IC) (Hurvich and Tsai, 1994), Bayesian IC (Schwarz, 1978), Hannan/Quinn IC (Hannan and Quinn, 1979), and Kashyap IC (Kashyap, 1982). These methods extend traditional goodness-of-fit measures to consider the number of calibrated parameters and observation data. The calibration component of this research applied selected IC metrics to multiple SRT scenarios involving nitrate-contamination.

3.5 Software Testing

A variety of numerical experiments were performed to test the OSTRICH software and verify its proper operation. A complete discussion of these tests is provided in Appendix A.

All numerical experiments developed for this dissertation were performed on parallel computing clusters maintained at the University at Buffalo Center for

Computational Research (UB CCR). These parallel computing facilities contain over 5,000 Linux-based processors, spread across 8 commodity dual-processor workstation clusters. While all UB CCR participants share most clusters, two clusters, “Clearwater” (32 1-GHz Pentium 3 processors w/ 1-GB RAM) and “MuddyWaters” (26 3.3-GHz Intel Xeon processors w/ 4-GB RAM), are committed to research performed by the UB Groundwater Research Group, and were dedicated resources for the research presented herein. Additional CCR resources that were utilized included the “Joplin” (512 2.4-GHz Pentium 4 processors w/ 2-GB RAM) and “U2” (2056 3.3-GHz Intel Xeon processors w/ 2-GB RAM) clusters. Access to the CCR clusters is via a Portable Batch System (PBS) resource manager and Maui scheduler, and the CCR supports parallel programs via the industry standard Message Passing Interface (MPI) specification.

4 PUMP-AND-TREAT OPTIMIZATION USING AEM FLOW MODELS

The material in Chapter 4 has been published as "Matott LS, Rabideau AJ, Craig JR. 2006. Pump-and-Treat Optimization Using Analytic Element Method Flow Models. *Advances in Water Resources*, vol. 29, no. 5, pg. 760-775", *copyright by Elsevier.*

4.1 Overview

Plume containment using pump-and-treat (PAT) technology continues to be a popular remediation technique for sites with extensive groundwater contamination. As such, optimization of PAT systems, where cost is minimized subject to various remediation constraints, is the focus of an important and growing body of research. While previous pump-and-treat optimization (PATO) studies have used discretized (finite element or finite difference) flow models, the present study examines the use of analytic element method (AEM) flow models. In a series of numerical experiments, two PATO problems adapted from the literature are optimized using a multi-algorithmic optimization software package coupled with an AEM flow model. The experiments apply several different optimization algorithms and explore the use of various pump-and-treat cost and constraint formulations. The results demonstrate that AEM models can be used to optimize the number, locations and pumping rates of wells in a pump-and-treat containment system. Furthermore, the results illustrate that a total outflux constraint placed along the plume boundary can be used to enforce plume containment. Such constraints are shown to be efficient and reliable alternatives to conventional particle tracking and gradient control techniques. Finally, the particle swarm optimization (PSO) technique is identified as an effective algorithm for solving pump-and-treat optimization problems. A parallel version of

the PSO algorithm is shown to have linear speedup, suggesting that the algorithm is suitable for application to problems that are computationally demanding and involve large numbers of wells.

4.2 Introduction

Remediation of contaminated groundwater is a continuing problem for the industrialized world. At many contaminated sites, a pump-and-treat system consisting of extraction and injection wells is installed to prevent further plume migration and remove contaminant mass. Designers typically determine the number, locations, and rates of extraction and injection wells such that plume containment is realized at the lowest cost. In this context, the *plume* is defined as a closed boundary delineating a fixed containment area (i.e. a region of groundwater contamination that must not be allowed to expand), and *plume containment* occurs when all groundwater initially residing within the containment area either remains within this boundary, or is extracted by a well during the remediation period.

Optimization of pump-and-treat systems using automated simulation-optimization techniques has been extensively studied over the past quarter century. Mayer et al. (2002) provided a detailed review of this body of research and set forth a suite of community problems intended to serve as a unifying benchmark for future work. While previously published studies of pump-and-treat optimization (PATO) have used finite-difference (FD) or finite-element (FE) flow models, this paper investigates the use of groundwater flow models based on the analytic element method (AEM). Therefore, a major contribution of this study is

that it is the first to assess the feasibility of AEM-based PATO. The purpose of this work is not to compare the merits of AEM versus FD/FE for PATO applications, but to examine the applicability of the AEM to this class of problems and develop guidelines for the appropriate PATO formulation.

Several major characteristics distinguish AEM groundwater models from their FD/FE counterparts. In AEM models, hydrologic features are treated as distinct model elements rather than distributed over a spatial grid or mesh. Continuously varying aquifer properties, such as hydraulic conductivity and recharge, are approximated using a set of parameter zones. While such zones are commonly assigned average or effective parameter values, solutions for continuous variation within a zone have been developed [e.g. the multi-quadric area sink (Strack and Jankovic, 1999)]. Point features (such as wells) are directly represented in AEM models and their spatial coordinates can be varied as continuous functions. Conversely, such point features can be only approximately located in common FD and FE modeling software, and the effects of such features are averaged over the entire grid- or mesh-cell in which they are placed. Finally, while FD/FE techniques result in a set of discrete nodal or grid cell solutions, AEM flow solutions are inherently continuous over the entire model domain. Introductory treatments of AEM modeling are provided in Strack (1989) and Haitjema (1995), while Jankovic (1997) and Jankovic and Barnes (1999) provide details on the high-order techniques underpinning the numerical engine used in this study. The particular AEM implementation used in this study assumes two-dimensional, steady state flow. Such assumptions are common

among published PATO studies and should not be a limitation for most PATO applications. Notable exceptions are problems involving time-varying pumping rates and/or flexible management periods [e.g. Chang et al. (1992), Culver and Shenk (1998), Culver and Shoemaker (1992, 1993 and 1997), and Lee and Kitanidis (1991)] and/or containing significant layering of aquifer permeability [e.g. Ahlfeld and Page (1995), and Sawyer et al. (1995)].

Given the fundamental differences between AEM and FD/FE flow modeling, the use of AEM introduces several unique possibilities with respect to PATO. For example, AEM-modeling allows for the coordinates of pump-and-treat wells to be directly represented as continuous design variables. Conversely, the majority of previous FD/FE-based PATO studies have optimized well coordinates using a discrete list of candidate well locations. Notable exceptions are found in Huang and Mayer (1997) and Wang and Ahlfeld (1994), but in these studies potential well locations were nonetheless limited to the nodes of the FE mesh (Huang and Mayer, 1997) or the cell center of a FD grid (Wang and Ahlfeld, 1994). Limitations in the placement of FD/FE wells can be overcome via spatial grid adaptation methods, but such methods can be computationally expensive and result in a more complicated linkage between the simulation and optimization software.

Another benefit of AEM-based PATO arises when particle-tracking techniques are used as plume containment indicators. Particle tracking, described by Mulligan and Ahlfeld (1999), considers the advection of a series of particles, initially located inside or along the perimeter of the plume. Plume

containment is indicated if all particles remain within the plume, or are extracted by pump-and-treat wells, at the conclusion of the remediation time frame. When particle tracking is applied to FD/FE model solutions, the accuracy of a particle track is sensitive to the level of grid or mesh discretization. Conversely, AEM flow solutions are grid-free and the corresponding particle tracks are not affected by domain discretization error.

In contrast to particle tracking, the hydraulic gradient control plume containment technique, introduced by Atwood and Gorelick (1985), specifies a series of control locations along the perimeter of the plume. When the head gradient at all control locations is oriented toward the interior of the plume, plume containment is presumed to occur. In FD/FE models, head gradients are approximated using a pair of head values defined at each control location, with one member of the pair located inside the plume and the other outside of the plume. The separation distance between gradient points in such models is restricted to discrete multiples of the grid spacing, limiting the accuracy of the numerical gradient calculations. Conversely, AEM-based PATO allows for exact, analytic computation of head gradients, and provides a unique opportunity to examine the sensitivity of PATO to the inaccuracies of the numerically computed gradient control approach.

While previous PATO studies have used particle tracking and/or gradient control pairs, the present study includes consideration of an alternative plume containment indicator, designated here as the “zone outflux constraint”. A complete mathematical description of the constraint is provided in Section 4.2.4,

and is derived from the decomposition of flux (vertically-integrated discharge) across an arbitrary transect into influx and outflux terms. A zone flux polygon is then assembled by connecting a series of transects. Plume containment is signified when the total outflux, summed over all transects in a plume-enclosing zone flux polygon, is identically zero.

In consideration of the possibilities suggested by AEM-based PATO, this study examines several AEM-based PATO formulations to identify those that are particularly efficient, effective and reliable. The following sub-sections summarize the various facets of PATO considered in this paper: (1) optimization algorithm, (2) system cost, and (3) constraint integration. Mathematical formulations associated with system cost and constraint integration are included in Appendix B.

4.2.1 Optimization algorithms

Numerous algorithms have been applied to pump-and-treat and related hydraulic optimization; a thorough review and tabulated summary is provided by Mayer et al. (2002). More recent studies have used various heuristic approaches (genetic algorithm, simulated annealing, tabu search, and/or artificial neural networks) [e.g. Chan Hilton and Culver (2005), ESTCP (2004), Guan and Aral (2004), Maskey et al. (2002), and Zheng and Wang (2003)], non-linear programming (e.g. Guan and Aral, 2004), and implicit filtering (e.g. Fowler et al., 2004a and 2004b).

For this study, five algorithms were considered, with the goal of discovering those most effective at solving AEM-based PATO problems. The

methods consisted of three heuristic algorithms: simulated annealing (SA) (Kirkpatrick et al., 1983), particle swarm optimization (PSO) (Kennedy and Eberhart, 1995), and a real-coded genetic algorithm (GA) [Goldberg (1989) and Yoon and Shoemaker (1999)], one non-linear programming algorithm [Fletcher-Reeves conjugate-gradient (CG) (Press et. al, 1995)], and a random (RND) search algorithm.

The choice of GA and SA algorithms was motivated by the fact that they are heuristic (global) algorithms successfully applied in previous PATO studies [e.g. Aly and Peralta (1999), Chan Hilton and Culver (2000 and 2005), Dougherty et al (1991), ESTCP (2004), Guan and Aral (2004), Huang and Mayer (1997), Maskey et al (2002), Rogers and Dowla (1994), and Yoon and Shoemaker (1999)]. The CG algorithm is representative of non-linear programming, a common approach in the PATO literature [e.g. Guan and Aral (2004), McKinney and Lin (1996), Mulligan and Ahlfeld (2001), Wang and Ahlfeld (1994), Yoon and Shoemaker (1999)]. The random search algorithm, where an optimal solution is selected from a random sample of solution sets, served as a control for the other algorithms.

Importantly, this paper represents the first application of the PSO algorithm to PATO problems. The algorithm was introduced by Kennedy and Eberhart (1995), and is an outgrowth of attempts to simulate the cooperative-competitive nature of social behavior. The algorithm can effectively solve a variety of engineering optimization problems, and Coelho et al. (2002) and Gies

and Rahmat-Samii (2003) demonstrated applications where PSO performance compared favorably with the GA and SA algorithms.

4.2.2 System cost

Mayer et al. (2002) summarized some of the more commonly used PATO cost formulations, which can be divided into three components: (1) C_{TOTQ}: total pumping rate as a surrogate for cost, (2) C_{OPER}: operational costs only (such as energy, treatment, disposal and labor costs), and (3) C_{OPER+}: both operational and capital (well installation and pump) costs. The numerical experiments in this study examined each of the three cost formulations in order to demonstrate the feasibility of their use in an AEM-based PATO problem, and to assess the influence of the cost function on *algorithm effectiveness* (the ability of a given optimization algorithm to determine the minimum cost plume containment system). Details on the three cost formulations, as implemented in this study, are provided in Appendix B.

4.2.3 Integration of constraints

The pump-and-treat objective can be mathematically formulated as a combination of the system cost function (either C_{TOTQ}, $C_{OPER,}$ or C_{OPER+}) and a penalty function, $P_{TOTAL,}$ which accounts for the cost of various constraint violations. Mayer et al (2002) provide a summary of the types of constraints that have been applied to pump-and-treat optimization, and this study demonstrates that AEM-based PATO is capable of handling commonly applied constraints on capacity, drawdown and plume containment. *Capacity* constraints limit total pumping so that the PAT system does not overload an established treatment

facility, *drawdown* constraints prevent aquifer dewatering, and plume *containment* constraints enforce the remedial goals of the PAT system. Formulas for P_{TOTAL} and associated constraints are given in the appendix.

Chan Hilton and Culver (2000) discuss several techniques for combining cost and P_{TOTAL} to form the objective function, including the additive penalty method (APM), the multiplicative penalty method (MPM), and the exponential penalty method (EPM); formulations for these methods are provided in the appendix. Following the reasoning of Mulligan and Ahlfeld (2001), the APM was initially viewed as the preferred penalty method for all experiments in this study because the MPM and EPM methods tend to over-penalize constraint violations, biasing the optimization to favor constraint reduction over cost reduction. However, a set of initial experiments indicated that while the APM was effective in problems utilizing particle-tracking constraints, the MPM performed better for gradient control and zone outflux constraints.

4.2.4 Zone outflux constraint

The zone outflux constraint enforces plume containment by utilizing the normal component of the vertically-integrated discharge, Q_η [L^2/T], which may be expressed as:

$$Q_\eta = \int_0^h q_\eta dz \tag{4.1}$$

where h [L] is the saturated thickness of the domain, q_η [L^3/T] is the specific discharge normal to some vertical plane through the aquifer, and z [L] is the vertical direction. Figure 4.1 illustrates the decomposition of Q_η across an

arbitrary transect into directional components, $Q_\eta^+(s)$ and $Q_\eta^-(s)$, that vary in a piecewise continuous manner between transect endpoints *a* and *b*. Total fluxes (F_{ab}^+ and F_{ab}^-) in each direction are computed via integration along transect *ab*, as shown in Equation 4.2.

$$F_{ab}^+ = \int_a^b Q_\eta^+(s)ds$$
$$F_{ab}^- = \int_a^b Q_\eta^-(s)ds \tag{4.2}$$

Where Q_η^+ and Q_η^- are strictly positive and $Q_\eta = Q_\eta^+ - Q_\eta^-$. A 'zone flux polygon' can be assembled by connecting a series of transects aligned such that Q_η^+ terms for all transects correspond to outflow from the polygon and Q_η^- terms correspond to inflow. Using this convention, the total outward flux (F_{ZFB}^+) and total inward flux (F_{ZFP}^-) across the boundary of a given zone flux polygon are computed by summing the appropriate transect fluxes, as shown in Equation 4.3.

$$F_{ZFP}^+ = \sum_{i=1}^{N} F_i^+ \qquad F_{ZFP}^- = \sum_{i=1}^{N} F_i^- \tag{4.3}$$

Where, *N* is the number of transects in the given zone flux polygon, and F_i^+ and F_i^- are the respective total outflux and total influx across the *i*-th transect boundary of the zone flux polygon.

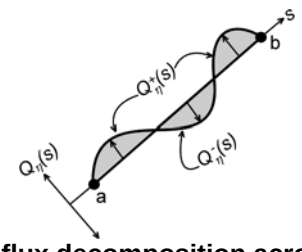

Figure 4.1: Example of flux decomposition across an arbitrary transect

For pump-and-treat optimization, a zone flux polygon is configured to match the plume boundary, and plume containment is enforced by constraining the total outward flux (F_{ZFB}^{+}) to be identically zero (i.e. no groundwater exits the plume, unless removed via a well). The zone outflux constraint may be considered equivalent to that of an infinite number of gradient control points placed along the plume boundary. For a given pump-and-treat system design, the zone outflux constraint is violated if the total outflux (F_{ZFB}^{+}) is nonzero. Such violations cause a penalty (proportional to F_{ZFB}^{+}) to be assessed to the pump-and-treat system cost.

Evaluation of the transect flux integrals in Equation 4.2 is dependent on the groundwater modeling strategy employed. For grid-based models, the flux terms Q_{η}^{+} and Q_{η}^{-} across each transect may be interpolated from the discretized flow solution and integrated numerically. Interpolation (and its associated numerical error) may be avoided if the geometry of the zone flux polygon is configured so that polygon sides coincide with cell faces. However, such a rectilinear geometry of the zone flux polygon may lead to an over-conservative constraint formulation. AEM-based models provide a continuous flow solution everywhere in the modeled domain and, regardless of zone flux polygon geometry, no interpolation is required to determine the flux across a given transect. Furthermore, the transect flux terms of an AEM-based flow solution can be integrated in two ways: strictly numerically or numerically with an analytic correction term (hereafter referred to as *semi-analytically*). For the semi-analytic method, the integrals in eq. (4.1) are first evaluated numerically. Then the *net* flux

through each transect, $F_{ab} = F_{ab}^{+} - F_{ab}^{-} = \int_{a}^{b} Q_{\eta}(s)ds$, is calculated analytically (as in Craig, 2005 (pg. 61-64), Craig and Rabideau, 2006 (section 3.1), and Craig and Rabideau, 2004 (pg. 385-387)). If, for a given transect, flow is unidirectional (i.e., $F_{ab} = F_{ab}^{+}$ or $F_{ab} = -F_{ab}^{-}$), then the analytic expression is used. Otherwise, a correction is applied to the numerically calculated total fluxes in order to be consistent with the analytic net flux:

$$\left(F_{ab}^{+}\right)_{CORR} = F_{ab}^{+}\left[1 + \frac{F_{ab} - F_{ab}^{+} + F_{ab}^{-}}{F_{ab}^{+} + F_{ab}^{-}}\right] \qquad \left(F_{ab}^{-}\right)_{CORR} = F_{ab}^{-}\left[1 - \frac{F_{ab} - F_{ab}^{+} + F_{ab}^{-}}{F_{ab}^{+} + F_{ab}^{-}}\right] \tag{4.4}$$

Note that $\left(F_{ab}^{+}\right)_{CORR} - \left(F_{ab}^{-}\right)_{CORR} = F_{ab}$, as desired.

In the AEM modeling software utilized in this study, calculation of transect fluxes in a plume-enclosing zone flux polygon is carried out using the semi-analytical technique. Computation of the constraint is highly accurate, fairly inexpensive and convenient in that no decisions regarding the number and location of gradient pairs and/or particles are required. The enhanced accuracy of the semi-analytic technique may be superfluous in the context of a pump-and-treat constraint, as a single outflux term in the numerical integration will trigger a penalty. The analytic correction simply adjusts the penalty value to more accurately represent the severity of the constraint violation, which is unlikely to affect the overall optimization results. However, the additional computation required for the analytic correction is minor compared to the numerical integration step, and the zone flux feature is a standard component of the AEM software used in this work.

4.3 Methods

To investigate the performance of AEM-based PATO, two problem formulations were developed: (1) a 'control' problem, selected from the community problems presented in Mayer et al (2002), and (2) a 'complex' problem, based on the twin-plume problem presented by Mulligan and Ahlfeld (2001). These problems were selected based on two criteria. First, they were readily adaptable to the AEM modeling software used in this study, which is limited to two-dimensional steady-state flow with homogeneous conductivity and recharge zones. Second, the two problems differ significantly in terms of domain size, plume geometry, and boundary conditions, allowing for meaningful generalization of observed optimization trends.

In each of the test problems, the optimization design variables were the location and rates of extraction and injection wells. Most optimizations were carried out using well coordinates varied as continuous functions; a subset of the experiments limited well location coordinates to evenly spaced intervals. The optimal number of wells was determined implicitly by allowing algorithms to consider a large maximum number of wells. Of this maximum number, only wells operating above a threshold value (1.5 m^3/day) were retained in the solution.

4.3.1 Control problem

The AEM setup of the control problem is illustrated in Figure 4.2. The problem is based on Application III of the community problems posed by Mayer et al (2002), and is located in an unconfined aquifer with no-flow boundaries to the south and west and specified head boundaries (i.e. a head gradient of 0.001)

to the north and east, resulting in a north-northeasterly flow direction near the plume. Following the guidelines for the community problem, aquifer porosity, hydraulic conductivity and recharge were set at 0.32, 4.33 m/day, and 0.00164 m/day, respectively. To facilitate comparison with Fowler et al (2004a), the plume containment boundary was delineated by the 50 ppb concentration contour resulting from 5 years of contaminant transport from the initial plume source. In this case, contaminant transport was simulated using Cardinal (Craig, 2005), a multi-species single-phase reactive-transport model that integrates an AEM flow solution with a finite-element or finite-difference transport model.

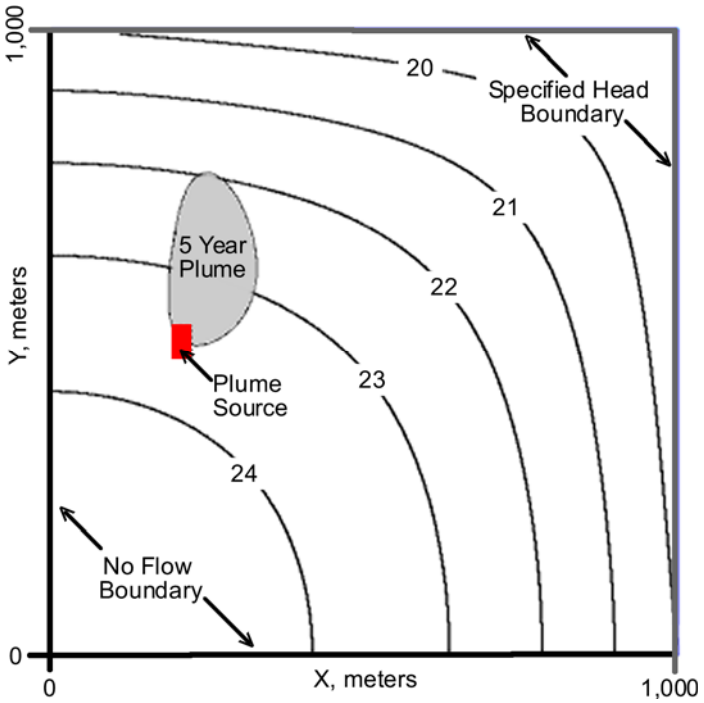

Figure 4.2: Control model setup (w/ simulated head contours [m])

4.3.2 Complex problem

The AEM setup of the complex problem is illustrated in Figure 4.3. The problem, adapted from a two-dimensional example developed by Mulligan and Ahlfeld (2001), is an unconfined aquifer containing no-flow boundaries in the

north and south, and specified heads in the west (head gradient of 3/3100) and east (head gradient of 3.17/3100), resulting in southeasterly flow through the plume. Following the description provided by Mulligan and Ahlfeld (2001), hydraulic conductivity, recharge and porosity were set to 5 m/day, 0 m/day and 0.3, respectively. The plume is presumed to result from the transport of contaminants from two separate source zones, leading to the dual-lobe shape. For this problem, precise values for the specified head boundaries were not provided in the published literature and were therefore estimated using trial and error to achieve a flow-field closely resembling the descriptions provided by Mulligan and Ahlfeld (2001).

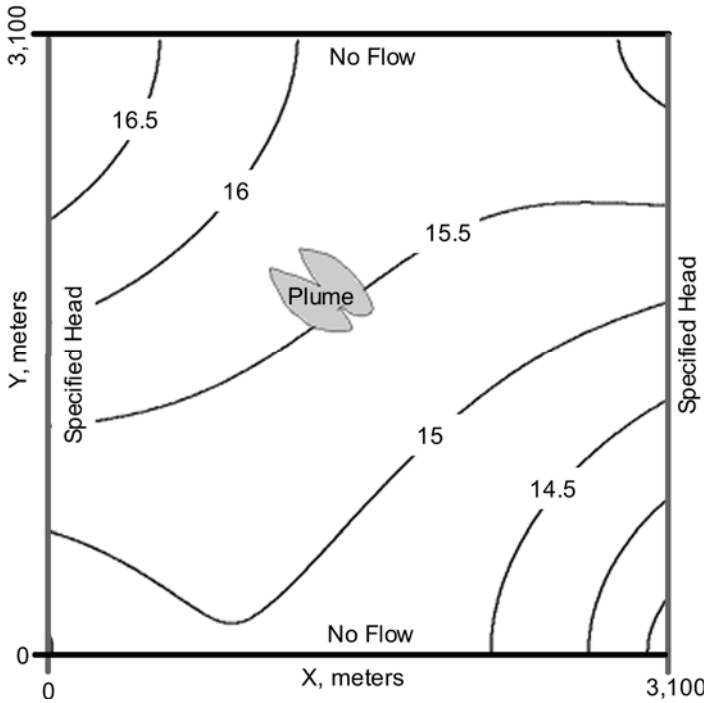

Figure 4.3: Complex problem setup (w/ simulated head contours [m])

4.3.3 Plume containment constraints

To assess the sensitivity of particle tracking and gradient control constraints to the number and distribution of particles and control pairs, several

different formulations of these constraints were implemented. Particle tracking and gradient control constraints were divided into three size-classes, corresponding to “low”, “medium” and “high” numbers of constraints, equal to 2, 5, and 10 times the maximum number of wells, respectively. Particle tracking constraints were further divided into two spatial categories: uniform placement of particles throughout the plume *body*, or uniform placement along the plume *perimeter*.

Hydraulic gradient constraints were always placed uniformly along the plume perimeter, but a distinction is made between whether the gradients were computed numerically (based on a distance of 10 meters between head inside and outside the plume) or analytically, which is not possible with standard FD/FE methods. In all, the particle tracking, hydraulic gradient, and zone outflux constraints provided a total of 13 different plume containment constraint configurations. Figure 4.4 illustrates selected constraints and Table 4.1 summarizes each of the formulations. In Figure 4.4, the arrows associated with gradient control constraints indicate an inward flow direction perpendicular to the plume boundary.

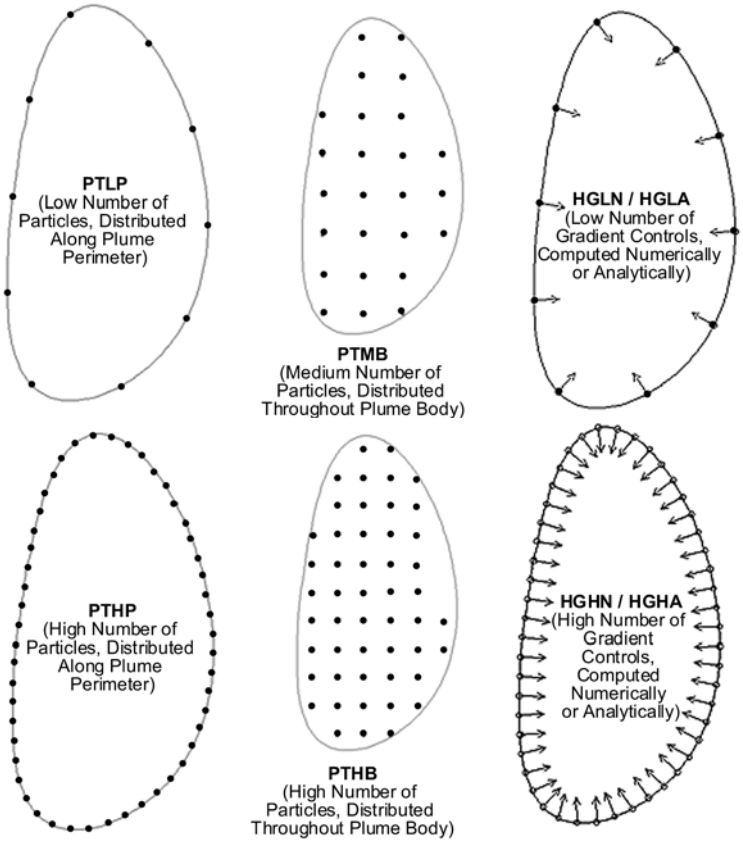

Figure 4.4: Selected Plume Containment Constraint Formulations

Table 4.1: Plume Containment Constraints

Acronym	Type	Number of Constraints (Control, Complex)	Distribution or Computation Technique
PTLB	**P**article **T**racking	**L**ow (10, 38)	Uniformly distributed throughout the plume **B**ody.
PTMB		**M**edium (25, 95)	
PTHB		**H**igh (50, 190)	
PTLP		**L**ow (10, 38)	Uniformly distributed along the plume **P**erimeter
PTMP		**M**edium (25, 95)	
PTHP		**H**igh (50, 190)	
HGLN	**H**ydraulic **G**radient Control (Control points uniformly distributed around plume perimeter)	**L**ow (10, 38)	Gradients computed **N**umerically
HGMN		**M**edium (25, 95)	
HGHN		**H**igh (50, 190)	
HGLA		**L**ow (10, 38)	Gradients computed **A**nalytically
HGMA		**M**edium (25, 95)	
HGHA		**H**igh (50, 190)	
ZONE	**ZONE** Outflux	n/a	n/a

4.3.4 Optimization algorithms

The performance of each of the optimization algorithms is dependent to some extent on the values assigned to various algorithmic parameters. Where possible, parameters were assigned values taken from published optimization studies, with preference given to references that specifically addressed pump-and-treat optimization. For example, PSO parameters values were taken from the tuning study of Beielstein et al (2002) and the guidelines of Zheng and Wang (2003) were used in the assignment of SA and GA parameters. Algorithm parameters related to computation time (for example, maximum number of generations) were assigned so that each algorithm would run to completion using a similar number of objective function evaluations.

4.3.5 Software packages

Three software packages were utilized in the experiments, which were run on a workstation cluster comprised of 32 1-GHz Intel Pentium III processors with 256-kB cache, 1-GB of RAM, and the Red Hat Linux 7.3 operating system. Two of the software packages, Split (Jankovic, 2005) and Bluebird (Craig and Matott, 2005), are AEM flow modeling engines that incorporate high-order elements. For experiments with particle tracking or numerical gradient control constraints, the Split engine was used, while the Bluebird engine was used for experiments involving zone outflux or analytic gradient control constraints. The two flow engines use identical system representation and solution algorithms; selection between the two was based solely on the availability of desired output. Both models use an over-specified high-order representation of line elements

[Jankovic (1997), and Jankovic and Barnes (1999)]. For this work, the element segments were configured with an order of 12 and 18 control points, yielding maximum simulated head errors of 0.2 and 2 mm for the Control and Complex problems, respectively.

The automated optimizations were performed using Ostrich (Matott, 2004), a model-independent, multi-algorithmic optimization tool. For this purpose, a pump-and-treat optimization module was developed and is available with version 1.4 of the public domain software.

4.3.6 Numerical experiments

To assess different aspects of AEM-based PATO, a series of numerical experiments was designed using the control and complex AEM models in conjunction with various configurations of the PATO problem. The goals of the experiments were: (1) demonstrate that PATO problems can effectively make use of AEM flow models, (2) compare the effectiveness of various optimization algorithms, as applied to PATO, (3) compare the *reliability* (defined below, in Section 4.3.6.1) of various plume containment constraint formulations, and (4) examine algorithm parallelization. To facilitate analysis of the experimental results, quantitative expressions for constraint reliability (R), algorithm effectiveness (F), and speedup (S) were developed, as discussed below.

4.3.6.1 Constraint reliability

Constraint reliability was computed following the completion of a given optimization run and measures the adequacy of the plume containment constraint formulation used in the optimization. Using the current optimal well-

field design, the flow model was run with a very large number of verification particles distributed uniformly throughout the plume and forward-tracked over the remediation time frame. The reliability of the constraints was computed as the percentage of verification particles successfully contained by the given optimal design.

$$R = \left(N_{con} / N_{total}\right) * 100\% \tag{4.5}$$

Where, N_{total} is the total number of verification particles and N_{con} is the number of these particles successfully contained.

4.3.6.2 Algorithm effectiveness

The measure of algorithm effectiveness was defined as the optimal objective function value discovered by a given algorithm, computed using the applicable additive or multiplicative penalty method (APM was used for particle tracking constraints, while MPM was used for gradient control and zone outflux constraints). As such, lower values indicate more effective algorithms.

4.3.6.3 Algorithm speedup

Algorithm speedup (S) was defined as the ratio of the wall-time required for optimization using a single processor (T_1) to the wall-time required when using p processors (T_p), where *wall-time* was the time required, from a human perspective, for an optimization to run to completion.

$$S = \left(T_1 / T_p\right) \tag{4.6}$$

Highly parallel algorithms may be expected to produce linear speedup ($S \rightarrow p$).

4.4 Results

More than 80 optimizations were performed. In general, a typical flow simulation for both the control and complex problems consumed less than one second of computation time. However, the use of particle tracking constraints significantly increased the model computation time. On average, the tracking of particles increased the AEM model run-time by approximately 1 second for every 25 particles. However, the increase was affected by the complexity of the local flow field and varied considerably between model configurations. Because of the additional model computation, optimization using “high” numbers of particle tracking constraints required considerably more computer time than other constraint formulations. The Split modeling engine supports parallel particle tracking, and while not utilized in the present study, this feature may provide substantial benefit to more complex problems involving hundreds or thousands of particles.

4.4.1 Algorithm comparisons

To assess algorithm effectiveness, the CG, GA, PSO, RND and SA algorithms were applied to the control AEM model. For each algorithm, separate optimizations were performed using the C_{TOTQ}, C_{OPER} and C_{OPER+} cost functions and the HGMN (medium number of numerically computed gradient control constraints) and PTMB (medium number of particle tracking constraints, placed throughout the plume body) plume containment constraint formulations. Additionally, two implementations of the conjugate gradient (CG) algorithm were examined, differentiated by the assignment of the initial well locations and rates.

One CG run (CG/AR) used randomly assigned initial parameter values, while the other run (CG/EJ) used initial values assigned based on engineering judgment and a limited number of manual trial-and-error runs.

In Figures 4.5 through 4.7, the effectiveness of each algorithm is presented for the various cost and constraint formulations. With the notable exception of the CG/EJ runs, the relative effectiveness of each algorithm was consistent across the different formulations. The particle swarm (PSO) algorithm was the most effective; the genetic algorithm (GA) also performed reasonably well across all formulations. For the C_{TOTQ} and C_{OPER} costs, the CG/EJ formulation was highly effective, but, as shown in Figure 4.7, the same algorithm was also the least effective at optimizing the C_{OPER+} cost formulation. It appears that the gradient-based CG algorithm was frustrated by the inclusion of capital costs in the C_{OPER+} cost function. These costs result in an optimization that is driven by the number of active wells in the system, a non-differentiable discrete parameter.

Based on their effectiveness at solving the control problem, the PSO and GA algorithms were applied to the complex problem. As shown in Figure 4.8, the PSO algorithm was much more effective at solving the complex problem, which was optimized using the C_{OPER+} cost function. In the complex problem, the maximum number of wells was nineteen, a value much larger than required for optimal satisfaction of the plume containment constraints (only one well is required). An examination of the optimization behavior of the two algorithms revealed that the PSO algorithm was much more effective at eliminating the

abundance of unnecessary wells. Given that the number of active wells drives the optimization of the C_{OPER+} cost function, the large difference between the effectiveness of the two algorithms is therefore attributed to the superior ability of the PSO algorithm to eliminate wells.

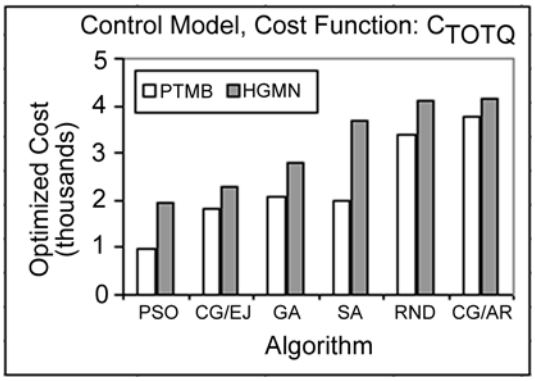

Figure 4.5: Comparison of algorithms applied to the control model optimization using PTMB and HGMN constraints and C_{TOTQ} cost

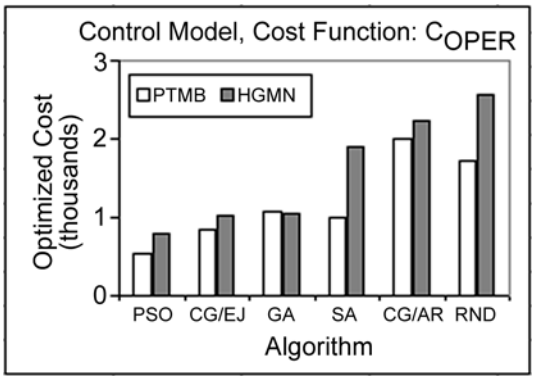

Figure 4.6: Comparison of algorithms applied to the control model optimization using PTMB and HGMN constraints and C_{OPER} cost

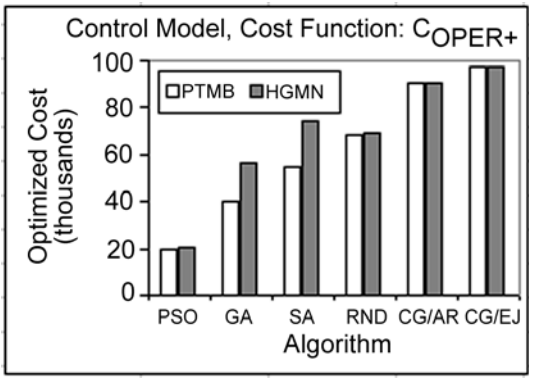

Figure 4.7: Comparison of algorithms applied to the control model optimization using PTMB and HGMN constraints and C_{OPER+} cost function

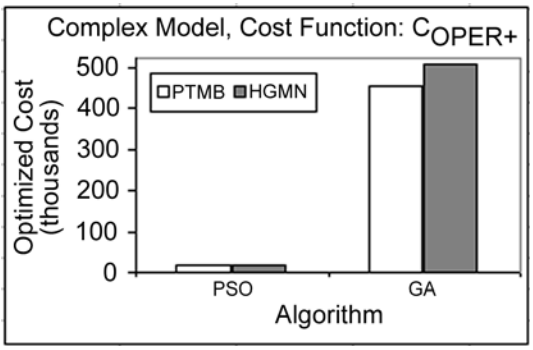

Figure 4.8: Comparison of algorithms applied to the complex model optimization using PTMB and HGMN constraints and C_{OPER+} cost function

4.4.2 Constraint comparisons

The experiments described above focused on the ability of various algorithms to minimize one of three cost functions utilizing a baseline set of plume containment constraint formulations. Another set of experiments examined the ability of alternative constraint formulations to represent the goal of plume containment in a reliable fashion. Optimizations were performed on both the control and complex problems using the C_{OPER+} cost function, the PSO algorithm, and each of the 13 constraint formulations listed in Table 4.1. Following each optimization, constraint reliability (as defined in Section 4.3.6.1) was computed based on the tracking of 1,000 particles initially located in and around the plume. Figures 4.9 and 4.10 summarize the resulting reliability measures for the various particle tracking and hydraulic gradient constraint formulations, respectively.

Among the particle tracking constraints, plume perimeter distributions were clearly more reliable than plume body distributions, but no configuration achieved 100% reliability (the 'Control, PTHP' configuration had a 99.5% reliability). For plume-perimeter particle distributions, the 'medium' setting yielded approximately 97% reliability, while 'high' numbers of particles were required to achieve similar reliability for plume-body distributions in the complex model (all of the plume-body distributions in the control model have less than 90% reliability). Conversely, 'low' numbers of gradient control constraints resulted in a range of 90-100% reliability while the 'medium' and 'high' gradient control settings were all between 97 and 100 percent reliable. Furthermore, the results show no

difference in reliability between the analytic and discretized gradient constraint formulations.

The zone outflux constraint (not shown) was found to be 100% reliable for both the control and complex problems. Average computation times required for the various constraint types (particle tracking, gradient control and zone outflux) are shown in Figure 4.11, and illustrate a significant computational advantage when using zone outflux or gradient control constraints. The reliability of the zone outflux constraint combined with its computational efficiency makes this constraint an attractive and powerful technique for constraining AEM-based PATO problems.

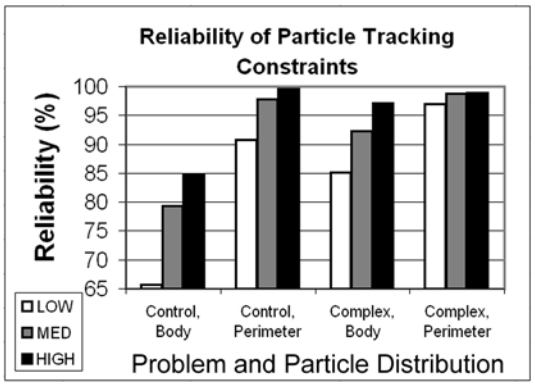

Figure 4.9: Comparison of particle tracking constraint reliabilities.

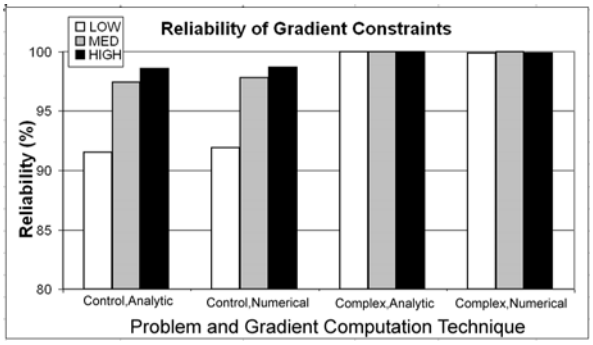

Figure 4.10: Comparison of gradient control constraint reliabilities.

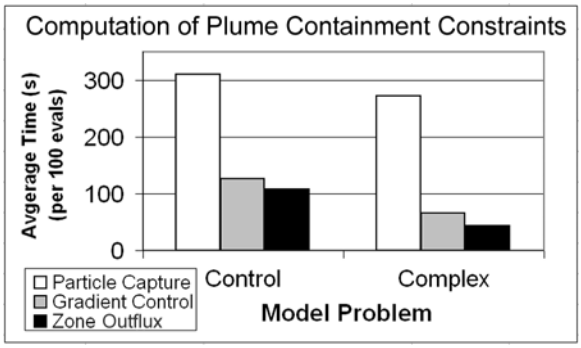

Figure 4.11: Average model computation times for various plume containment constraints

4.4.3 Comparison with published solutions

Table 4.2 provides a summary of the solutions to the control problem, using the zone outflux constraint and the most reliable particle tracking and gradient control constraint formulations. Also included in the table are the solution found by Fowler et al (2004a), using a finite difference flow model, and a solution found using the type curve procedures described by Javandel and Tsang (1986) and Grubb (1993). The type curve analysis is based on the simplifying assumption of uniform flow through the plume. The most reliable solution is that of the zone outflux constraint, whose optimal design is roughly 5½ percent less costly than the published FD-based solution. One possible explanation for the lower reliability of the published FD-based solution is that it used relatively few gradient control points (examination of Figure 10 indicates that low numbers of gradient control points are associated with reduced reliability). A possible explanation for the increased cost of the FD-based solution is that the gradient control constraint was more restrictive than the one presented in the current study. In the FD-based study, the gradient control formulation constrained flow to

be precisely directed toward an installed well, whereas the present study required flow to be towards the interior of the plume.

Table 4.3 provides a summary of solutions to the complex problem, using (1) the zone outflux constraint, (2) the most reliable gradient control constraint formulation (HGHA), (3) a particle tracking constraint formulation (PTMP) analogous to the constraint formulation used in the reference study (Mulligan and Ahlfeld, 2001), (4) the optimal solution reported in Mulligan and Ahlfeld (2001), which used a finite difference flow model and a particle tracking containment constraint formulation consisting of 110 particles placed along the plume perimeter, and (5) the optimal two-well solution using type curve analysis (as with the control problem, this requires the assumption of uniform flow through the plume body).

Table 4.2: Solutions to the Control Problem

Cost Function	Constraint Formulation (or Literature Reference)	Optimized Cost	Number of Wells	Well-field Configuration (Q [m^3/day], X [m], Y [m])	Reliability
OPER+	PTHP	$20,273	1	(178.1, 264, 726)	99.5%
	HGHA	$20,570	1	(219.3, 249, 711)	98.6%
	ZONE	$20,745	1	(241.6, 242, 705)	100.0%
	Fowler et al (2004a)	$21,957	1	(371.5, 250, 650)	96.8%
	Type Curve Analysis	$20,107	1	(152.5, 289, 741)	86.6%

Examination of the FD-based Complex solution and the analogous AEM-based solution (PTMP) reveals a close correspondence between the pumping rates of the two required wells. However, it is noted that the locations of the low-rate and high-rate wells for the two solutions are inverted. The low-rate (7 m^3/day) well in the AEM solution is associated with the eastern lobe of the plume, whereas the low-rate (8 m^3/day) well in the FD-based solution is associated with

the western lobe of the plume. Furthermore, the reliability of the FD-based solution (computed by configuring the AEM-based complex model with the reported FD-based solution) is fairly poor (less than 90%). The discrepancies between the FD- and AEM-based solutions, when using comparable plume containment constraints, suggests differences in the aquifer properties of the two models (recall that the specified head boundary conditions of the AEM-based complex model were estimated using trial-and-error).

Table 4.3: Solutions to the Complex Problem

Cost Function	Constraint Formulation (or Literature Reference)	Optimized Cost (Total Rate)	Number of Wells	Well-field Configuration (Q [m^3/day], X [m], Y [m])	Reliability
TOTQ	HGHA	$3,385 (62.8)	3	(8.3, 1462, 1664) (28.2, 1432, 1759) (26.3, 1540, 1811)	100.0%
	ZONE	$3,489 (64.7)	3	(14.6, 1441, 1670) (11.9, 1435, 1745) (38.2, 1520, 1819)	100.0%
	PTMP	$1,694 (31.4)	2	(24.4, 1449, 1679) (7.0, 1569, 1702)	97.6%
	Mulligan and Ahlfeld (2001)	$1,565 (29.0)	2	(8.0, 1347, 1680) (21.0, 1573, 1720)	88.7%
	Type Curve Analysis	$1,511 (28.0)	2	(14.0, 1504, 1676) (14.0, 1537, 1706)	89.9%

The type curve solutions for both problems are low cost, but also have low reliability. Two aspects of the type curve analysis account for its low reliability: (1) the simplifying assumption of uniform flow results in a less-than-optimal rate for plume containment, and (2) the analysis applies to the steady-state capture zone (i.e. at infinite time), rather than the actual remediation time frames used in this study (5 and 30 years for the control and complex problems, respectively).

For the complex model, examination of the gradient control (HGHA) and zone outflux constraint (ZONE) solutions reveals that, relative to the particle

tracking constraint formulation, one additional well is required and the total pumping rate is significantly higher (roughly double). This increase in cost and number of wells is likely due to the dual-lobed shape of the plume. As shown by the capture zones in Figure 4.12, the gradient control and zone outflux constraints prevent the “clean” region between the two lobes from being contaminated during remediation, while the particle tracking solution drags contaminated groundwater through this region and then back into the confines of the plume boundary. Maintaining an inward flux along the plume boundary where the two lobes converge (thus preventing contamination of the clean region) is a more restrictive constraint, and necessitates an increased number of wells and increased total pumping rate.

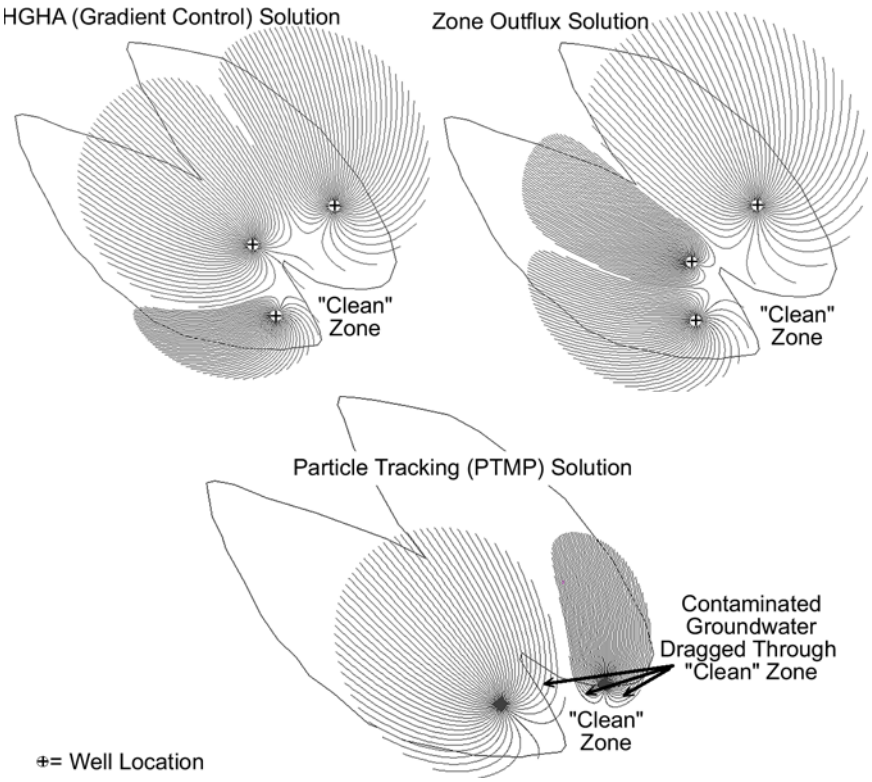

Figure 4.12: 30-year Capture Zones for the Complex Problem

4.4.4 Continuous vs. discretized well coordinates

Tables 4.4 and 4.5 summarize optimal solutions for various constraint formulations using continuous and discretized well coordinates. For discrete well-coordinates, candidate well locations were set at 10 meter intervals in the x- and y- directions. Examination of Tables 4.4 and 4.5 reveals that discretization produces results nearly equivalent to those in which well coordinates are varied as continuous functions, both in terms of cost (the maximum cost difference is 4%) and well location. Since both methods provide equivalent results, the choice between discretized and continuous well coordinates (if continuous well coordinates can be handled by the given flow-modeling engine, and if the PATO problem is similar to those presented in this study) can be based on computational considerations. For example, conjugate-gradient algorithms require continuous variables, to facilitate computation of partial derivatives. Conversely, a binary-encoded GA is more amenable to the use of discretized (integer-based) values.

Table 4.4: Well-Coordinate Comparisons (Control Problem)

Cost Function	Constraint Formulation	Discretized?	Cost	Number of Wells	Well-field Configuration (Q [m^3/day], X [m], Y [m])	Reliability
C_{OPER+}	PTHP	No	$20,273	1	(178.1, 264, 726)	99.5%
		Yes	$20,333	1	(186.0, 280, 730)	98.5%
	HGHA	No	$20,570	1	(219.4, 249, 711)	98.6%
		Yes	$20,588	1	(221.7, 250, 710)	98.8%
	ZONE	No	$20,745	1	(241.6, 242, 705)	100.0%
		Yes	$20,850	1	(253.9, 230, 710)	100.0%

Table 4.5: Well-Coordinate Comparisons (Complex Problem)

Cost Function	Constraint Formulation	Discretized?	Cost (Total Rate)	Number of Wells	Well-field Configuration (Q [m^3/day], X [m], Y [m])	Reliability
C_{TOTQ}	PTHP	No	\$2,015 (37.4)	2	(33.8, 1507, 1728) (3.6, 1449, 1646)	99.1%
		Yes	\$2,018 (37.3)	2	(33.9, 1510, 1720) (3.4, 1440, 1640)	99.6%
	HGHA	No	\$3,385 (62.8)	3	(8.3, 1462, 1664) (28.2, 1432, 1759) (26.3, 1540, 1811)	100.0%
		Yes	\$3,526 (65.3)	3	(7.5, 1460, 1660) (30.8, 1430, 1760) (27.0, 1540, 1820)	99.9%
	ZONE	No	\$3,489 (64.7)	3	(14.6, 1441, 1670) (11.9, 1435, 1745) (38.2, 1520, 1819)	100.0%
		Yes	\$3,580 (66.3)	3	(17.8, 1420, 1660) (17.4, 1440, 1760) (31.1, 1540, 1820)	100.0%

4.4.5 Algorithm parallelization

A final set of optimizations examined improvements in computation speed achievable via parallelization of the optimization algorithm. The PSO algorithm was parallelized for distributed, cluster-based processors using the message-passing interface (MPI) (e.g., Gropp et al, 1999). In the parallel PSO algorithm, a supervisor processor begins iteration by broadcasting a revised population set (particle swarm) to a set of subordinate processors. Each subordinate processor computes the objective function of one or more of the revised particles and sends the results back to the supervisor. The supervisor completes the iteration by revising algorithmic data (i.e. local and global memory) associated with each particle, and the entire process begins again with the next iteration.

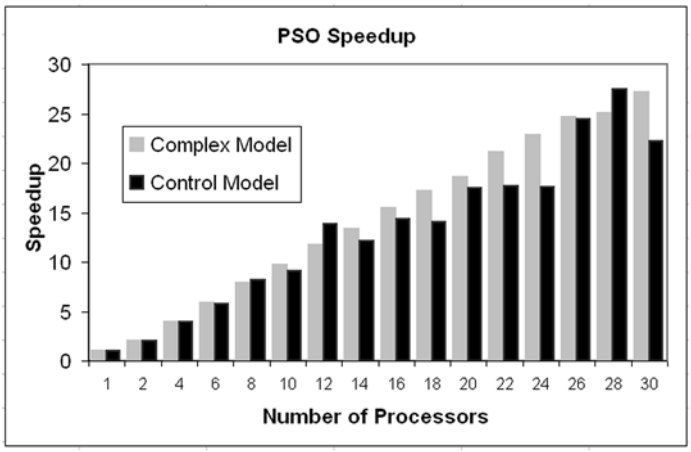

Figure 4.13: Parallel speedup of the PSO algorithm

As shown in Figure 4.13, nearly linear speedup of the PSO algorithm was achieved using up to thirty parallel processors. The complex model appeared to benefit slightly more from the parallel processing, which is attributed to the use of a larger swarm size (i.e. number of candidate solutions) in solving the complex problem. Evaluation of this larger swarm by the subordinate processors necessarily consumed more computation time and therefore diminished the relative amount of time spent performing MPI communication.

4.5 Discussion And Conclusion

In this paper, the use of AEM flow models in the automated optimization of pump-and-treat systems has been demonstrated for the first time. Two hydraulic control problems were adapted from published literature and numerous optimizations were successfully performed using a variety of algorithms, cost functions, penalty techniques, and plume containment constraints. Although the chosen problems are amenable to solution by elementary type-curve analysis, they are also rather complex from the viewpoint of a general-purpose optimizer. When expressed in a constrained optimization framework, the problems are

highly non-linear and contain a multitude of design variables, and are therefore a useful means to benchmark AEM-based PATO against other simulation-optimization approaches.

Of the algorithms investigated, the particle swarm (PSO) algorithm performed most effectively and exhibited linear parallel speedup. Of particular note is the ability of the PSO to reduce the number of extraction wells when the maximum number is highly over-estimated. This paper also marks the first application of the PSO algorithm to PATO problems, and its superior performance suggests that it should be evaluated for more complex environmental optimization problems.

The use of analytic element (AEM) flow models for pump-and-treat optimization provides several interesting capabilities that are either not possible or not yet utilized within standard finite difference (FD) and finite element (FE) flow models. For example, the optimizations in this paper varied well coordinates as continuous functions, an approach that is not possible with grid-based FD/FE models. Furthermore, while AEM models can readily incorporate commonly used particle tracking and gradient control plume containment constraints, the method also supports the use of a zone outflux constraint (not presently implemented in FD/FE models) and the analytic computation of gradient control constraints (not possible in FD/FE models). The zone outflux constraint was shown to be extremely reliable and, like the gradient control constraint, required significantly less computation time than particle tracking techniques. Conversely, in the context of pump-and-treat optimization, the results fail to demonstrate that other

features of AEM (such as well coordinates varied as continuous functions and analytically computed head gradients) offer a particular advantage.

Limitations associated with the AEM modeling software used in this study include the assumptions of steady-state two-dimensional flow with zoned heterogeneity (i.e. piecewise constant regions of aquifer heterogeneity). Other public domain AEM software, such as Tim^{ML} (Bakker, 2004), can overcome some of these limitations, suggesting that the AEM-based PATO concepts discussed in this paper may be applicable to more complex aquifer systems. Alternatively, the particular advantages associated with the use of AEM-based PATO could be utilized in a preliminary optimization exercise, to be followed by optimization of a more complex (e.g. three-dimensional, time-varying and/or heterogeneous) FD/FE model. Such a preliminary model could be used to identify candidate well locations and estimate the required number of wells and total pumping rate.

5 APPLICATION OF HEURISTIC OPTIMIZATION TECHNIQUES AND ALGORITHM TUNING TO MULTI-LAYERED SORPTIVE BARRIER DESIGN

The material in Chapter 5 has been accepted for publication as "Matott LS, Bartelt-Hunt SL, Rabideau AJ, Fowler KR. accepted. Application of Heuristic Optimization Techniques and Algorithm Tuning to Multi-Layered Sorptive Barrier Design. *Environmental Science and Technology*", *copyright by American Chemical Society.*

5.1 Overview

Although heuristic optimization techniques are increasingly applied in environmental engineering applications, algorithm selection and configuration are often approached in an ad hoc fashion. In this study, the design of a multi-layer sorptive barrier system served as a benchmark problem for evaluating several algorithm-tuning procedures, as applied to three global optimization techniques (genetic algorithms, simulated annealing, and particle swarm optimization). Each design problem was configured as a combinatorial optimization in which sorptive materials were selected for inclusion in a landfill liner to minimize the transport of three common organic contaminants. Relative to multi-layer sorptive barrier design, study results indicate (1) the binary-coded genetic algorithm is highly efficient and requires minimal tuning, (2) constraint violations must be carefully integrated to avoid poor algorithm convergence, and (3) search algorithm performance is strongly influenced by the physical-chemical properties of the organic contaminants of concern. More generally, the results suggest that formal algorithm tuning, which has not been widely applied to environmental engineering optimization, can significantly improve algorithm performance and provide insight into the physical processes that control environmental systems.

5.2 Introduction

Heuristic optimization algorithms have been applied to an increasing number of environmental engineering applications because they are capable of overcoming common challenges of environmental problems, such as extreme non-linearity, mixed parameter types, and the presence of local minima and/or discontinuities. With a few notable exceptions [e.g. Matott et al (2006), Yoon and Shoemaker (1999), Maskey et al (2002), and Solomatine (1999)], comparisons of alternative search algorithms are uncommon and often characterized by ad-hoc algorithm selection and configuration. Rardin and Uzsoy (2001) argue that meaningful comparisons should be anchored by a procedure (known as *algorithm tuning*) in which each optimization algorithm is adapted to the specific problem under consideration to maximize algorithm performance.

While algorithm tuning is uncommon in environmental studies, several systematic approaches have been proposed in the optimization literature, including the use of experimental techniques and/or sensitivity analysis (Coy et al, 2001), the development of self-adaptive algorithms (Hinterding et al, 1997), and the use of meta-optimization algorithms (Talbi, 2002). The present work focuses on algorithm tuning via experimental techniques and, in particular, adopts the Taguchi *design of experiments* (DOE) approach (Roy, 2001), a popular method within process engineering for tuning various manufacturing processes. While Beielstein et al. (2002) applied Taguchi analysis to various benchmark optimization problems, the present approach differs from Beielstein et al. (2002) by (1) considering non-linear behavior and interactions among tuning

parameters, (2) performing confirmation of tuning effectiveness, (3) comparing multiple search algorithms, and (4) examining a real-world environmental application.

The optimization studies considered in this paper involve the design of multi-layer sorptive landfill liners, an application that is representative of a broad class of remediation problems involving multiple sequential barriers or treatment units. While subsurface barrier design frequently emphasizes the minimization of advection through low permeability materials, several studies have demonstrated the significance of diffusion (Johnson et al, 1995, and Khandelwal et al, 1998), and this has motivated an interest in low permeability sorbing barriers capable of simultaneously controlling both advective and diffusive contaminant transport (Gullick and Weber, 2001, and Deitsch et al, 1998).

Numerous studies have modeled contaminant transport through barrier systems (Bartelt-Hunt et al, 2005), and a few have investigated optimal barrier design using a simulation-optimization approach (Bartelt-Hunt et al, in press). The benchmark application for this study was a multi-layer sorptive liner design problem developed by Bartelt-Hunt et al (in press), in which sorptive materials are added to a multi-layer liner to inhibit organic solute transport. A detailed problem description is provided in the supporting information (Appendix C). Transport of three organic solutes [benzene, trichloroethylene (TCE) and 1,2-dichlorobenzene (1,2-DCB)] with different nonlinear sorption behavior was considered, resulting in three distinct optimization problems.

This study makes a dual contribution by investigating a formal algorithm tuning methodology in the context of an important class of environmental engineering problems. Specific research objectives were to (1) assess the performance of several heuristic algorithms by comparing alternative formulations, using a DOE approach to enhance the efficiency and robustness of the process, (2) explore techniques for integrating design constraints into the liner cost function, (3) examine relationships between algorithm performance and liner problem formulation, and (4) assess the merits of the Taguchi DOE approach as a formal algorithm tuning procedure. For each liner problem and for a variety of constraint integration methods, three popular heuristic search procedures [particle swarm optimization (PSO) (Kennedy and Eberhart, 1995), genetic algorithms (GA) (Goldberg, 1989), and simulated annealing (SA) (Kirkpatrick et al, 1983)] were applied, tuned, and compared. Algorithm analysis focused on measures of *efficiency* (amount of computation time required, in terms of objective function evaluations) and *effectiveness* (ability of an algorithm to identify the globally optimal design), and was aided by the identification of the true global optimum for each liner problem, determined via an exhaustive search involving millions of simulations on a massively parallel computing system.

5.3 Methods

5.3.1 Heuristic optimization algorithms

The computational effort required for an exhaustive search of the multi-layer landfill liner design space is probably infeasible for routine applications and motivates the development of more efficient strategies. Traditional numerical

optimization methods are mathematically derived, deterministic, and gradient-based. Conversely, heuristic optimization techniques are derived from natural optimization processes and incorporate structured randomness. For the selected liner design problems, heuristic algorithms were preferred because the design space is discontinuous and has local minima, as shown in Appendix C (Figure C.3). Gradient-based methods can be frustrated by these factors, while heuristic methods are more robust. This study considered four heuristic algorithms: two genetic algorithm variants (with different parameter encoding techniques), particle swarm optimization, and simulated annealing. A brief overview of each algorithm is provided below and Matott (2005) provides additional implementation details.

5.3.1.1 Genetic algorithm (GA)

The GA (Goldberg, 1989) utilizes a population of candidate solutions (parameter sets) and applies selection, crossover, mutation, and elitism operators to successive generations of the population. The chosen RGA (real-coded GA) implements two-member tournament selection, uses real-valued parameter encoding and mutation, and implements crossover as a non-biased random-weighted average of randomly-selected parent parameters. Conversely, the selected BGA (binary-coded GA) also uses two-member tournament selection, but encodes parameters into binary bit-strings, mutates by inverting random bits, and performs crossover via between-parent bit swapping. For both algorithms, four configurable parameters were considered: the population size, the number of generations, the elitism level (the number of unchanged members

between generations), and the mutation rate (the probability of randomly re-assigning the parameter values of a population member).

5.3.1.2 Simulated annealing (SA)

The SA algorithm (Kirkpatrick et al, 1983) is analogous to physical annealing, where a solid is heated to a high energy-state and slowly cooled to drive the material to its lowest energy state. During each SA step, a randomness control parameter (the temperature) is reduced and an equilibration procedure is performed, where the design space is explored by a series of random-walk parameter adjustments. Each random-walk step is subject to an acceptance probability, allowing the equilibration procedure to accept uphill moves. The selected SA estimates the initial temperature via a set of 'melting' trials consisting of random-walk steps with a 100% acceptance probability. This study considered four SA tuning parameters: the number of temperature reductions, the number of equilibration steps at each temperature reduction, the number of melting trials, and the temperature reduction rate.

5.3.1.3 Particle swarm optimization (PSO)

PSO (Kennedy and Eberhart, 1995) mimics the cooperative-competitive behavior of birds, fish and other animals. The algorithm utilizes a population of parameter sets (the *particle swarm)*. During each algorithm step, particles move through the design space and revised locations and velocities (i.e. step sizes) are computed using simple vector calculations. In these calculations, each particle retains a fraction of its velocity (the inertia weight) and the direction of movement is computed as a biased-but-random combination of two vectors pointing from a

particle's current location to the globally (visited by any particle) and locally (visited by a given particle) best solutions. Preference for global or local descent is determined by two PSO parameters: the cognitive weight and the social weight. A high cognitive weight biases particles towards the local best, while a high social weight biases particles toward the global best. This study considered five PSO tuning parameters: the swarm size, the number of generations, the inertia weight, the cognitive weight, and the social weight.

5.3.2 Overview of experimental approach

The numerical experiments performed in the study proceeded as follows: First, for each pairing of algorithm, optimization problem, and constraint integration technique, a set of Taguchi DOE tuning experiments were performed, requiring numerous optimizations and yielding optimal, problem-specific, configurations of algorithm and penalty parameters. For each individual optimization, a given algorithm sought the optimal liner design via repeated executions of a solute transport model. Output from a contaminant transport simulator was forwarded to a constraint-integration step that determined whether the given design violated constraints, in which case the design was considered infeasible and a penalty was assessed to the overall liner cost. After completing the DOE experiments, tuned algorithms were utilized in a set of confirmation optimizations, which facilitated a rigorous comparison and evaluation of the various algorithms with respect to each of the three organic solutes. A graphical illustration of the experimental setup is provided in Appendix C (Figure C.4).

5.3.3 Taguchi DOE method

Robust comparisons of heuristic algorithms should be preceded by an algorithm tuning procedure that maximizes algorithm performance. The selected Taguchi DOE method configures preliminary optimizations using a variety of values (*levels*) for the various tuning parameters (*factors*). Rather than evaluating all factor-level combinations, the Taguchi method utilizes a combination of fractional experimental layout and statistical and/or graphical analysis to efficiently determine the optimal parameter settings for a given *optimization process* (i.e. a combination of heuristic algorithm, organic solute, and constraint integration technique). Tuned parameter settings for each process were determined via separate applications of the Taguchi method, which is described below.

5.3.3.1 Selection of experimental layout

Table 5.1 summarizes the factors considered for each algorithm, with four levels per factor selected to allow consideration of non-linear effects. To simplify the representation of the Taguchi experimental setup, each factor and level in Table 5.1 was assigned an alphanumeric value, defined in the parentheses of row and column headings. Because up to six four-level factors were considered, a truncated L_{32} orthogonal array (requiring 32 experiments and replicated in Table 5.2) was selected for the experimental layout. Published material (Beielstein et al, 2002, Goldberg, 1989, and Zheng and Wang, 2003) and exploratory numerical experiments determined the range of values represented by the four levels of each factor.

Table 5.1: Factor-Level mapping of tuning parameters. Parenthetic values in the row and column headings define alphanumeric short-hand for the algorithm parameters (A-F) and the range of considered values (1-4)

GA (Genetic Algorithm)	Levels			
Factor	(1)	(2)	(3)	(4)
(A) Penalty Weight [$/µg]	0.1	1	10*	100
(B) Population Size [C]	20	50	100*	200
(C) Number of Generations [C]	10	20*	50	100
(D) Number of Elites	1	3*	5	10
(E) Mutation Rate	0.1%	1%	5%*	15%
PSO (particle swarm optimization)	Levels			
Factor	(1)	(2)	(3)	(4)
(A) Penalty Weight [$/µg]	0.1	1	10*	100
(B) Swarm Size [C]	20	50	100*	200
(C) Number of Generations [C]	10	20*	50	100
(D) Initial Inertia Weight	0.25	1*	2	4
(E) Cognitive Weight	0.25	1	2*	4
(F) Social Weight	0.25	1	2*	4
SA (Simulated Annealing)	Levels			
Factor	(1)	(2)	(3)	(4)
(A) Penalty Weight [$/µg]	0.1	1	10*	100
(B) Equilibration Steps [C]	20	50	100*	200
(C) Temperature Reductions [C]	10	20*	50	100
(D) Melting Trials [C]	10	20	50*	100
(E) Cooling Rate	1%	10%*	25%	50%

* Denotes nominal values.
[C] Denotes a computational parameter.

5.3.3.2 Experiment evaluation

Because heuristic optimization algorithms contain randomness, a single optimization was insufficient to characterize a given experiment. Therefore, each experiment evaluation was based on multiple repetitions (*10 samples*) of the given optimization process. Preliminary numerical experiments (with configurations of up to 100 samples) established that 10 samples yielded good computational performance with acceptably small error in the estimated median (less than 5%).

Table 5.2: Portion of the L32 orthogonal array used in this study. For algorithms involving only five factors, column F is ignored. For each experiment, the array identifies the required factor-level settings using the alphanumeric short-hand defined in Table 5.1

Experiment Number	Factor Levels						Experiment Number	Factor Levels					
	A	B	C	D	E	F		A	B	C	D	E	F
1	1	1	1	1	1	1	17	1	1	4	1	4	2
2	1	2	2	2	2	2	18	1	2	3	2	3	1
3	1	3	3	3	3	3	19	1	3	2	3	2	4
4	1	4	4	4	4	4	20	1	4	1	4	1	3
5	2	1	1	2	2	3	21	2	1	4	2	3	4
6	2	2	2	1	1	4	22	2	2	3	1	4	3
7	2	3	3	4	4	1	23	2	3	2	4	1	2
8	2	4	4	3	3	2	24	2	4	1	3	2	1
9	3	1	2	3	4	1	25	3	1	3	3	1	2
10	3	2	1	4	3	2	26	3	2	4	4	2	1
11	3	3	4	1	2	3	27	3	3	1	1	3	4
12	3	4	3	2	1	4	28	3	4	2	2	4	3
13	4	1	2	4	3	3	29	4	1	3	4	2	4
14	4	2	1	3	4	4	30	4	2	4	3	1	3
15	4	3	4	2	1	1	31	4	3	1	2	4	2
16	4	4	3	1	2	2	32	4	4	2	1	3	1

5.3.3.3 Calculation of experiment performance

Each optimization yielded a measure of sample performance, computed using Equation 5.1.

$$S_i = 10 \times C_i + 90 \times E_i \qquad (5.1a)$$

$$C_i = 1 - \left(\frac{N_i - 1}{N_R} \right) \qquad (5.1b)$$

$$E_i = 1 - \left(\frac{F\left(\overline{X}\right)_i - F\left(\overline{X}\right)_{\min}}{F\left(\overline{X}\right)_R} \right) \qquad (5.1c)$$

where, S_i is the performance of the *i*-th sample, computed as a weighted combination of the efficiency (C_i) and effectiveness (E_i) terms, N_i is the number of objective function evaluations required by the *i*-th sample and is normalized by the range (N_R) of evaluations required by the various optimizations, $F\left(\overline{X}\right)_i$ is the

optimal objective function value discovered by the *i*-th sampled optimization, and $F(\overline{X})_{\min}$ and $F(\overline{X})_R$ are the true optimal objective function value and the range of optima reported by all optimizations of the given problem, respectively. As shown in equation 5.1a, a 90:10 effectiveness-efficiency ratio was utilized, biasing the optimizations to favor effectiveness. The fast (approximately one second) run-times of the transport simulations suggest this weighting scheme is appropriate for the selected problems. For more computationally demanding applications, the higher cost of computer resources may be accommodated via an increased efficiency weight.

The formulation of sample performance defined by equations (5.1a-5.1c) is non-dimensional and scaled to have a range from zero (worst) to one hundred (best). After evaluating all samples for a given experiment, overall experiment performance (*Y*) was computed using the *median* value of the sample performances. The median was preferred because of the small number of experiment samples, the structured-but-random nature of the search algorithms, and the skewed, non-random, sample distribution resulting from the optimization objective.

5.3.3.4 Experiment analysis

Two forms of experiment analysis were applied to the Taguchi method utilized in this work. The first method computed the average experiment performance of each factor at each level and utilized these averages in a 'main-effects' tuning procedure, which assigned optimal factor-level settings by selecting factor levels with the highest average performance. The second method

involved the inspection of two-way interaction plots, a graphical procedure in which the performance of a given factor-level was plotted for fixed levels of another factor. Selected interaction plots are presented in Figure 5.1 and in Appendix C (Figure C.2). For a given analysis, intersection of any of the four factor-level lines indicates factor interaction. In such cases, assignment of optimal factor-level settings to peak interaction points may provide superior tuned performance relative to main effects tuning. However, tuning using factor interaction plots was sometimes confounded by the presence of multiple, nearly equivalent, peaks in a given plot, and different interaction plots occasionally pointed toward conflicting settings. These difficulties necessitated a somewhat subjective trial-and-error approach, in which various interaction plot interpretations were evaluated. The optimization processes in this study were tuned using both the main effects and the interaction tuning procedures, resulting in a pair of optimal factor-level configurations for each process.

5.3.3.5 Confirmation of Taguchi analysis

For each completed Taguchi application, a confirmation procedure was applied to the factor-level settings resulting from the two tuning analyses. The first confirmation step involved performing experiments using 'tuned' process settings. The resulting measures of experiment performance were then compared to a 90% confidence interval on the tuned performance value, computed using an analysis of variance (ANOVA) on the tabulated experiment data, as described in Roy (2001). Confirmation results were also compared with a 'nominal' configuration of factor-level settings (nominal settings are identified in

Table 5.1). The confidence interval comparison estimated the statistical reliability of the Taguchi tuning procedure, while the comparison against nominal assessed the practical usefulness of the approach.

5.3.4 Solute transport model

The migration of leachate contaminants through a given landfill liner was modeled as transient one-dimensional solute transport through multiple layers of low-permeability sorptive material. In this study, the one-dimensional advective-dispersive-reactive equation was solved using the MOUSER software (Rabideau, 2003), modified to support multiple layers. Solute sorption behavior was defined in terms of empirical nonlinear isotherm parameters, using values established by previous work (Bartelt-Hunt et al, 2005). Appendix C provides a lengthier treatment of the solute transport model.

5.3.5 Sorbing additives

In this study, a given liner design was represented by six combinatorial parameters ($\overline{X} = [L_1, L_2, L_3, L_4, L_5, L_6]^T$) defining the order and material composition of 150-mm thick liner layers. Each layer parameter (L_i) was represented by an integer value and the material composition (and costs) corresponding to these values is given in Table 5.3 (organoclay and GAC costs were vendor-provided, while shale costs were derived from Gullick (1998)). The final layers included a "no layer" composition, allowing for consideration of a variable number of layers. The basis for the selected additives is a recent study considering liner design using sorptive amendments (Bartelt-Hunt et al, 2005). While the liners considered in this study consist of (possibly amended) earthen

layers, the current state-of-practice favors composite geomembrane-earthen materials. The optimization and tuning methods presented in this study would apply equally well to these more conventional systems, provided the solute transport model was adapted to include composite barrier components (e.g. Edil, 2003).

Table 5.3: Combinatorial encoding of layer parameters

Coded Value	Material Composition of the Layer	Cost (w_L [\$/m^2])
1	87% sand, 10% bentonite, 3% BTEA-bentonite[a]	19.33
2	84% sand, 10% bentonite, 6% BTEA-bentonite	36.50
3	81% sand, 10% bentonite, 9% BTEA-bentonite	53.46
4	87% sand, 10% bentonite, 3% HDTMA-bentonite[b]	20.32
5	84% sand, 10% bentonite, 6% HDTMA-bentonite	37.68
6	81% sand, 10% bentonite, 9% HDTMA-bentonite	53.46
7	87% sand, 10% bentonite, 3% shale	2.08
8	84% sand, 10% bentonite, 6% shale	2.20
9	81% sand, 10% bentonite, 9% shale	2.31
10	87% sand, 10% bentonite, 3% GAC[c]	10.65
11	84% sand, 10% bentonite, 6% GAC	19.34
12	81% sand, 10% bentonite, 9% GAC	28.03
13	90 % sand, 10% bentonite	1.96
14	no layer	0.00

[a]BTEA-bentonite: benzyltriethylammonium bentonite
[b]HDTMA-bentonite: hexadecyltrimethylammonium bentonite
[c]GAC: granular activated carbon

5.3.6 Cost function and constraint integration

The financial cost associated with the construction of a given landfill liner was computed using Equation 5.2, simplified from (Bartelt-Hunt et al, in press).

$$f\left(\overline{X}\right) = \underbrace{w_{oc}\left(h_l - h_{\min}\right)}_{\text{opportunity cost}} + \underbrace{\sum_{i=1}^{6} w_{L_i}}_{\text{material cost}} \tag{5.2}$$

where $f(\overline{X})$ is the financial cost (in \$/m^2) of the landfill liner, h_l is the actual height of the liner, h_{min} is the minimum height of the liner (0.6 m), w_{oc} is the opportunity cost factor [37.5 \$/m^3, derived from nationally averaged tipping fees], and w_{L_i} is the material cost of the i^{th} layer, which includes the cost of grading and excavation plus the bulk cost of individual sorptive amendments. Opportunity costs reflect the revenue lost due to excess liner thickness (0.6 m is the regulated minimum), which decreases the amount of waste that can be accommodated by the landfill. While tipping fees and materials costs could change with time and location, such fluctuations were not considered.

Besides minimizing financial cost, each liner was required to satisfy a constraint on the amount of contaminant released during the design lifetime, quantified using Equation 5.3:

$$P(\overline{X}) = w_{vio} \times \max\left[0, g(\overline{X}) - b\right] \tag{5.3}$$

where $P(\overline{X})$ is the penalty associated with a given liner design, $\overline{X}$ is a layer vector, $g(\overline{X})$ is the cumulative leachate mass per area exiting the liner after one hundred years of simulated transport, b is the maximum tolerable 100-year leachate mass per area (5 μg/m^2), and w_{vio} is the penalty weight, identified as one of the tuning parameters of the Taguchi analysis. Incorporation of the penalty function, $P(\overline{X})$, into the overall objective function can be done in a variety of ways (Chan Hilton and Culver, 2000), and is referred to as *constraint integration*. In this study, two constraint integration techniques were considered:

the Additive Penalty Method (APM) and the Multiplicative Penalty Method (MPM). Objective function formulations for each method are given in Equation 5.4.

$$F(\overline{X}) = \begin{cases} f(\overline{X}) + P(\overline{X}) & \text{if APM} \\ f(\overline{X})(1 + P(\overline{X})) & \text{if MPM} \end{cases} \tag{5.4}$$

where the objective function, $F(\overline{X})$, combines the financial cost and penalty function, and depends on the choice of penalty method.

5.3.7 Summary of numerical experiments

A typical 100-year leachate transport simulation required 0.8 seconds of computation time. All optimizations were performed using OSTRICH (Matott, 2005), run on parallel computing clusters maintained by the University at Buffalo Center for Computational Research (CCR). Appendix C provides additional detail on the numerical experiments.

5.4 Results and Discussion

5.4.1 Comparison of tuning procedures

A total of 7,680 samples and 768 experiments were required by the Taguchi method for tuning the 24 selected optimization processes. As illustrated in Figure 5.1, interaction plots suggest significant interaction between algorithm parameters. Tuned parameter settings for each algorithm and for each solute are tabulated in Appendix C (Table C.1).

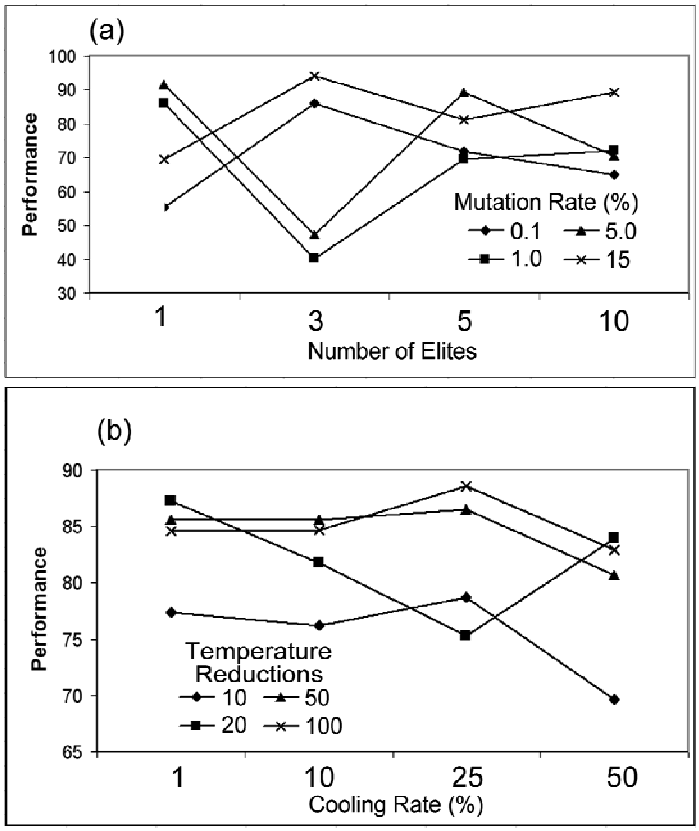

Figure 5.1: Typical interaction plots for the considered problems. Significant crisscrossing indicates the presence of an interaction. These plots suggest that (a) for the BGA, an elitism of 3 should be combined with a 15% mutation rate, and (b) for the SA, 100 temperature reductions should be coupled with a 25% cooling rate

Figure 5.2 compares interaction and main-effects confirmation runs against nominal algorithm configurations. Confirmation runs were also compared with ANOVA-generated lower confidence limits on predicted performance (ANOVA results are tabulated in Appendix C, Table C.2). For the problems investigated, the main-effects tuning procedure was found to be unreliable. Only 67% of the main-effects confirmation runs were within ANOVA-generated confidence limits, and several confirmation runs failed to improve over the nominal configuration. Conversely, interaction tuning was found to improve the nominal performance of *all* of the considered algorithms, and 92% of the interaction-tuned confirmation runs were within the confidence limits. However,

deriving effective algorithm settings from interaction plots was a manual process and the development of automation procedures requires further investigation.

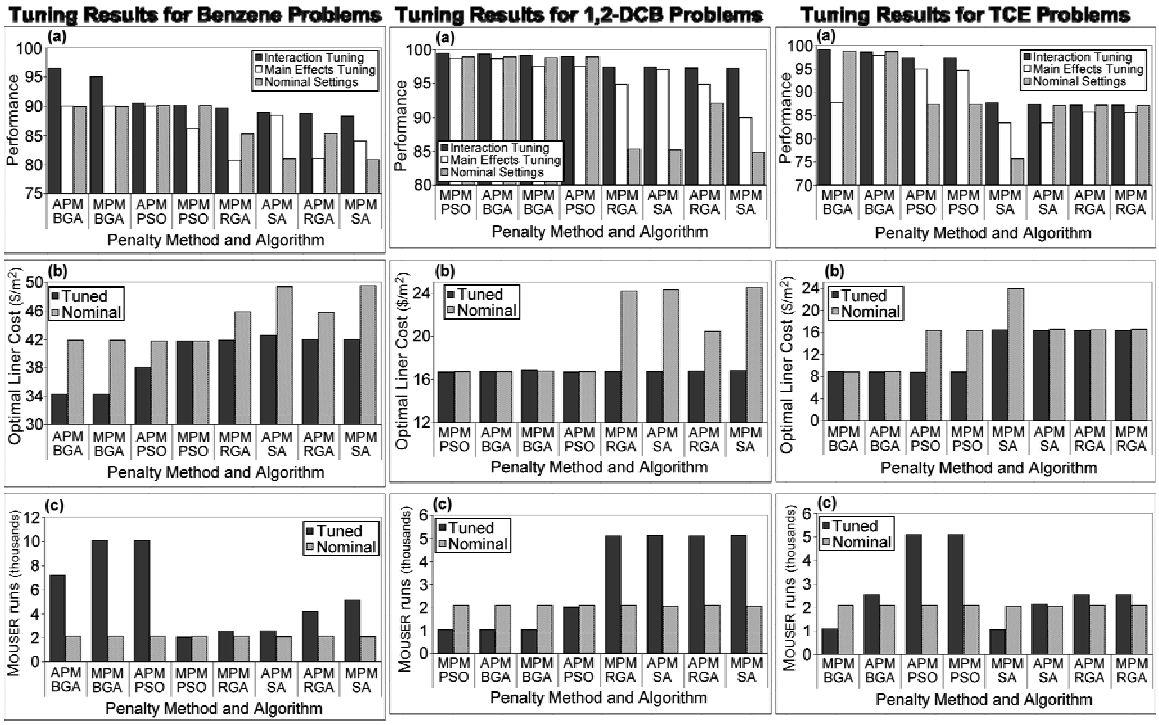

Figure 5.2: Effects of algorithm tuning vs. nominal behavior for four algorithms (BGA, RGA, PSO and SA) and using the additive (APM) and multiplicative (MPM) penalty methods. (a) Comparison of the overall performance (using a 90:10 effectiveness-efficiency weighting), of two types of tuning and the nominal algorithm settings, (b) Comparison of the effectiveness (liner cost) of interaction-tuned and nominal configurations, and (c) Comparison of the efficiency (computational cost) of the interaction-tuned and nominal configurations

5.4.2 Exhaustive searches

Optimal liner configurations discovered by the massively parallel exhaustive searches are given in Table 5.4. Liner designs with identical layer materials, but containing different layer ordering, were extracted from the exhaustive searches and compared. These comparisons revealed considerable variation in simulated exit mass and in some cases the feasibility/infeasibility of a given set of layer materials was altered when an alternative layer ordering was

considered. The observed sensitivity of sorptive liners to layer ordering is the focus of ongoing research, and may be influenced by artifacts related to the modeling of non-linear sorption at low concentrations using empirically derived isotherms.

Table 5.4: Optimal layer configurations. For each layer entry (L_1-L_6), the top value is the coded parameter value and the bottom value is the corresponding amendment percentage.

Leachate Material	Optimal Cost ($/m^2)	Optimal Layer Configuration					
		L_1	L_2	L_3	L_4	L_5	L_6
benzene	34.27	9 (9% shale)	10 (3% GAC)	10 (3% GAC)	10 (3% GAC)	14 (no layer)	
1,2-DCB	16.66	7 (3% shale)	10 (3% GAC)	13 (conv)	13 (conv)		
TCE	8.66	13 (conv)	9 (9% shale)	7 (3% shale)	9 (9% shale)		
conv : 90% sand and 10% bentonite (conventional materials with no sorbing additives)							

5.4.3 Comparison of tuned algorithms

Care should be taken in interpreting and/or extrapolating the results of any study involving algorithm comparisons. In this study, conclusions about algorithm efficacy are applicable to a specific set of problem formulations and algorithm implementations, namely variable-layered sorptive barrier problems with discrete parameter values, formulated using a penalty function approach to constraint handling, and solved using the RGA, BGA, SA, and PSO algorithms, as implemented in the OSTRICH software package. With these caveats in mind, the binary coded GA (BGA) was found to be the overall most efficient and effective algorithm. The tuned BGA was the only algorithm that correctly identified the true optimal for all three of the problem formulations. Although generally effective, the tuned PSO algorithm was less efficient than the BGA and did not identify the true solution of the benzene problem. Finally, while the performances of the SA and

RGA algorithms were significantly improved by tuning, these tuned algorithms nonetheless could not identify the true solutions of two of the three problems. A possible explanation for the superior performance of the BGA is the use of bit-wise parameter encoding, which maps favorably with the discrete-valued formulation of the layer parameters.

5.4.4 Sensitivity to penalty weight

Analysis of optimization convergence behavior suggests that the selected algorithms are sensitive to both the penalty method and the value of the penalty weight. When the lowest penalty weight ($0.10/μg) was used in combination with the additive penalty method, there was a tendency to converge on an infeasible solution. Importantly, this behavior was not observed for the multiplicative penalty method. With respect to the population-based GA and PSO algorithms, convergence on a sub-optimal design occurred when an artificially high ($100/μg) penalty weight was observed. The SA algorithm displayed an opposite trend in which a low ($1/μg) penalty weight could result in sub-optimal convergence. These differing behaviors suggest an important and complex interplay between algorithm, penalty method, and penalty weight. Application of tuning analysis to determine an appropriate penalty weight is therefore an important pre-optimization step.

5.4.5 Insight into problem formulation

The results in Figure 5.2 suggest that the design of a variable-layer sorptive liner for different organic solutes presented different levels of difficulty for the selected algorithms. The 1,2-dichlorobenzene formulation seemed to be the

most straightforward problem. All tuned algorithms, as well as the nominal PSO and BGA configurations, discovered the optimal 1,2-dichlorobenzene solution and required as few as one thousand model runs. In contrast, the true solution to the trichloroethylene problem was only discovered by the BGA (both nominal and tuned) and the tuned PSO algorithms. The most difficult problem was the benzene formulation, as the true optimal was only discovered by the tuned BGA algorithm and required more than ten thousand model executions.

The exhaustive searches of the design space provided further insight into the problem formulation. While all optimal solutions correspond to a 4-layer configuration, each algorithm was allowed to consider as many as six layers. Using data from the exhaustive searches, the number of feasible designs versus the number of active layers for each organic solute was determined. Relative to feasible four-layer designs, benzene has the fewest feasible solutions (3,159), followed by TCE (6,556) and 1,2-DCB (18,293). The number of feasible designs was found to be inversely related to the number of sorptive-amended layers required in each optimal design: 1,2-DCB required two amended layers, TCE required three, and benzene required four. Because solutes requiring more sorptive layers had fewer feasible solutions, search algorithms were discouraged from considering potential four-layer solutions. Thus, for multi-layered sorbing barrier systems, algorithm effectiveness is significantly influenced by the sorption properties of the solute and liner materials.

Since layer elimination appeared to be a major difficulty for most of the algorithms, additional numerical experiments were performed in which the

sorptive barrier problems were reformulated to require exactly four layers. Using this four-layer formulation, all algorithms were able to locate the optimal liner design, regardless of solute. The finding that some algorithms have difficulty with layer elimination is consistent with a study involving plume containment (Matott et al, 2006), which considered a variable number of pump-and-treat wells. The study found that the RGA and SA algorithms were relatively ineffective and had difficulty eliminating unnecessary wells, while the PSO algorithm was highly effective and capable of eliminating numerous wells while maintaining a feasible solution. With respect to similarly formulated variable-parameter environmental engineering problems, these findings suggest that the ability to eliminate design components is an important algorithm criterion.

5.4.6 Guidelines for algorithm tuning

This study explored the use of Taguchi DOE techniques to formally tune a variety of heuristic algorithms to a set of problems involving the design of multi-layer sorptive landfill liners. The study incurred enormous computational costs due to the large size of the experimental layout and the inclusion of computational tuning parameters (indicated with a 'C' superscript in Table 5.1). Such a layout is best suited for studies involving algorithm comparisons and/or seeking insight into a given problem. Conversely, for the optimization of a single problem using a single algorithm, the payoffs of algorithm tuning must be weighed against the computational cost. In this regard, study results have been organized into the following guidelines for algorithm selection, tuning, and analysis:

- For algorithm selection, the presence/absence of a variable number of engineered components (e.g. liner layers, wells, etc.) in the problem formulation is important, in addition to the usual considerations of whether or not the problem has local/multiple minima, is linear/non-linear and/or discrete/continuous. Depending on the selected algorithm, a variable-component formulation may impede algorithm effectiveness and lead to sub-optimal solutions.
- For single-problem/single-algorithm uses, computational considerations may limit tuned parameters to the penalty weight and algorithm parameters that do not directly alter the number of required simulations.
- Tuning using a straightforward main-effects analysis may be inadequate if parameters interact significantly. In such cases, tuning via the analysis of interaction plots may provide superior results.
- Because the use of formal algorithm tuning is relatively recent, optimal results reported for a tuned algorithm should be compared against a nominal algorithm configuration. This information can then be incorporated into future optimization projects.

5.4.7 Broader implications for sorptive barrier design

A comparison of tuned heuristic algorithms suggests the binary coded genetic algorithm (BGA) is a suitable choice for solving the multi-layer sorptive barrier design problems considered in this study, which contain discrete-valued

parameters and allow for a variable number of layers. Relative to barrier design, this study also revealed a correlation between organic solute sorption behavior and optimization performance. When many sorptive layers were required to optimally contain a given organic contaminant, the algorithms had difficulty finding feasible reduced-layer configurations and tended to converge on solutions that incorporated unnecessary additional layers. In addition to landfill problems, similar considerations apply to other multi-component systems, such as sequential permeable reactive barriers and multi-layered sediment caps.

Analysis of exhaustive searches revealed the sensitivity of barrier performance to the order in which sorptive materials are assembled, which influences the simulated mass of contaminants released from the liner. The sensitivity to layer ordering is counterintuitive and underscores the value of the simulation-optimization approach to liner design. However, differences due to layer ordering may also be influenced by the assumptions and procedures used to model nonlinear sorption at low solute concentrations; this issue is the subject of additional investigations.

5.5 Supporting Information Available

Available supporting information: (1) illustrative liner design, (2) illustrative factor interaction plots, (3) plots of the design surface, (4) descriptions of solute transport model and numerical experiments, (5) table of tuned parameter settings for each algorithm, (6) table of tuning results vs. lower confidence limits, and (7) plot of feasible solutions vs. number of active layers. This material is provided in Appendix C.

6 SELECTION AND CALIBRATION OF REACTIVE TRANSPORT MODELS USING A SURROGATE-MODEL APPROACH

6.1 Overview

While standard techniques for uncertainty analysis have been successfully applied to groundwater flow models, extension to reactive transport is frustrated by numerous difficulties, including excessive computational burden and parameter non-uniqueness. This chapter introduces a novel surrogate-based method that overcomes such difficulties by utilizing a global search technique that samples from a hierarchy of candidate reactive transport models. During calibration, the search algorithm is driven toward least-squares minimization of the most parsimonious model that best matches the available calibration data. This surrogate-model approach is demonstrated via application to several nitrate contamination problems. Results indicate that, due to the utilization of simpler models in regions of parameter insensitivity, the method is able to identify quality model fits at reduced computational expense, relative to traditional techniques. Furthermore, comparisons with a formal multi-model ranking procedure suggest the new approach is a promising tool for multi-model ranking and selection.

6.2 Introduction

The practice of subsurface reactive transport modeling has matured significantly due to increasingly powerful computer hardware and the development of new solution methods that enable integrated modeling of an array of physical, geochemical and microbiological processes controlled by kinetic and equilibrium conditions [e.g. Barry et al. (2002), Brun and Engesgaard

(2002), Fang et al. (2003), MacQuarrie and Sudicky (2001), and Parkhurst and Appelo (1999)]. For such models to be useful in a management context, model uncertainty must be rigorously assessed and, ideally, minimized via automated uncertainty analysis procedures (Environmental Protection Agency, 2002). Several aspects of subsurface reactive transport modeling make uncertainty analysis difficult, including (1) selection of an appropriate model, (2) excessive computational costs, and (3) parameter non-uniqueness.

6.2.1 Model selection

Given the variety and number of field-data typically available for calibrating subsurface reactive transport models, the appropriate level of model complexity may not be obvious. For example, Watson et al. (2003) found competitive microbiology and mineral-phase availability to be important components of a bench-scale system. However, the study also noted that a lack of supporting data often hinders detailed field-scale modeling of such processes. Keating and Bahr (1998) experienced similar problems when they studied reactive transport modeling at a Wisconsin field site. In that study, the authors acknowledged the presence of a geologically complex subsurface regime but opted to utilize simplified zero-order reaction kinetics because additional complexity would result in poorly constrained rate parameters. More recently, Haws et al. (2006) compared alternative batch-reaction models based on a series of hypothetical case studies. The results indicated that model discrimination was especially problematic when aqueous-phase concentrations were the only available evaluation criteria. This underscores the difficulty of subjectively choosing an

appropriate level of model complexity. Focusing on ground water flow modeling, Poeter and Anderson (2005) utilized Kullback-Leibler information criteria to rank and select from multiple models. While providing a structured and objective method for model selection, a drawback of the method is that accurate model rankings are contingent upon separate calibrations of all candidate models. For reactive transport modeling, this requirement may render such 'brute-force' ranking and selection techniques computationally infeasible.

6.2.2 Computational costs

Detailed reactive transport models can incur immense computational costs. For example, MacQuarrie et al. (2001) report computation times for a field scale nitrogen transport application in excess of sixty hours. These costs are further exacerbated by automated calibration, which can require thousands of model evaluations [e.g. Bell and Binning (2004)]. One technique for addressing such computational burden is the use of surrogates (Booker et al., 1999). As surrogate-based calibration proceeds, cheaper models or expressions are evaluated in lieu of the overlying model of interest. Previous environmental modeling studies have utilized *surrogate-expressions*, in which surrogates are defined as functional approximations of a more complex mechanistic model [e.g. Regis and Shoemaker (2004), and Mugunthan and Shoemaker (2005)]. Examples of commonly employed function approximations are best-fit polynomials and radial basis functions. In contrast to the surrogate-expression approach, this study considers a *surrogate-model* approach, where surrogates constitute a hierarchy of candidate reactive-transport models. Relative to

surrogate-expressions, the surrogate-model approach is attractive because it yields an automated procedure that is capable of simultaneous model ranking, selection, and calibration.

6.2.3 Parameter non-uniqueness

Available evidence suggests that complex reactive transport models suffer from parameter non-uniqueness, a characteristic that can frustrate traditional regression-based calibration algorithms. For example, Essaid et al. (2003) investigated the calibration of a hydrocarbon dissolution and degradation model and found that fitting a Monod-based kinetic formulation using traditional non-linear regression was impractical due to excessive parameter correlation and insensitivity. A number of alternative algorithms (variously classified as heuristic or global search algorithms) have been developed that are capable of overcoming parameter non-uniqueness. Classic examples of such algorithms are simulated annealing (Kirkpatrick et al., 1983) and genetic and evolutionary algorithms (Goldberg, 1989). More recent developments include particle swarm optimization (Kennedy and Eberhart, 1995), tribes (Clerc, 2003), ant colony optimization (Dorigo and Stutzle, 2004), and the big-bang big-crunch algorithm (Erol and Eksin, 2006). A major hindrance for applying such algorithms to reactive transport calibration is that they generally require a large number of model evaluations to achieve good performance. Additionally, heuristic algorithms lack the robust suite of post-regression statistical and diagnostic measures commonly produced by Jacobian-based regression methods. This particular limitation may be overcome by hybridizing a heuristic-based calibration

with a regression-based ‘polishing’ step. In such an approach, the starting point for non-linear regression is set equal to the optimal parameter set discovered by the heuristic.

6.3 Research Objectives

To address the difficulties of selecting and calibrating reactive transport models, this paper introduces a novel calibration method, referred to herein as the *surrogate-model* approach. The new method combines the robustness of a hybridized heuristic calibration search procedure with the computational advantage afforded by the use of surrogate models. The approach utilizes a run-time decision module that interfaces between a given calibration search procedure and a hierarchy of candidate models. During calibration, the decision module adapts to the calibration design space using information from previous model evaluations. When evaluating each new design point, the decision module dynamically selects the model that provides the best tradeoff between model complexity and quality of fit. The result is a powerful technique capable of simultaneous model ranking, selection, and calibration. This paper details the development of the surrogate-model approach and demonstrates it for a set of realistic batch and one-dimensional transport scenarios, based on a field site.

The test problems considered in this study are based on hypothetical scenarios involving contamination of groundwater by nitrate. Excessive nitrogen levels in ground and surface-water are associated with a number of adverse outcomes, including fish kills, algal growth, hypoxia, eutrophication, and outbreaks of toxic bacteria. Nitrate is a commonly identified pollutant (EPA,

1999) and discharge of nitrate-contaminated groundwater into surface water bodies may be a significant component of nitrogen loading. These factors have led to an increased interest in the detailed modeling of nitrogen transformation and transport in the subsurface, and the test problems are representative of such applications.

6.4 Methods

The methods section is organized as follows: section 6.4.1 contains a detailed description of the surrogate-model approach introduced in this work, section 6.4.2 contains a description of the test problems that are utilized to demonstrate and assess the new approach, and section 6.4.3 contains an overview of the numerical experiments performed for this study.

6.4.1 Development of the surrogate-based approach

In groundwater flow and transport modeling, the dominant problem formulation for automated calibration is weighted least squares minimization. As shown in Equation 6.1, the approach seeks to minimize the sum of squared errors between field-measured and model-computed observations by adjusting uncertain parameter values. For clarity, model-computed observations are sometimes referred to as *simulated equivalents*.

$$\begin{aligned} &\min \quad WSSE = (\mathbf{Y}_{\mathbf{obs}} - \mathbf{Y}_{\mathbf{sim}})^T \mathbf{Q} (\mathbf{Y}_{\mathbf{obs}} - \mathbf{Y}_{\mathbf{sim}}) \\ &\text{s.t.} \quad \mathbf{X}_{\mathbf{L}} < \mathbf{X} < \mathbf{X}_{\mathbf{U}} \\ &\text{where } \mathbf{Y}_{\mathbf{sim}} = F(\mathbf{X}) \end{aligned} \tag{6.1}$$

Where, *WSSE* is the weighted sum of squared errors objective function, $\mathbf{Y}_{\mathbf{obs}}$ is a vector of m measured observation values, $\mathbf{Q}$ is an $m \times m$ observation weight matrix that reflects uncertainties associated with the measured observations, $\mathbf{X}$ is

a vector of *p* uncertain parameter values, $\mathbf{Y_{sim}}$ is a vector of *m* simulated equivalents computed via evaluation of the model for a given set of uncertain parameter values, and the $\mathbf{X_L}$ and $\mathbf{X_U}$ vectors are the lower and upper bounds of the uncertain parameters. Note that in Equation 6.1, model evaluation is represented generically as *F()*. For reactive transport modeling, the appropriate level of model complexity (i.e. the appropriate form of *F()*) is often uncertain. This uncertainty motivates the consideration of multiple models.

Figure 6.1 compares the traditional multi-model selection and calibration approach with the new surrogate-model approach. Figure 6.1a illustrates the determination of the best-ranked model ($F^*()$) and corresponding best-fit parameter set ($\mathbf{X}^*$) using traditional uncertainty analysis methods. The approach proceeds by first calibrating each model and then performing model ranking and selection based on the results of these calibrations. In contrast, the surrogate-model approach performs simultaneous model selection and calibration via the use of a decision module. As shown in Figure 6.1b, the decision module receives model evaluation requests for various parameter configurations ($\mathbf{X_{S0}}$) of the most complex model (*S0*). For each of these requests, the decision module computes a corresponding WSSE value that is possibly evaluated via one of the *n* surrogate models. As illustrated in Figure 6.2 and described below, an adaptive model-selection algorithm makes the determination of which model to evaluate.

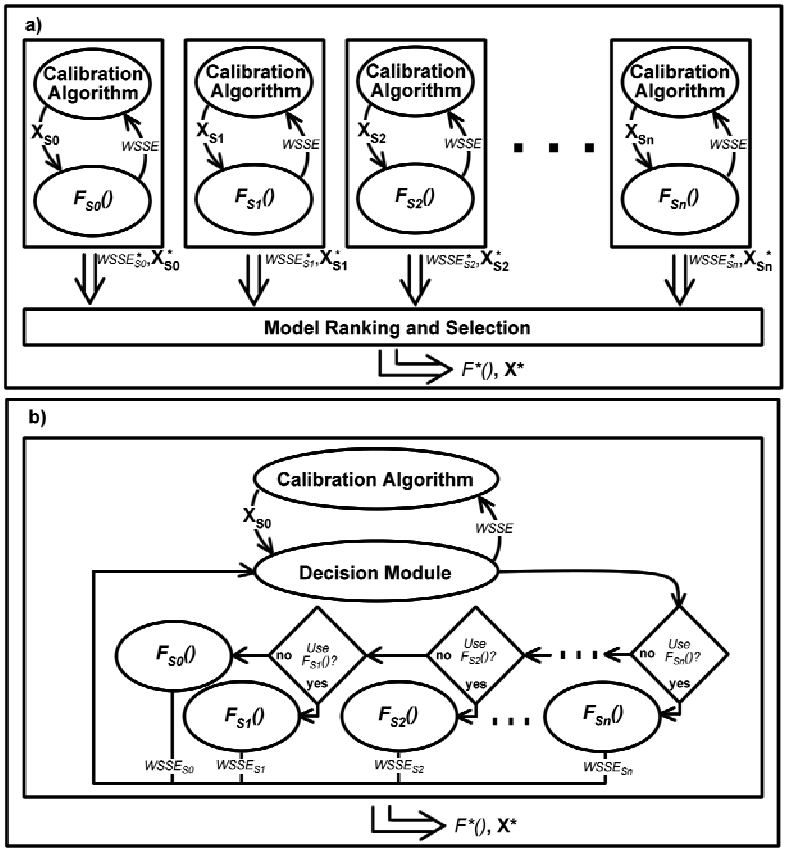

Figure 6.1: Comparison of (a) traditional and (b) surrogate-model approaches to calibration and model selection. $F_{S0}()$ is the most complex model with uncertain parameter vector X_{S0}, calibrated parameter vector X_{S0}^*, and calibrated WSSE value of $WSSE_{S0}^*$, $F_{S1}()$, $F_{S2}()$, … $F_{Sn}()$ are *n* simplified alternative models, with uncertain parameter vectors X_{S1}, X_{S2}…X_{Sn}, best-fit parameter vectors X_{S1}^*, X_{S2}^*…X_{Sn}^*, and best-fit WSSE values of $WSSE_{S1}^*$, $WSSE_{S2}^*$, …, $WSSE_{Sn}^*$, and $F^*()$ is the best-ranked model (one of $F_{S0}()$, $F_{S1}()$, $F_{S2}()$, …, $F_{Sn}()$), with corresponding best-fit parameters X^*.

Figure 6.2 illustrates the model selection procedure that is followed by the decision module. In Step #1, a problem-specific set of mapping functions ($f_1()$, $f_2()$ … $f_n()$) converts complex model parameter values into corresponding surrogate model parameter values. These mapping functions serve as a coupling mechanism for the various models, allowing the adaptive model selection strategy to operate independently of the calibration algorithm. As a result, the calibration algorithm operates solely in the parameter space of the complex model and proceeds as if performing a single-model calibration.

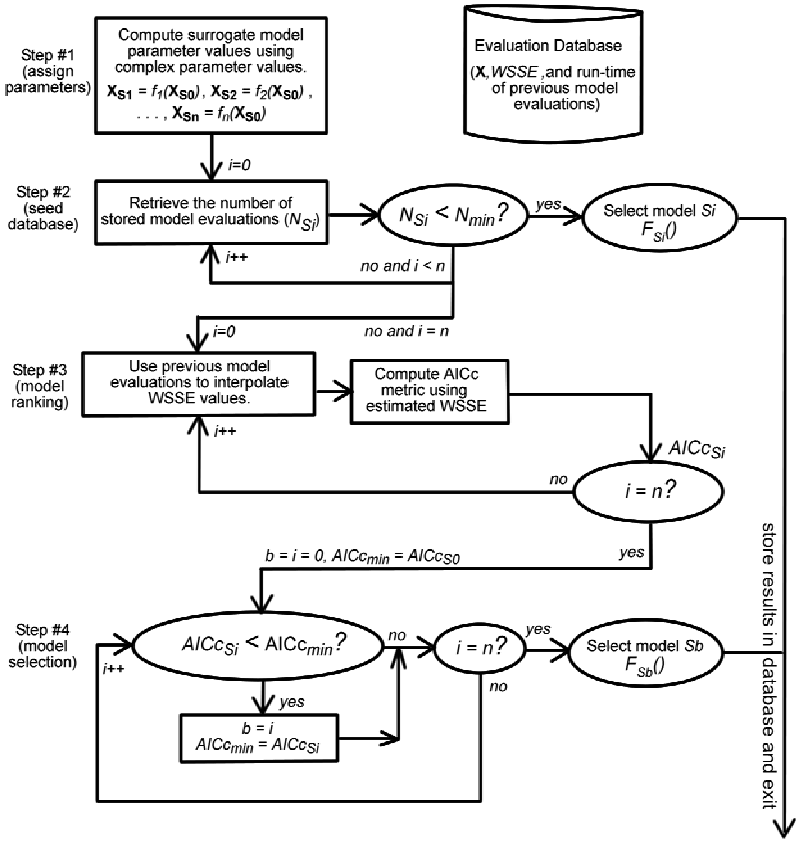

Figure 6.2: Decision module for calibration using surrogate-models. Subscript $_{Si}$ *(i = 0 to n)* **identifies a candidate model, which are (loosely) ordered from most complex (*S0*) to most simplified (*Sn*),** X_{Si} **is an uncertain parameter vector,** $F_{Si}()$ **specifies model evaluation at** X_{Si}**,** $f_1(), f_2(), \ldots, f_n()$ **are mapping functions relating complex and surrogate model parameters,** N_{min} **is the minimum number of model evaluations required for interpolation,** $AICc_{Si}$ **is the model ranking (lower is better), based on an AICc quality-of-fit and adjusted for computational expense, and *b* identifies the model with the lowest ranking (**$AICc_{min}$**).**

While mapping functions are necessarily problem specific, a few examples involving sorption and biokinetics are presented to illustrate the concept.

6.4.1.1 Mapping example 1: sorption modeling

The sorption of aqueous phase contaminants to aquifer solids is an important process in subsurface contaminant transport, and a variety of models are used in practice. In this example, consider a hierarchy of equilibrium sorption models in which the most complex model (*S0*) presumes Langmuir sorption, an

intermediate model (*S1*) assumes linear sorption, and the simplest model (*S2*) assumes zero-order sorption (i.e. a constant sorbed concentration). General expressions for each of these models are given in Equations 6.2 - 6.4.

$$q_{S0} = \frac{Q_{\max} bC}{1 + bC} \tag{6.2}$$

$$q_{S1} = K_d C \tag{6.3}$$

$$q_{S2} = Q_0 \tag{6.4}$$

Where, C is the aqueous concentration, q_{S0} is the sorbed concentration computed using the Langmuir isotherm, Q_{max} [M/M] is the maximum sorption density, b [L^3/M] is the affinity of adsorbent to the adsorbate, q_{S1} is the sorbed concentration computed using the linear isotherm, K_d [L^3/M] is the linear sorption distribution coefficient, q_{S2} [M/M] is the sorbed concentration computed using the zero-order expression, and Q_0 is the constant sorbed concentration.

Given these models, the uncertain parameters are $\mathbf{X_{S0}} = [Q_{max}, b]^T$, $\mathbf{X_{S1}} = K_d$, and $\mathbf{X_{S2}} = Q_0$. For $bC << 1$, the complex model reduces to $q_{S0} = (Q_{max}\, b)\, C$, yielding the following relationship between the parameters of model *S0* and *S1*:

$$f_1(\mathbf{X_{S0}}) \rightarrow K_d = Q_{\max} b \tag{6.5}$$

Where, $f_1()$ is the mapping function for model *S1* which specifies, in this case, that the K_d parameter is the product of the two parameters of the Langmuir model. For the simplest model, if one assumes $bC >> 1$, the complex model reduces to $q_{S0} = Q_{max}$, yielding:

$$f_2(\mathbf{X_{S0}}) \rightarrow Q_0 = Q_{\max} \tag{6.6}$$

Where, $f_2()$ is the mapping function for model *S2* and indicates that the constant sorbed concentration (Q_0) in model *S2* is equal to the maximum sorption density (Q_{max}) of model *S0*.

6.4.1.2 Mapping example 2: biokinetics modeling

In this example, a complex dual-Monod model (*S0*) of biodegradation kinetics is paired with five simpler surrogate models. The surrogate models reflect parallel simplification pathways and are determined by whether the system is assumed to be substrate-limited or electron-acceptor (e-a) limited. Surrogates *S1* and *S3* assume that biokinetics are e-a limited, surrogates *S2* and *S4* assume substrate-limited biokinetics, and surrogate *S5* assumes that biokinetics are neither substrate nor e-a limited. With these assumptions in mind, surrogates *S1* and *S2* are single-Monod models, surrogates *S3* and *S4* are 1st order biokinetics models, and surrogate *S5* expresses biokinetics as a zero-order expression.

$$R_{S0} = k_{S0,\max}\left(\frac{E}{k_{S0,E}+E}\right)\left(\frac{S}{k_{S0,S}+S}\right) \tag{6.7}$$

$$R_{S1} = k_{S1,\max}\left(\frac{E}{k_{S1,E}+E}\right) \tag{6.8a}$$

$$R_{S2} = k_{S2,\max}\left(\frac{S}{k_{S2,S}+S}\right) \tag{6.8b}$$

$$R_{S3} = k_{S3}E \tag{6.9a}$$

$$R_{S4} = k_{S4}S \tag{6.9b}$$

$$R_{S5} = k_{S5} \tag{6.10}$$

where, R_{S0}-R_{S5} are the degradation rates [M/L^3-T] for each of the candidate models, E is the terminal electron-acceptor concentration [M/L^3], S is the substrate concentration [M/L^3], $k_{S0,max}$ is the dual-Monod maximum degradation rate [M/L^3-T], $k_{S0,E}$ is the dual-Monod half-saturation constant for the terminal electron-acceptor [M/L^3], $k_{S0,S}$ is the dual-Monod half-saturation constant for the substrate [M/L^3], $k_{S1,max}$ is the single-Monod maximum degradation rate, assuming e-a limited biokinetics [M/L^3-T], $k_{S1,E}$ is the single-Monod half-saturation constant for the terminal electron acceptor [M/L^3], $k_{S2,max}$ is the single-Monod maximum degradation rate, assuming substrate-limited biokinetics [M/L^3-T], $k_{S2,S}$ is the corresponding single-Monod half-saturation constant for the substrate [M/L^3], k_{S3} is the first-order degradation rate for the e-a limited pathway [1/T], k_{S4} is the first-order degradation rate for the substrate-limited pathway [1/T], k_{S5} is the zero-order degradation rate [M/L^3-T], and k_{S6} is the zero-order degradation rate [M/L^3-T].

The complex model may be reduced into the forms of the various surrogate models in a number of ways, and here we make the following assumptions: For surrogate *S1*, assume S >> $k_{S0,S}$. For surrogate *S3*, additionally assume that E << k_E. For surrogate *S2*, assume E >> $k_{S0,E}$. For surrogate *S4*, additionally assume that S << k_S. For surrogate *S5*, assume E >> $k_{S0,E}$ and S >> $k_{S0,S}$. These assumptions yield the following mapping functions:

$$f_1(\mathbf{X_{S0}}) \rightarrow \begin{cases} k_{S1,\max} = k_{S0,\max} \\ k_{S1,E} = k_{S0,E} \end{cases} \tag{6.11a}$$

$$f_2(\mathbf{X_{S0}}) \rightarrow \begin{cases} k_{S2,\max} = k_{S0,\max} \\ k_{S2,S} = k_{S0,S} \end{cases} \tag{6.11b}$$

$$f_3(\mathbf{X_{S0}}) \rightarrow k_{S3} = \frac{k_{S0,\max}}{k_{S0,E}} \tag{6.12a}$$

$$f_4(\mathbf{X_{S0}}) \rightarrow k_{S4} = \frac{k_{S0,\max}}{k_{S0,S}} \tag{6.12b}$$

$$f_5(\mathbf{X_{S0}}) \rightarrow k_{S5} = k_{S0,\max} \tag{6.13}$$

6.4.1.3 Model ranking and selection

After mapping surrogate model parameter values, the decision module determines how many previous evaluations of each candidate model have been stored in an evaluation database. If too few model evaluations are stored, subsequent WSSE interpolation will not be sufficiently accurate. Therefore, the decision module will automatically select a given model if it is found to have fewer than N_{min} stored evaluations. At the start of calibration, this procedure results in the initialization of the decision module and its evaluation database.

Once the model evaluation database has been properly seeded, subsequent calls to the decision module result in the dynamic ranking of each model. The first step in ranking each model is the calculation of an estimated WSSE value. These WSSE estimates are interpolated from the evaluation database, which will, in general, contain a collection of scattered data points. Based on this characterization, the selected interpolation scheme is a multi-quadric radial basis function (Kansa, 1990), which is capable of robust interpolation using an irregularly spaced network of data points.

After a WSSE estimate is generated for a given model, model quality is computed using an appropriate measure. This study utilizes the bias-corrected Akaike Information Criteria measure (AICc) (Hurvich and Tsai, 1994):

$$AICc_i = n\log_e\left(\frac{WSSE_i}{n}\right) + 2p_i + \left(\frac{2p_i(p_i+1)}{n-p_i-1}\right) \quad (6.14)$$

where $AICc_i$ is the AICc value of the i-th model, n is the number of observations, p_i is the number of uncertain model parameters for the i-th model, and $WSSE_i$ is the estimated WSSE value of the i-th model. As shown in Step #4 of Figure 6.2, the decision module completes a given iteration of the model ranking and selection process by choosing and evaluating the model with the lowest estimated AICc value. The true WSSE value corresponding to this model evaluation is then stored in the model evaluation database and returned to the calibration algorithm.

6.4.2 Description of the test problems

The performance of the new surrogate-model approach was explored using carefully formulated reactive transport scenarios based on a highly detailed configuration of biokinetic and geochemical reactions. The selected test problems for the surrogate-model approach focus on nitrate contamination in hypothetical (but realistic) batch and one-dimensional transport scenarios. To develop the surrogate-model calibration exercises, a “true” model was established for each hypothetical scenario. The “true” batch model contained an extensive set of biogeochemical reaction processes including multiple-Monod biokinetics, secondary inorganic redox kinetics, and numerous geochemical equilibrium processes. The “true” transport model problem also considered biokinetics, but neglected secondary reactions and considered a reduced number of equilibrium processes.

In developing the “true” models, uncertain kinetic parameters were assigned realistic literature-derived values, as tabulated in Appendix D, Table D.2. Forward runs of these truth models were used to generate a set of synthetic observation values, to be used in subsequent calibration experiments. To develop appropriate observation weights for use in the calibration experiments, each synthetic observation was treated as if it contained a certain amount of measurement error. These errors were assigned following Hem (1985), and are as follows:

(1) measurements greater than 1 mg/L have an error of +/- 5%,

(2) measurements less than 1 mg/L incur an error of +/- 10%,

(3) measurements less than 0.1 microgram per liter are below typical detection limits and are assumed to be in the range of 0-0.1 micrograms per liter, and

(4) pH measurements are assumed to be accurate within +/- 0.02 pH units.

Estimates of measurement error were converted to appropriate relative observation weights following the guidelines of Hill (1998).

Conceptually, the batch-reaction test model may be considered an approximation of the effects of natural degradation, with transport within the system domain neglected. In this scenario, a spike of contaminated groundwater is presumed to have infiltrated from the unsaturated zone and the batch model is used to estimate the biodegradation timeframe of various contaminants, most notably nitrate. Synthetic observations sampled from the ‘true’ batch model

consisted of fifteen commonly collected aqueous-phase constituents (pH and total Na, K, Ca, Mg, Cl, HCO_3, SO_4, Fe, Mn, HS, NH_4, O_2, NO_3, and DOC). These constituents were sampled twice-per-year over a 20-year simulation period. To capture fast non-equilibrium kinetics, early-time samples of 1 hour, 1 day, 1 week and 1 month were also collected. The overall sampling regime resulted in a total of 660 observation measurements available for a given calibration exercise.

The transport problem extended the batch reaction scenario to include the vertical transport of a continuous contaminant source through a hypothetical aquifer column. For the transport model, eight aqueous-phase constituents were sampled (pH, HCO_3, DOC, O_2, NO_3, Mg, Ca and Cl) at column depths of 0.5, 2.5 and 4.7 meters. These locations were sampled after one day of transport simulation and then every four days for 52 days of simulation. This sampling scheme resulted in a total of 336 observations for use in the transport model calibration experiments. The sampling schedule for the transport test problem was designed to emulate realistic site-characterization activities, in which a short period of intense sampling is typical.

Initial and boundary conditions for the test problems were motivated by data collection activities at the Lizzie Research Station, in Greene County, North Carolina. The research site is located on an actively operated hog farm in which liquid hog waste is applied to cropland as a fertilizer, resulting in high concentrations of nitrate in the groundwater. From 1999 to 2002, the U.S. EPA studied the site extensively, collecting groundwater samples from a number of

monitoring wells installed on the site and analyzing these samples for the aqueous-phase concentrations of nearly 20 chemical constituents (Spruill et al., 2005). These aqueous-phase concentrations, along with hydrologic data gathered at the site and solid-phase and kinetic data taken from the literature, were utilized to develop a realistic set of biodegradation models.

The remainder of this section is organized as follows: sections 6.4.2.1 and 6.4.2.2 provide an overview of the subsurface reactive transport processes and related solution methods considered in this work, and sections 6.4.2.3 and 6.4.2.4 describe the setup of the batch and one-dimensional transport test problems, respectively.

6.4.2.1 Subsurface reactive transport model

Barry et al. (2002) provided a thorough review of the various processes that influence subsurface reactive transport, which may include sorption/desorption (e.g. hydrophobic partitioning, cation exchange and/or surface complexation), mineral precipitation and dissolution, microbial activity, and equilibrium and kinetic geochemistry. Apart from neglecting a given process, the simplest modeling approach is to assume local equilibrium for all reactions [e.g. Engesgaard and Kipp (1992), and Postma et al. (1991)]. Intermediate methods (in terms of complexity) consider kinetic processes using zero- or first-order rate expressions [e.g. McNab and Narasimhan (1994), van Breukelen et al. (1998), Hunter et al. (1998), and Keating and Bahr (1998)].

With regard to biotransformation in the subsurface, the most complex modeling approaches use multiple-Monod biokinetics in which growth inhibition

due to substrate, nutrient and/or electron acceptor availability is enforced via one or more empirically defined inhibition terms [e.g. MacQuarrie et al. (2001), and Killingstad et al. (2002)]. A further complexity is that microbial growth is often treated as a diffusion-limited process. Here, nutrients, substrate, and/or electron acceptors must diffuse from aqueous solution into an immobile bio-phase [eg. Kinzelbach and Schafer (1991), Baveye and Valocchi (1989), Doussan et al. (1997), Lensing et al. (1994), Schafer et al. (1998), Schafer and Therrien (1995), Prommer et al. (1999), and Widdowson et al. (1988)].

The reactive transport application considered in this study focused on the natural degradation and transport of groundwater contaminated by agricultural practices. As such, the primary contaminant of concern was nitrate (NO_3^-), with a secondary emphasis on sulfur compounds, including sulfate (SO_4^{2-}). A commonly applied transformation pathway for both nitrate and sulfate is degradation via microbially mediated redox processes. In oxygen-depleted environments, specialized microorganisms will preferentially utilize nitrate, manganese, iron and sulfate as terminal electron acceptors. Substrate for these microorganisms is commonly assumed to be an organic carbon source, often generically referred to as CH_2O. A number of inorganic geochemical reactions influence microbial degradation, and for the hypothetical test problems, the considered biogeochemical processes included:

(1) Microbially-mediated kinetic reactions including aerobic degradation, denitrification, and manganese, iron and sulfate reduction. Diffusion into the bio-phase was assumed to occur rapidly and was ignored.

(2) Kinetically controlled inorganic secondary redox reactions involving manganese, iron, and sulfur.

(3) Aqueous equilibrium chemistry involving the carbonate, sulfate, and sulfide systems.

(4) Equilibrium speciation of calcium, magnesium, sodium, potassium, iron, manganese, and ammonium.

(5) Equilibrium precipitation and dissolution of calcite, siderite, rhodochrosite, gypsum, and iron sulfide.

(6) Linear partitioning of sorbed and aqueous phase organic carbon. For this work, the partition coefficient was assigned so that the initial aqueous phase DOC concentration was 2.0 mg/L.

(7) Competitive cation exchange involving sodium, calcium, magnesium and potassium. This process was modeled using the Gaines-Thomas convention, where equivalent fractions are used for the activity of exchangeable cations.

(8) Surface complexation of iron, manganese, and hydrogen onto hydrous ferric oxide. This was modeled using the approach of Dzombek and Morel (1990), in which sorbing ions must overcome electrostatic effects before reacting with high (strong) and low (weak) affinity surface sites.

The chemical reactions and modeling technique(s) associated with each of these processes are summarized in Table 6.1.

Table 6.1: Reaction Network for the Hypothetical Modeling Scenarios

Microbial-mediated reactions (modeled using multiple-Monod, single-Monod, 1st order, or zero order kinetics)	
Aerobic degradation*	R_1: $CH_2O + O_2 \rightarrow CO_2 + H_2O$
Denitrification*	R_2: $\frac{5}{2}CH_2O + 2NO_3^- + 2H^+ \rightarrow N_2 + \frac{5}{2}CO_2 + \frac{7}{2}H_2O$
Mn(IV)-reducers	R_3: $MnO_2(s) + \frac{1}{2}CH_2O + 2H^+ \rightarrow Mn^{2+} + \frac{1}{2}CO_2 + \frac{3}{2}H_2O$
Fe(III)-reducers	R_4: $Fe(OH)_3(s) + \frac{1}{4}CH_2O + 2H^+ \rightarrow Fe^{2+} + \frac{1}{4}CO_2 + \frac{11}{4}H_2O$
Sulfate reducers	R_5: $SO_4^{2-} + 2CH_2O + H^+ \rightarrow 2CO_2 + HS^- + 2H_2O$
Secondary Redox Reactions (modeled using 1st order kinetics or zero order kinetics)	
Manganese redox	R_6: $Mn^{2+} + \frac{1}{2}O_2 + H_2O \rightarrow MnO_2(s) + 2H^+$
Iron redox	R_7: $Fe^{2+} + \frac{1}{4}O_2 + \frac{5}{2}H_2O \rightarrow Fe(OH)_3(s) + 2H^+$
Iron-Manganese redox	R_8: $2Fe^{2+} + MnO_2(s) + 4H_2O \rightarrow 2Fe(OH)_3(s) + Mn^{2+} + 2H^+$
Sulfide redox	R_9: $H_2S + 2O_2 \rightarrow SO_4^{2-} + 2H^+$
Iron sulfide redox	R_{10}: $FeS(s) + 2O_2 \rightarrow Fe^{2+} + SO_4^{2-}$
Sulfide-Manganese redox	R_{11}: $H_2S + MnO_2(s) + 2H^+ \rightarrow Mn^{2+} + S^0 + 2H_2O$
Sulfide-Iron redox	R_{12}: $H_2S + 2Fe(OH)_3(s) + 4H^+ \rightarrow 2Fe^{2+} + S^0 + 6H_2O$
Aqueous Equilibrium Chemistry (modeled as equilibrium reactions)	
Carbonate system*	R_{13}: $H_2O \leftrightarrow H^+ + OH^-$ R_{14}: $CO_3^{2-} + H^+ \leftrightarrow HCO_3^-$ R_{15}: $HCO_3^- + H^+ \leftrightarrow CO_2 + H_2O$
Sulfide System	R_{16}: $H_2S \leftrightarrow H^+ + HS^-$ R_{17}: $HS^- \leftrightarrow H^+ + S^{2-}$
Sulfate System	R_{18}: $H^+ + SO_4^{2-} \leftrightarrow HSO_4^-$ R_{19}: $Ca^{2+} + SO_4^{2-} \leftrightarrow CaSO_4$ R_{20}: $Mg^{2+} + SO_4^{2-} \leftrightarrow MgSO_4$ R_{21}: $Na^+ + SO_4^{2-} \leftrightarrow NaSO_4^-$ R_{22}: $K^+ + SO_4^{2-} \leftrightarrow KSO_4^-$ R_{23}: $Fe^{2+} + SO_4^{2-} \leftrightarrow FeSO_4$ R_{24}: $Mn^{2+} + SO_4^{2-} \leftrightarrow MnSO_4$
Calcium Speciation	R_{25}: $Ca^{2+} + CO_3^{2-} \leftrightarrow CaCO_3$ R_{26}: $Ca^{2+} + CO_3^{2-} + H^+ \leftrightarrow CaHCO_3^+$

Magnesium Speciation	R_{27}: $Mg^{2+} + CO_3^{2-} \leftrightarrow MgCO_3$ R_{28}: $Mg^{2+} + CO_3^{2-} + H^+ \leftrightarrow MgHCO_3^+$
Sodium Speciation	R_{29}: $Na^+ + CO_3^{2-} \leftrightarrow NaCO_3^-$ R_{30}: $Na^+ + HCO_3^- \leftrightarrow NaHCO_3$
Iron Speciation	R_{31}: $Fe^{2+} + H_2O \leftrightarrow FeOH^+ + H^+$ R_{32}: $Fe^{2+} + CO_3^{2-} \leftrightarrow FeCO_3$ R_{33}: $Fe^{2+} + HCO_3^- \leftrightarrow FeHCO_3^+$
Manganese Speciation	R_{34}: $Mn^{2+} + Cl^- \leftrightarrow MnCl^+$ R_{35}: $Mn^{2+} + CO_3^{2-} \leftrightarrow MnCO_3$ R_{36}: $Mn^{2+} + HCO_3^- \leftrightarrow MnHCO_3^+$
Ammonium Speciation	R_{37}: $NH_3 + H^+ \leftrightarrow NH_4^+$
Mineral Precipitation/Dissolution (modeled as equilibrium reactions)	
Calcite*	R_{38}: $CaCO_3(s) \leftrightarrow CO_3^{2-} + Ca^{2+}$
Rhodochrosite	R_{39}: $MnCO_3(s) \leftrightarrow Mn^{2+} + CO_3^{2-}$
Siderite	R_{40}: $FeCO_3(s) \leftrightarrow Fe^{2+} + CO_3^{2-}$
Iron Sulfide	R_{41}: $FeS_{(s)} \leftrightarrow Fe^{2+} + S^{2-}$
Gypsum	R_{42}: $CaSO_4(H_2O)_2(s) \leftrightarrow Ca^{2+} + SO_4^{2-} + 2H_2O$
Additional Solid-Aqueous Phase Reaction Processes (modeled as equilibrium reactions)	
Carbon Partitioning	R_{43}: $CH_2O(ads) \leftrightarrow CH_2O$
Surface Complexation ($\equiv HFO^w$: weak sites, $\equiv HFO^s$: strong sites)	R_{44}: $\equiv HFO^wOH + H^+ \leftrightarrow \equiv HFO^wOH_2^+$ R_{45}: $\equiv HFO^wOH + Fe^{2+} \leftrightarrow \equiv HFO^wOFe^+ + H^+$ R_{46}: $\equiv HFO^wOH \leftrightarrow \equiv HFO^wO^- + H^+$ R_{47}: $\equiv HFO^wOFe^+ + H_2O \leftrightarrow \equiv HFO^wOFeOH + H^+$ R_{48}: $\equiv HFO^wOH + Mn^{2+} \leftrightarrow \equiv HFO^wOMn^+ + H^+$ R_{49}: $\equiv HFO^sOH + H^+ \leftrightarrow \equiv HFO^sOH_2^+$ R_{50}: $\equiv HFO^sOH \leftrightarrow \equiv HFO^sO^- + H^+$ R_{51}: $\equiv HFO^sOH + Fe^{2+} \leftrightarrow \equiv HFO^sOFe^+ + H^+$ R_{52}: $\equiv HFO^sOH + Mn^{2+} \leftrightarrow \equiv HFO^sOMn^+ + H^+$
Ion Exchange (X: solid exchanger)	R_{53}: $NaX + K^+ \leftrightarrow Na^+ + KX$ R_{54}: $2NaX + Ca^{2+} \leftrightarrow 2Na^+ + CaX_2$ R_{55}: $2NaX + Mg^{2+} \leftrightarrow 2Na^+ + MgX_2$ R_{56}: $CaX_2 + 2K^+ \leftrightarrow Ca^{2+} + 2KX$ R_{57}: $MgX_2 + 2K^+ \leftrightarrow Mg^{2+} + 2KX$ R_{58}: $MgX_2 + Ca^{2+} \leftrightarrow Mg^{2+} + CaX_2$
Summary: 65 species, 46 equilibrium reactions, 12 kinetic reactions All reactions listed were utilized in the 'true' batch reaction model. Only the reactions indicated with an asterisk (*) were considered for the 'true' transport model.	

6.4.2.2 Numerical methods

In this study, equilibrium reactions (R_{13} through R_{58} in Table 6.1) were modeled using 'fast' kinetics. Using this approach, all reversible equilibrium reactions are re-written as complementary pairs of high-rate forward and backward reactions. For example, the reaction $A^- + B^+ \leftrightarrow AB$ with equilibrium constant $K_{eq}=[AB]/([A][B])$, would be re-written as $A^- + B^+ \rightarrow AB$, with forward rate K_f, and $AB \rightarrow A^- + B^+$, with backward rate K_b. To maintain equivalency with the equilibrium expression, the ratio of reaction rates was selected to be consistent with the equilibrium constant (i.e. $(K_f/K_b) = K_{eq}$). Furthermore, both rates were made sufficiently large so that equilibrium amongst the reacting species is achieved rapidly relative to the time step of interest. Following MacQuarrie and Sudicky (2001), these complementary reaction pairs combined with irreversible kinetic reactions (R_1 through R_{12} in Table 6.1) to form a stiff set of coupled ordinary differential equations. These equations are summarized in Appendix D and their solution requires a robust numerical solver. For this work, a number of solvers were investigated before selecting the CVODE solver (Hindmarsh and Serban, 2006), which is part of the SUNDIALS package (Hindmarsh et. al, 2005). Attempts at solving the entire reaction network in Table 6.1 using PHREEQC (Parkhurst and Appelo, 1999) (which utilizes a differential/algebraic equation solver) were unsuccessful. This difficulty motivated the consideration and subsequent adoption of the aforementioned fully kinetic approach. The correctness of the fully kinetic implementation was established by solving

subsets of the overall reaction network and comparing the results with those obtained using PHREEQC.

Zheng and Bennett (2002) and Steefel and Maquarrie (1996) provide excellent reviews of the various approaches to reactive transport modeling. The experiments in this study utilized the sequential non-iterative approach (SNIA). This operator splitting technique separates reactive transport into an advective-dispersive time-step followed by a reaction time-step. The governing equation for the advective-dispersive transport of each solute through a one-dimensional unidirectional flow field is given in Equation 6.15:

$$\frac{\partial C_i}{\partial t} = D\frac{\partial^2 C_i}{\partial x^2} - v\frac{\partial C_i}{\partial x} \tag{6.15}$$

where C_i is the concentration of the *i*-th species, v is the seepage velocity, and D is the dispersion coefficient such that $D=\alpha v$, where α is the longitudinal dispersivity. In this study, equation 6.15 was discretized using finite-differences (as in Zheng and Bennett (2002), pg. 180, eqn. 7.20) and solved using a fully implicit temporal weighting scheme and an upstream spatial weighting scheme. For each time step, all reactive species were first advected and dispersed. Next, each finite-difference cell was batch-reacted for one time step using the previously described fully kinetic reaction solver.

6.4.2.3 Batch-reaction test problem

The batch-reaction model configuration was developed using well data collected at the Lizzie Research Station (Spruill et al., 2005). The well of interest is located within the central spray field area and contains the highest levels of nitrate contamination. The well was screened at three depth levels (shallow,

medium and deep) and the shallow well measurements provided the aqueous-phase initial conditions for the batch reaction model. The Lizzie data did not include the initial conditions of the solid-phase components of the model (i.e. mineral content, surface complexes, organic carbon partitioning, or ion exchange capacity) and these initial conditions were assigned based on literature-derived values. Solid phase concentrations were normalized to pore-volume concentrations by using typical porosity (0.3), soil density (2.65 kg/L), and bulk density (1.86 kg/L) values, as reported in Charbeneau (2000). Initial conditions for the batch-reaction test problem are given in Table 6.2.

Table 6.2: Initial Conditions for Batch-Reaction Scenario.
(CEC is the cation exchange capacity, SA_{HFO} is the surface area of hydrous ferric oxide, HFO^s and HFO^w denote the strong and weak surface complexation sites, respectively.)

Aqueous-phase Constituent	Concentration (mol/L)	Solid-phase Constituent	Concentration (mol/L)
H+	2.51E-05	CEC (meq/L)	203.43 [a]
TOT Na	1.31E-03	SA_{HFO} (m^2)	180.68 [b]
TOT K	3.33E-04	TOT HFO^w	6.77E-04 [b]
TOT Ca	1.06E-03	TOT HFO^s	1.69E-05 [b]
TOT Mg	6.02E-04	MnO_2(s)	8.87E-03 [c]
TOT Cl	2.14E-03	$Fe(OH)_3$(s)	3.41E-03 [c]
TOT HCO_3	1.17E-04	CH_2O(ads)	4.34E-02 [c]
TOT SO_4	2.53E-04	FeS(s)	0.00
TOT Fe	4.73E-06	$CaSO_4(H_2O)_2$ (s)	0.00
TOT Mn	4.02E-06	$FeCO_3$(s)	0.00
TOT HS	3.10E-06	$CaCO_3$(s)	0.00
TOT NH_4	5.56E-06	Data Sources a – Tucker (1999) b – Dzombak and Morel (1990), Knapp et al. (1998) c – Barcelona and Holm (1991)	
TOT O_2	1.56E-04		
TOT NO_3	2.50E-03		
TOT CH_2O (as C)	4.16E-04		

6.4.2.3.1 Candidate reaction models

To demonstrate the surrogate-model calibration approach, a number of plausible candidate reaction models were developed. For the most complex candidate model, a 'kitchen-sink' approach was taken, such that the 58 reactions in Table 6.1 were included in the model. Additionally, the complex model utilized

dual-Monod kinetic expressions (as in Equation 6.7) for the sequence of five microbially mediated reactions. To develop the surrogate candidate reaction models, graphical analysis of the sampled synthetic observation data motivated the selection and exclusion of various reactive processes. Figure 6.3 contains representative plots of the synthetic observations that were investigated as part of this process. Analysis of the concentration data provided the following evidence for subsequent model development:

(1) DOC concentrations are well buffered and remained nearly constant for the sampled timeframe. Therefore, any active biokinetics processes will not be substrate limited and the dual-Monod formulation of Equation 6.7 is unnecessary.

(2) Major cations and anions also remained nearly constant for the sampled time frame. This suggested that cation exchange processes could be neglected.

(3) Concentrations of dissolved-oxygen, nitrate and sulfate reduced in sequence over time, suggesting the influence of aerobic, denitrifying and sulfate-reducing biokinetics processes.

(4) Early in the simulation, pH was buffered via the removal of Fe and Mn from solution. Such buffering indicated the presence of surface complexation.

(5) The early-time samples indicated an increase in Fe, Mn and sulfate with a corresponding decrease in HS. This was taken as evidence of secondary redox reactions, namely R_8, R_9, R_{11} and R_{12} in Table 6.1.

(6) During years 2 through 13, Mn, Fe and carbonate concentrations were significantly reduced. This was interpreted as evidence of biokinetics processes that *produce* Fe, Mn and CO_2 and *consume* H^+. Buffering of pH via surface complexation and precipitation of Fe-/Mn-carbonate minerals explains how the biokinetic production of Fe and Mn can actually drive these species from solution.

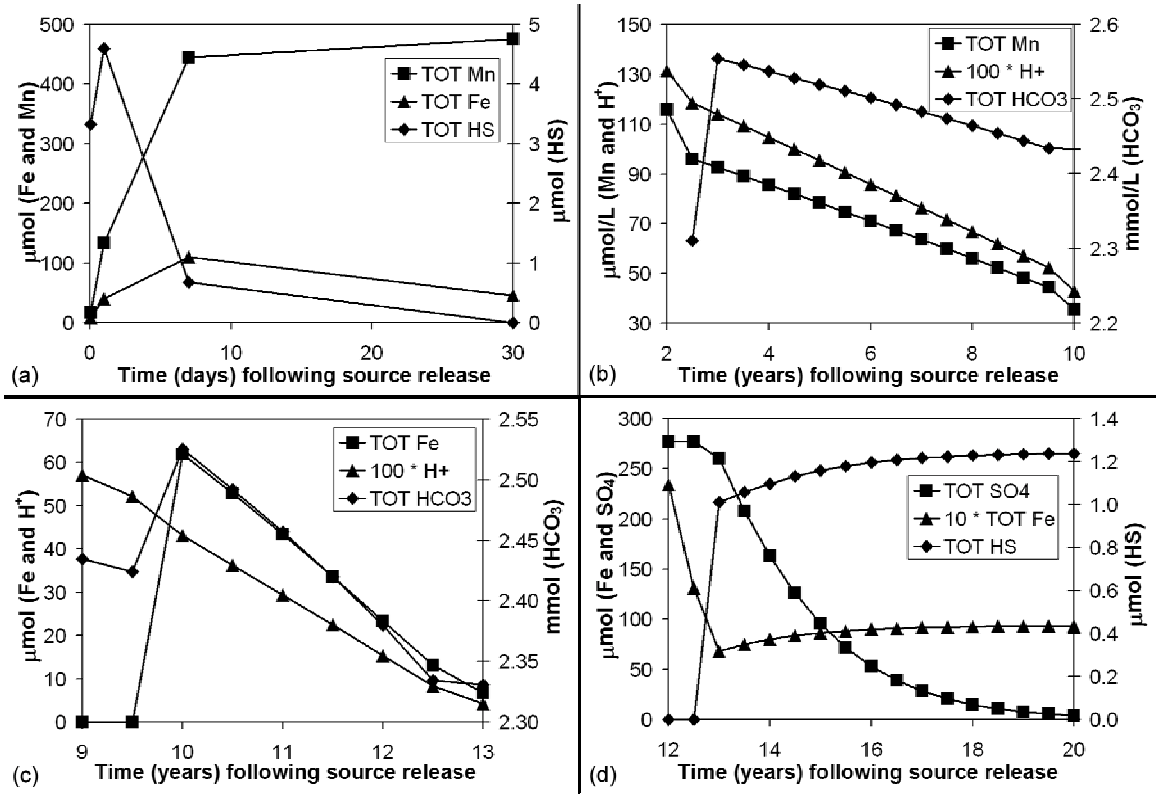

Figure 6.3: Selected plots of synthetically generated observations of the batch-reaction system. (a) early-time increase in Mn and Fe, with corresponding decrease in HS, (b-c) evidence of manganese and iron reduction, where biokinetic production of Mn^{+2}/Fe^{+2} is thought to trigger manganese and iron removal via surface-complexation and mineral precipitation reactions, (d) evidence of sulfate reduction late in the simulation

Based on the above analysis of observation data, three secondary reactions (R_6, R_7 and R_{10}) and the ion exchange reactions (R_{53} to R_{58}) were excluded from consideration in the surrogate models. Additionally, the dual-

Monod biokinetics formulation was neglected, and considered biokinetics formulations were limited to zero-order, and e-a limited first-order and single-Monod expressions. The resulting set of six surrogate models are summarized in Table 6.3 along with the complex model. Also identified in Table 6.3 are the equations used to assemble the complete set of mapping functions required for each surrogate model. For example, using the equations specified for surrogate S1 would result in the following vector of 14 mapping functions (one mapping function per parameter):

$$f_{S1}(\mathbf{X_{S0}}) \rightarrow \begin{cases} k^1_{S1,\max} = k^1_{S0,\max} \;,\; k^1_{S1,E} = k^1_{S0,E} \\ k^2_{S1,\max} = k^2_{S0,\max} \;,\; k^2_{S1,E} = k^2_{S0,E} \\ k^3_{S1,\max} = k^3_{S0,\max} \;,\; k^3_{S1,E} = k^3_{S0,E} \\ k^4_{S1,\max} = k^4_{S0,\max} \;,\; k^4_{S1,E} = k^4_{S0,E} \\ k^5_{S1,\max} = k^5_{S0,\max} \;,\; k^5_{S1,E} = k^5_{S0,E} \\ k^8_{S1} = k^8_{S0}[Fe^{2+}]_0 \;,\; k^9_{S1} = k^8_{S0}[O_2]_0 \\ k^{11}_{S1} = k^8_{S0}[H_2S]_0 \;,\; k^{12}_{S1} = k^8_{S0}[H_2S]_0 \end{cases} \tag{6.16}$$

where superscripts identify a reaction in Table 6.1; the '*S1*' and '*S0*' subscripts identify surrogate model S1 and S0, respectively; a '*max*' subscript identifies a maximum degradation rate; an '*E*' subscript signifies an electron acceptor half-saturation constant; and $[Fe^{2+}]_0$, $[O_2]_0$, and $[H_2S]_0$ are the initial concentrations of iron, dissolved oxygen, and hydrogen sulfide.

To constrain the calibration exercises, values for the upper and lower limits of each parameter were assigned based on initial experimentation. Ranges reported in the literature served as a useful guide for this process, particularly

Mayer et al. (2001) (for biokinetic rates), and Hunter et al. (1998) (for secondary redox rates).

Table 6.3: Configurations of the batch-reaction candidate models.

Reac-tion	Batch-Reaction Model						
	Complex (S0)	Surro-gate 1 (S1)	Surro-gate 2 (S2)	Surro-gate 3 (S3)	Surro-gate 4 (S4)	Surro-gate 5 (S5)	Surro-gate 6 (S6)
R_1	dual	single	single	zero [a]	zero [a]	zero [a]	zero [a]
R_2	dual	single	single	single	single	single	zero [a]
R_3	dual	single	single	single	zero [a]	zero [a]	zero [a]
R_4	dual	single	single	single	zero [a]	zero [a]	zero [a]
R_5	dual	single	single	zero [a]	single	first [c]	first [c]
R_6	first [a]	*n/a*	*n/a*	*n/a*	*n/a*	*n/a*	*n/a*
R_7	first [a]	*n/a*	*n/a*	*n/a*	*n/a*	*n/a*	*n/a*
R_8	first [a]	first [b]	zero [b]	zero [b]	zero [b]	zero [b]	zero [b]
R_9	first [a]	first [b]	zero [b]	zero [b]	zero [b]	zero [b]	zero [b]
R_{10}	first [a]	*n/a*	*n/a*	*n/a*	*n/a*	*n/a*	*n/a*
R_{11}	first [a]	first [b]	zero [b]	zero [b]	zero [b]	zero [b]	zero [b]
R_{12}	first [a]	first [b]	zero [b]	zero [b]	zero [b]	zero [b]	zero [b]
Num. param-eters	22	14	14	12	11	10	9
Key to terminology, with mapping functions in parentheses. wrt – with respect to; dual – dual-Monod; first [a] – first-order wrt to all reactants; single – e-a limited single-Monod (Eq. 6.11a); first [b] – first-order wrt a single reactant (Eq. 6.18); first [c] – e-a limited first-order (Eq. 6.12a); zero[a] – zero-order biokinetics (Eq. 6.13); zero[b] – zero-order secondary redox (Eq. 6.19)							

6.4.2.3.2 Mapping functions for secondary redox reactions

In this study, secondary redox reaction rates were presumed to take on one of three forms, depending on the level of model complexity:

$$R_i = k^i [A_1^i][A_2^i], \text{ or} \tag{6.17a}$$

$$R_i = k_1^i [A_1^i], \text{ or} \tag{6.17b}$$

$$R_i = k_0^i \tag{6.17c}$$

where R_i is the rate of a secondary reaction listed in Table 6.1 (i = 6 – 12); $[A_1^i]$ and $[A_2^i]$ are the concentrations of the reactants involved in the given

reaction, where $\mathbf{A_1}^T$ = [Mn^{2+}, Fe^{2+}, Fe^{2+}, O_2, O_2, H_2S, H_2S], and $\mathbf{A_2}^T$ = [O_2, O_2, $MnO_2(s)$, H_2S, $FeS(s)$, $MnO_2(s)$, $Fe(OH)_3(s)$]; and the reaction rate may be first-order with respect to both reactants (k^i), first-order respect to reactant A_1^i (k_1^i), or zero-order (k_0^i).

Mapping functions for k_1^i and k_0^i are given in Eq. 6.18 and 6.19 respectively, and were derived by assuming constant reactant concentration(s):

$$k_1^i = k^i [A_2^i]_0 \tag{6.18}$$

$$k_0^i = k^i [A_1^i]_0 [A_2^i]_0 \tag{6.19}$$

where, $[A_1^i]_0$ and $[A_2^i]_0$ are the initial reactant concentrations.

6.4.2.4 One-dimensional reactive transport test problem

The hypothetical transport scenario considered the simulation of nearly two months (52 days) of extensively monitored nitrate transport. Because of the short monitoring period and focus on nitrate, the 'true' one-dimensional transport model considered a reduced number of reactive processes, relative to the batch-reaction problem. As indicated by the asterisked entries in Table 6.1, the transport problem involved 6 reactions and a total of 12 species.

Initial conditions throughout the one-dimensional aquifer column were derived from a well at the Lizzie Research Station located up gradient of the spray fields. Measurements taken at this well were assumed to represent background aquifer conditions. As summarized in Table 6.4, the aquifer column was divided into five zones: a shallow zone, a medium zone, a deep zone, and two transition zones. Initial conditions for the shallow, medium and deep portions

of the aquifer column were derived from corresponding up gradient well data. Initial conditions for each transition zone were assigned via inverse-distance weighting of the concentration values of adjacent zones. Calcium carbonate mineral concentrations were assumed to be initially zero everywhere in the column.

Entrance boundary conditions for the column consisted of a constant-concentration source of contaminated groundwater, presumably infiltrating from the unsaturated zone. Entrance concentrations were derived from shallow-well data collected at the in-spray-field well, and are tabulated in the relevant entries of Table 6.2. The exit boundary condition for the column was a zero concentration gradient for all species, a commonly employed condition for this type of problem (e.g. Doussan et al., 1997).

Advective-dispersive components of the 'true' transport model were assigned as follows: dispserivity was set at 0.1 m, the Darcy velocity was 4.5 mm/day, porosity was assumed to be 0.3, and the retardation factor was set to 1.0. To facilitate numerical solution of the transport problem, the 5-meter spatial domain was discretized into 100 50-centimeter cells. Furthermore, the time domain was broken into 52 steps of 1-day each. This configuration yielded grid-Peclet (*Pe*) and Courant (*Cr*) numbers of 0.5 and 0.3, respectively. When applying the sequential non-iterative operator splitting technique to systems involving fast reactions, $Cr < 0.1$ is generally required for good accuracy. For this study, initial experimentation established that, relative to $Cr=0.01$, $Cr = 0.3$ yielded an average error of less than 2%.

Table 6.4: Initial Conditions for One-Dimensional Transport

Constituent	Aquifer Zones (values in parentheses are the zone thicknesses)				
	Shallow (0.9 m)	Shallow-Med. (0.35 m)	Medium (2.75 m)	Med.-Deep (0.4 m)	Deep (0.6 m)
pH	5.10	Assigned using inverse-distance weighting.	4.60	Assigned using inverse-distance weighting.	5.20
TOT HCO_3	1.64×10^{-5}		1.64×10^{-5}		1.64×10^{-4}
TOT O_2	1.31×10^{-4}		1.06×10^{-4}		1.88×10^{-5}
TOT NO_3	1.86×10^{-4}		2.93×10^{-4}		6.35×10^{-5}
TOT DOC (as C)	1.17×10^{-4}		5.00×10^{-5}		4.16×10^{-5}
TOT Ca	5.49×10^{-5}		8.73×10^{-5}		1.50×10^{-4}
TOT Mg	1.83×10^{-4}		1.83×10^{-4}		2.85×10^{-4}
TOT Cl	2.82×10^{-4}		2.57×10^{-4}		6.49×10^{-4}

After establishing the truth model for the reactive-transport benchmark problem, a series of candidate transport models were developed. Graphical analysis of the synthetic transport observation suggested that denitrification, if present, was likely to be substrate-limited. The seven candidate reactive transport models that were considered are summarized in Table 6.5. Calibration of the uncertain parameters of these candidate models provided an experimental framework for evaluating alternative methods for model ranking, selection and calibration.

Table 6.5: Configuration of the candidate transport models

	Reactive-Transport Model						
	Complex (S0)	Surro-gate 1 (S1)	Surro-gate 2 (S2)	Surro-gate 3 (S3)	Surro-gate 4 (S4)	Surro-gate 5 (S5)	Surro-gate 6 (S6)
Uncertain reaction parameters							
R_1	dual	single [a]	first [a]	first [a]	zero	zero	n/a
R_2	dual	single [b]	first [b]	zero	first [b]	zero	n/a
Uncertain advection-dispersion parameters (directly mapped [e.g. $v_{S6} = v_{S0}$])							
dispersivity	α_{S0}	α_{S1}	α_{S2}	α_{S3}	α_{S4}	α_{S5}	α_{S6}
velocity	v_{S0}	v_{S1}	v_{S2}	v_{S3}	v_{S4}	v_{S5}	v_{S6}
Num. parameters	8	6	4	4	4	4	2

Key to terminology, with mapping functions in parentheses.
wrt – with respect to; dual – dual-Monod; single [a] – e-a limited single-Monod (Eq. 6.11a); single [b] – substrate-limited single-Monod (Eq. 6.11b); first [a] – e-a limited first-order (Eq. 6.12a); first [b] – substrate-limited first-order (Eq. 6.12b); zero – zero-order biokinetics (Eq. 6.13)

As shown in Table 6.5, all models considered uncertain advection-dispersion parameters. The most complex model also considered dual-Monod biokinetics, while models S1 through S5 considered various biokinetics simplifications and the simplest model (S6) neglected biokinetics entirely.

6.4.3 Setup of the numerical experiments

To evaluate the surrogate-model approach, a series of numerical experiments were performed. The experiments sought to calibrate and rank the various batch and one-dimensional transport models using synthetic observations generated from the corresponding 'truth' model. The experiments are summarized in Table 6.6, and consisted of combinations of calibration algorithm, test problem and model complexity. As shown in Table 6.6, for each test problem and level of model complexity, three non-surrogate calibrations were performed. One non-surrogate utilized a multi-start regression (MSR) algorithm, another utilized particle swarm optimization (PSO), and the third used a hybridized particle swarm optimization algorithm. These calibrations (and subsequent model ranking and selection) served as a baseline for assessing the surrogate-model approach introduced in this work. For the MSR algorithm, the Levenberg-Marquardt regression procedure was initiated from randomly generated initial guesses. This enhancement provided the gradient-based algorithm with a limited ability to avoid local minima. Four and eight initial guesses were used for the batch-reaction and reactive transport problems, respectively.

Besides the aforementioned baseline experiments, the surrogate-model approach was also applied to each test problem. For this study, the surrogate-model approach was implemented by linking the PSO algorithm with the previously described surrogate-model decision module. The effect of 'polishing' the surrogate-model approach with a regression step was also examined. For this polishing step, the best configuration of each candidate model was extracted from the surrogate-model calibration results. These configurations furnished the initial parameter values for a subsequent set of Levenberg-Marquardt regression runs (one regression per candidate model).

Because the considered calibration algorithms (i.e. PSO and MSR) contain elements of randomness, the corresponding experiments were repeated multiple times in order to capture the central tendency of a given approach. Following previous work involving optimization algorithms (Matott et al., 2006b), between 10 and 20 samples were collected for each experiment.

A final set of numerical experiments focused on a qualitative evaluation of the degree of parameter non-uniqueness and non-linearity associated with the selected calibration problems. For these experiments, massively parallel computing infrastructure was utilized to evaluate and map a series of two-dimensional slices through the design space of selected calibration problems.

All calibrations were run on parallel computing clusters maintained by the University at Buffalo Center for Computational Research (CCR). The clusters consisted of dual-processor 3.2-GHz Intel Xeon processors, with 2-GB of RAM and version 7.6 of the RedHat Linux operating system. Calibrations were

performed using Ostrich (Matott, 2006a), a model-independent, multi-algorithmic optimization tool that includes a surrogate-model calibration module (available with version 1.8 of the public domain software).

Table 6.6: Experimental Setup

Exp.	Test Problem	Algorithm	Model	Exp.	Test Problem	Algorithm	Model
1	Batch-reaction	Multi-start Regression	S6	17	One-dimensional transport	Multi-start Regression	S6
2			S5	18			S5
3			S4	19			S4
4			S3	20			S3
5			S2	21			S2
6			S1	22			S1
7			S0	23			S0
8a-b		(a) Particle Swarm Optimization, (b) Hybrid PSO	S6	24a-b		(a) Particle Swarm Optimization, (b) Hybrid PSO	S6
9a-b			S5	25a-b			S5
10a-b			S4	26a-b			S4
11a-b			S3	27a-b			S3
12a-b			S2	28a-b			S2
13a-b			S1	29a-b			S1
14a-b			S0	30a-b			S0
15		Surrogate-model	S*	31		Surrogate-model	S*
16		Surrogate-model w/ polishing	S*	32		Surrogate-model w/ polishing	S*
S* - all batch or transport models, individual batch models are described in Table 6.3 and individual transport models are described in Table 6.5.							

6.5 Results and Discussion

Typical batch-reaction model calibrations required between two and four hours of wall-time on the parallel clusters, corresponding to several days of computation time. Individual complex batch-reaction model evaluations required as many as 2 minutes of computation time, while the suite of surrogate models required between 30 and 90 seconds of computer time per evaluation. Because the reactive transport models involved fewer parameters that the batch-reaction models, the transport model calibrations generally required fewer model evaluations. However, computation times for a given transport model evaluation

could be as much as ten minutes for the complex model, and ranged between one and five minutes for the surrogate models. As a result, the typical parallel cluster wall-time for the transport model calibrations was between four and twelve hours. On a single-processor system, such transport calibrations would have taken somewhere between five days to two weeks.

6.5.1 Visualization of the Calibration Design Space

Results from the two-dimensional mapping of selected calibration problems are provided in Figure 6.4. These graphical slices through the calibration design space reveal a highly non-linear objective function surface. Large patches of the design space are relatively flat indicating parameter insensitivity. Conversely, other regions displayed extreme sensitivity and contain a heterogeneous mixture of closely grouped peaks and valleys.

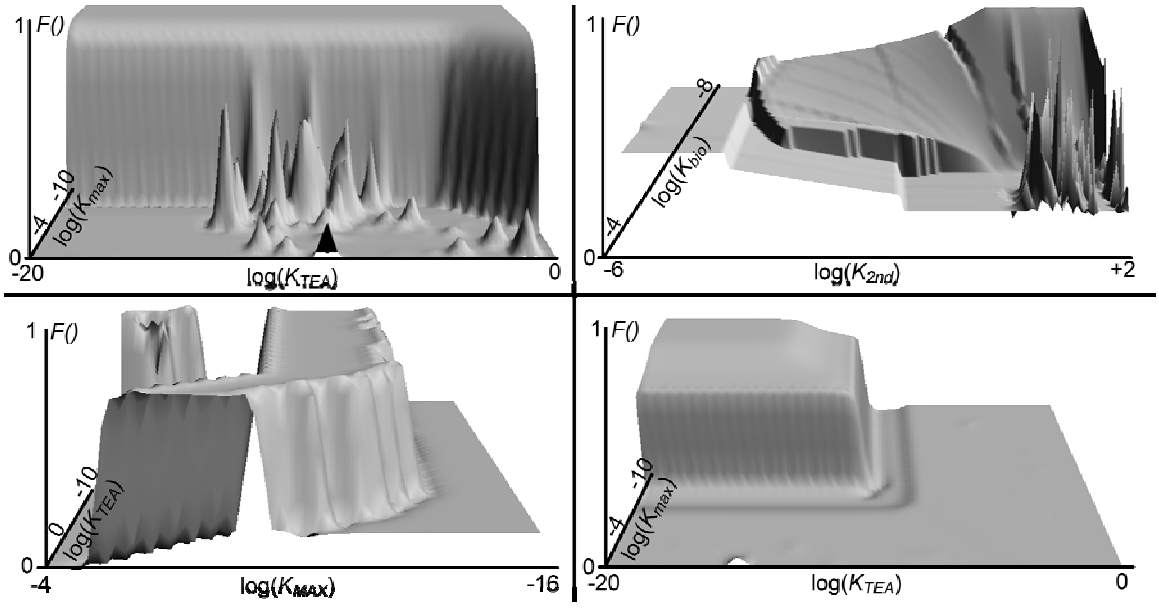

Figure 6.4: Two-dimensional slices of the calibration objective function surface. Unless noted, the plots compare the calibration objective function to changes in biokinetic parameters, where K_{max} is the maximum degradation rate, K_{TEA} is the electron acceptor half-saturation constant, and $F()=log(WSSE)/log(WSSE_{max})$ is the normalized objective function value. (top left) denitrification process, TEA is NO_3^-, (top right) lumped first-order biokinetic (K_{bio}) rate vs. lumped first-order 2nd-ary redox rate (K_{2nd}), (bottom left) sulfate reduction, TEA is SO_4^{2-}, (bottom right) manganese reduction, TEA is MnO_2(s).

6.5.2 Calibration and Ranking of the Batch Reaction Models

Table 6.7 summarizes the AICc-based model rankings of the candidate batch-reaction models, as determined by the considered algorithms. Taken as a whole, these rankings support the partitioning of the candidate models into three groups. First, the complex model (S0) and the most complicated surrogate (S1) were generally the highest ranked models. Next, the least complicated surrogates (S5 and S6) also tended to be highly ranked, with AICc values typically within 20% of the highest ranked model. Finally, the remaining intermediate-complexity surrogates (S2 though S4) tended to be ranked lowest, with AICc values markedly higher (i.e. worse) than the alternative models.

Examination of the batch-reaction model configurations (listed in Table 6.3) suggests a possible explanation for the somewhat counterintuitive model ranking: the intermediate complexity models (S2-S4) paired simplified secondary redox reactions with complex single-Monod biokinetics processes. Conversely, the more preferred models paired complex secondary-redox and complex biokinetics expressions (S0 and S1), or paired simple secondary reactions with simple biokinetics formulations. Apparently, mixing the complexity levels of the two reaction types was not a favorable way to represent the 'true' system. The convergence behavior of selected intermediate-model calibrations was supportive of this assertion. In such calibrations, algorithms tended to drive all single-Monod half-saturation constants toward their upper or lower limits, effectively reducing such expressions to either zero- or first-order kinetics. Such

algorithm behavior can be viewed as an attempt to simplify the biokinetics in order to make them compatible with the secondary reactions.

Of the search algorithms, the PSO-regression hybrid generally provided the lowest AICc values for each candidate model. The corresponding model rankings were therefore thought to be the most reliable, and served as a benchmark for evaluating the ranking capability of the surrogate-model approach. The model rankings provided by the basic surrogate-model approach (without polishing) qualitatively agreed with the rankings of the hybrid PSO, with one important exception: surrogate model S1 was ranked very poorly by the surrogate-model approach, but was ranked very highly by the hybrid PSO. Following up the surrogate-model approach with a polishing step significantly reduced the AICc value of model S1, and the polished S1 model was within 8% of the 2nd place S5 model.

Table 6.7: AICc Model Rankings for the Candidate Batch-Reaction Models

Model ID	Multi-Start Regression		Particle Swarm Optimization		Hybrid PSO		Surrogate-model Approach		Surrogate-model w/ Polishing	
	AICc	Rank	AICc	Rank	AICc	Rank	AICc	Rank	AICc	Rank
S0	3016	3	2575	2	1957	1	2375	1	2110	1
S1	1951	1	2524	1	2017	2	3851	6	2540	4
S2	10306	7	2685	4	2475	6	3456	5	3329	6
S3	6210	4	2697	5	2501	7	3968	7	3609	7
S4	6430	6	2652	3	2455	5	2946	4	2946	5
S5	6417	5	2797	6	2328	3	2777	3	2346	2
S6	2710	2	2926	7	2344	4	2655	2	2420	3

Figure 6.5 compares the performance (i.e. efficiency and effectiveness) of the selected calibration algorithms, as applied to the set of candidate batch-reaction models. For this work, algorithm efficiency was measured in terms of the

number of required model evaluations and effectiveness was measured in terms of root-mean-squared error ($RMSE=[WSSE/(n-p)]^{1/2}$).

In terms of efficiency, the results demonstrated that the surrogate-model approach required far fewer model runs than the considered non-surrogate alternatives. Calibration of all candidate models using the highly effective, but computationally expensive, hybrid PSO method required more than 25,000 evaluations of the various models. Conversely, the surrogate-model approach required less than 9,000 total evaluations, and the surrogate-model approach with additional polishing required slightly more than 11,000 total evaluations. The most inefficient method was multi-start regression, which required more than 27,000 total evaluations. Given the high computational cost of the MSR technique, it was surprisingly ineffective when applied to models S2 through S5, where it reported extremely high best-fit RMSE values of 2400, 109, 129 and 128, respectively. For these problems, the algorithm appeared to slowly converge on local minima.

The bottom portion of Figure 6.5 compares algorithm effectiveness, in terms of RMSE values. Overall, the hybrid particle swarm optimization algorithm was the most effective of the considered algorithms. For most of the models, the effectiveness of the less expensive 'polished' surrogate-model approach was comparable to that of the hybrid PSO. Notable exceptions are the results of the S2 and S3 calibrations, where the surrogate-model approach had difficulty even when followed with a polishing step.

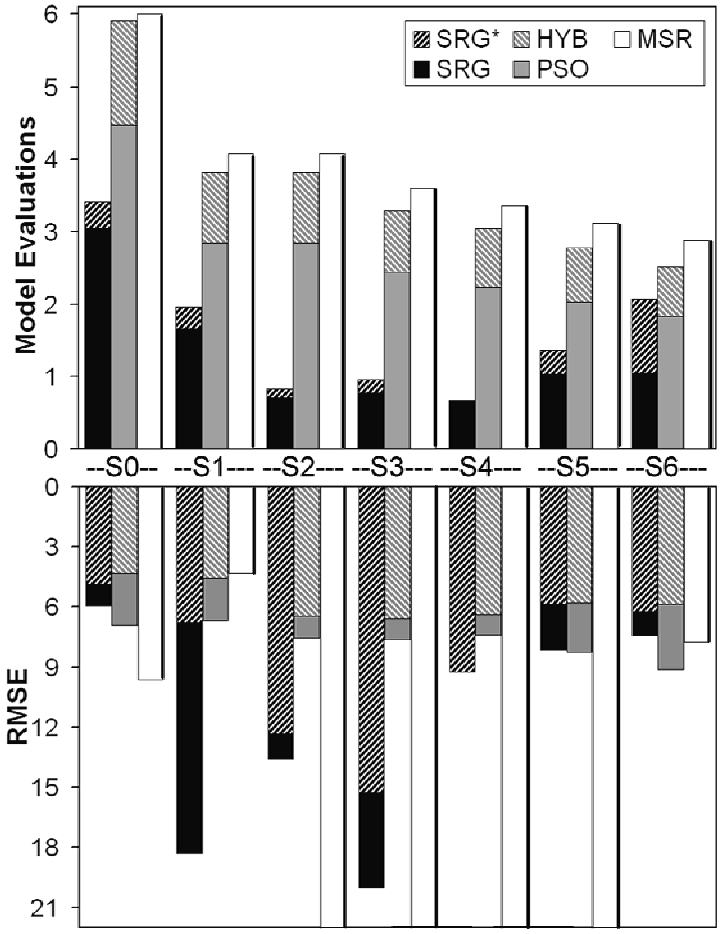

Figure 6.5: Comparison of Algorithm Performance for the Batch-Reaction Models. Model evaluations are in thousands. MSR – multi-start regression, PSO – particle swarm optimization, HYB – hybrid particle swarm optimization, SRG – surrogate model approach, SRG* - surrogate model approach with additional polishing step, configurations of models S0-S6 are given in Table 6.3.

Recall that the S2 and S3 models were poorly ranked and that non-surrogate calibration procedures attempted to drive the Monod-kinetics of these models into simpler zero- and first-order behavior. The number of S2 and S3 model evaluations under the surrogate-model approach was around 700 evaluations each. Conversely, the number of S5 and S6 model evaluations was just over 1000 each. Therefore, rather than spending model evaluations driving the parameters of the S2 and S3 models toward simpler kinetics, in the

surrogate-model approach it appears that the decision module instead simply selected and evaluated simpler (i.e. S5 or S6) models, as appropriate.

6.5.3 Comparisons of Calibrated and "True" Batch-Reaction Models

For the selected test problems, a set of simulated concentration profiles were generated for the best-ranked models, as determined by the surrogate- and non-surrogate approaches. For comparison, these profiles also include a profile generated using the appropriate "true" model. Visual comparison of the profiles provides a qualitative analysis of model appropriateness. Figure 6.6 contains profiles of (a) oxygen, (b) nitrate, (c) sulfate, and (d) pH for the batch-reaction calibrations.

The profiles of dissolved oxygen in Figure 6.6a indicate significant differences among the various calibrated models. At the extremes, the calibrated S2 model prolonged the degradation of oxygen for an additional day, relative to the 'true' model. Conversely, the calibrated S1 model preferred a degradation rate that depleted oxygen in less than three hours. In terms of denitrification (see Figure 6.6b), the best-ranked calibrated models (i.e. models S0*, S0, S5 and S6) were in very good agreement with the 'true' model, which required about 2.5 years to fully degrade the nitrate concentrations from the initial contaminant release. Conversely, the poorly ranked models (i.e. models S2-S4) preferred rapid denitrification rates that fully degraded the contaminant source in less than 6 months. As shown in Figure 6.6c, the sulfate reduction process of the true model was not well represented by models of simple (i.e. S5 and S6) or intermediate (i.e. S2-S4) complexity.

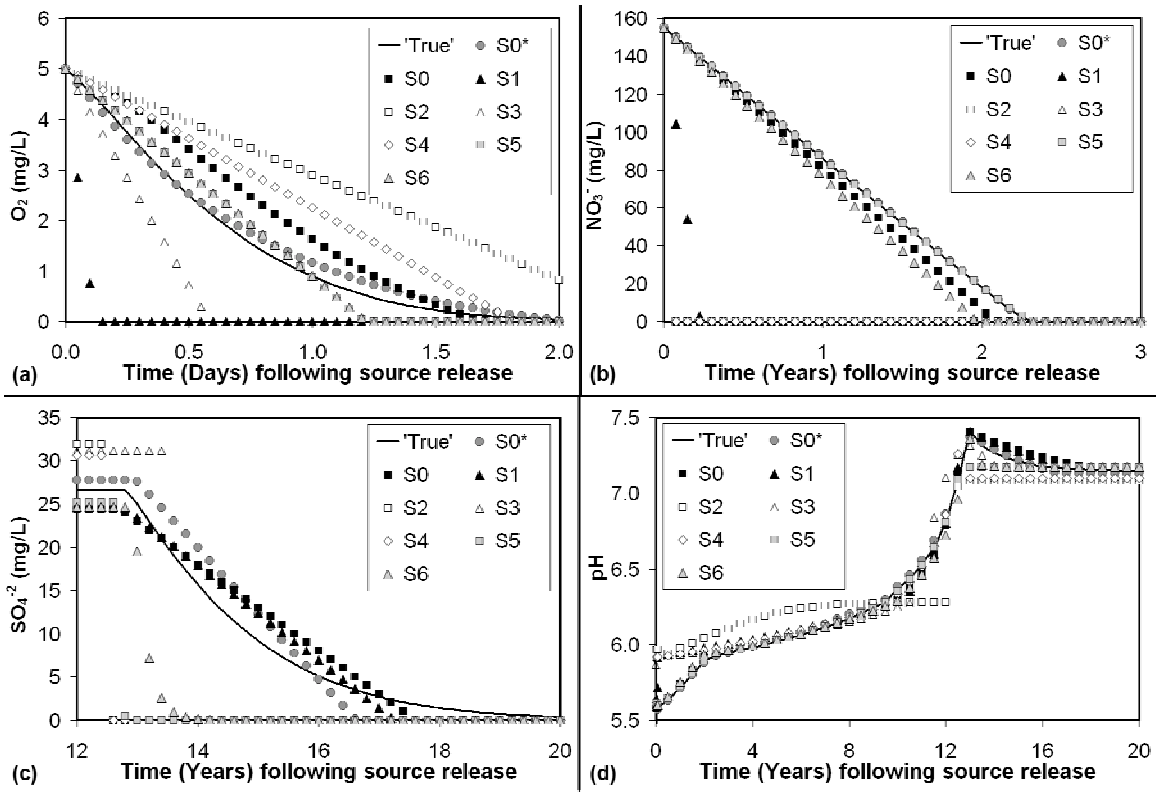

Figure 6.6: Comparison of simulated concentration profiles for the batch-reaction test problem. Profiles S0-S6 correspond to models S0-S6, calibrated using surrogate-model approach with an additional polishing step. Profile S0* is the S0 model calibrated using the PSO-regression hybrid.

6.5.4 Calibration and Ranking of the Reactive-Transport Models

Table 6.8 summarizes the AICc-based model rankings of the candidate reactive transport models. Overall, the model rankings were consistent across the various algorithms. Four of the five methods ranked model S5 best, and all algorithms also preferentially ranked models S0 and S1. Conversely, model S6 was by far the worst ranked model and models S2 through S4 were given intermediate rankings. Comparison of these rankings with the model configurations given in Table 6.5 suggests that while neglecting biokinetics entirely (i.e. model S6) was inadequate, inclusion of simple zero-order biokinetics (i.e. model S5) provided the best tradeoff between model complexity and quality

of fit. Additionally, for the selected reactive transport problem, it appears that approximating aerobic degradation and/or denitrification using first order kinetics (i.e. models S2-S4) was not favored.

For the reactive transport problems, the AICc values of the multi-start regression were the lowest. Therefore, the corresponding MSR rankings were used to benchmark the rankings of the surrogate-model approach. Qualitatively, the rankings and AICc values of the basic surrogate-model approach were in good agreement with the MSR results. Applying a polishing step to the surrogate-model approach quantitatively improved the AICc values of various candidate models, particularly models S0 and S2-S4. The resulting 'polished' model rankings match the multi-start regression rankings exactly.

Table 6.8: AICc Model Rankings for the Candidate Reactive Transport Models

Model ID	Multi-Start Regression		Particle Swarm Optimization		Hybrid PSO		Surrogate-model Approach		Surrogate-model w/ Polishing	
	AICc	Rank	AICc	Rank	AICc	Rank	AICc	Rank	AICc	Rank
S0	-764	2	-330	1	-395	3	-247	3	-763	2
S1	-597	3	0.60	3	-438	2	-443	2	-443	3
S2	3.11	4	9.75	5	3.13	5	827	5	3.11	4
S3	3.15	5	6.47	4	3.11	4	207	4	3.14	5
S4	128	6	138	6	128	6	1123	6	128	6
S5	-769	1	-323	2	-767	1	-755	1	-770	1
S6	1225	7	1225	7	1225	7	1225	7	1225	7

Figure 6.7 compares the performance of the selected calibration algorithms, as applied to the set of candidate reactive transport models. With the exception of model S1, the surrogate-model approach required significantly fewer individual candidate-model evaluations, relative to non-surrogate approaches. Overall, the total evaluations required by the surrogate-model approach (3850) and the surrogate-model with polishing (4392) were significantly less than the

non-surrogate PSO (7040), hybrid PSO (7467), and multi-start regression (8206) algorithms. Like the batch-reaction problems, the MSR algorithm tended to be the least efficient algorithm. However, unlike the batch-reaction problems, the MSR algorithm was highly effective when applied to the reactive transport problems.

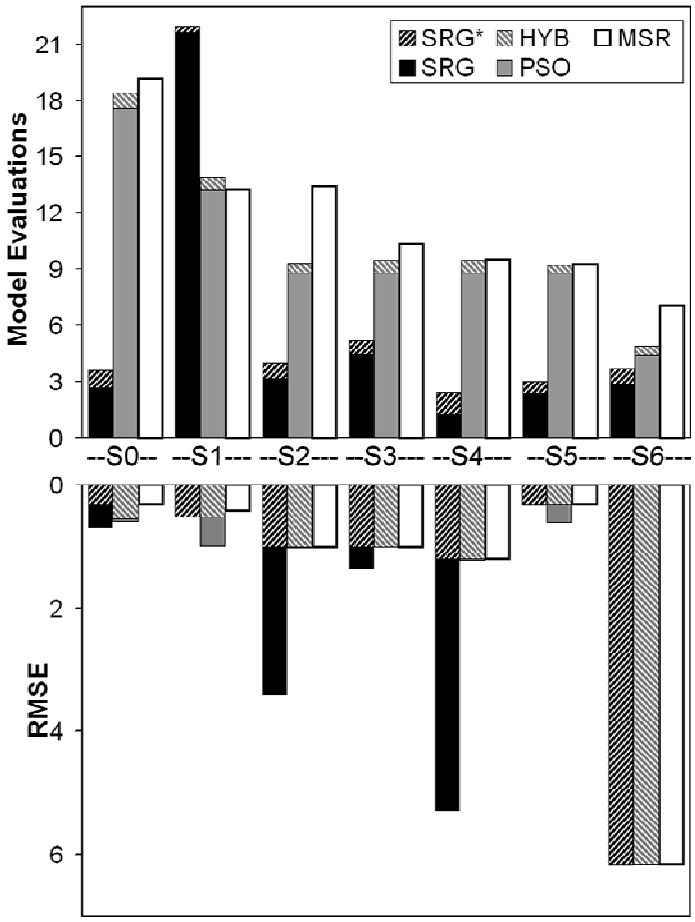

Figure 6.7: Comparison of Algorithm Performance for the Reactive Transport Models. Model evaluations are in hundreds. MSR – multi-start regression, PSO – particle swarm optimization, HYB – hybrid particle swarm optimization, SRG – surrogate model approach, SRG* - surrogate model approach with additional polishing step, configurations of models S0-S6 are given in Table 6.5.

In terms of algorithm effectiveness, the various non-surrogate algorithms and the polished surrogate-model all tended to be equally effective. The basic

surrogate-model approach was effective for most of the candidate models, but performed poorly on models S2 and S4. In this regard, inspection of the surrogate-model behavior provided useful insight. Evidently, early algorithm exploration resulted in parameter configurations that favored the intermediate-complexity biokinetics of models S2-S4. This early exploration quickly led the PSO calibration algorithm toward parameter configurations that favored the single-Monod biokinetics of the S1 model. For the majority of subsequent PSO iterations, the decision module continued to favor the S1 model. However, as the PSO progressed it began selecting parameter configurations in which the zero-order simplification of the S5 model became more and more competitive with the single-Monod S1 model. Finally, in the late stages of the PSO algorithm, the decision module began favoring the S5 model.

6.5.5 Comparisons of Calibrated and "True" Reactive Transport Models

Figure 6.8 contains profiles of oxygen and nitrogen gas at the shallow well for the calibrated and 'true' reactive-transport models. As shown in Figure 6.8a, relative to the 'true' model, reactive transport of dissolved oxygen was well replicated by almost all of the calibrated candidate models. The lone exception is model S6, which neglected biokinetics. The nitrogen gas profiles in Figure 6.8b indicate that denitrification at shallow depths was just beginning at the end of the 52-day simulation. Therefore, it is not surprising that the majority of the calibrated candidate models preferred to ignore denitrification by adjusting the relevant rate parameters toward zero. To allow for a more rigorous consideration of denitrification processes, a revised set of reactive-transport calibrations have

been undertaken. These revised experiments extend the simulated reactive-transport time period to one year, allowing for a more complete denitrification profile to develop throughout the 5-meter column.

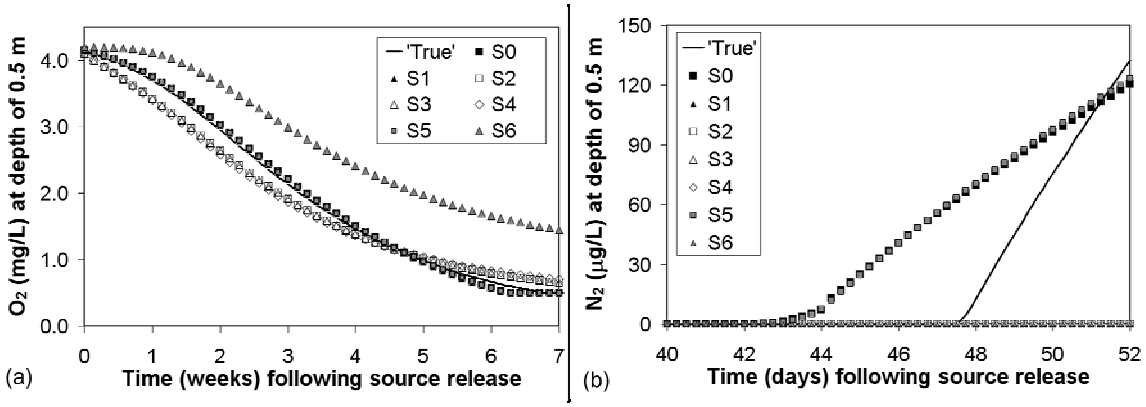

Figure 6.8: Comparison of simulated shallow-depth concentration profiles for the reactive transport problem. Profiles S0-S6 correspond to models S0-S6, calibrated using the surrogate-model approach, followed by an additional polishing step.

6.6 Conclusions

This study has introduced an integrated approach to the calibration, ranking and selection of alternative reactive transport models. The new method utilizes a surrogate-based approach, in which a suite of candidate reaction models is evaluated as surrogate representations of a more complex (and computationally expensive) model. During automated calibration, an adaptive interpolation scheme is utilized to dynamically rank and select an appropriate model for a given configuration of calibration parameters.

The new method was demonstrated using a set of hypothetical batch- and one-dimensional reactive transport scenarios. For both test problems, the surrogate-model approach was capable of efficiently and simultaneously performing the tasks of model ranking, selection and calibration. Additional experiments examined the effect of following up a surrogate-model calibration

with a relatively inexpensive regression-based polishing step. Such polishing further enhanced both the accuracy of model rankings and the overall quality of model fits.

In the regulatory and research communities, there has been increased interest in large-scale regional modeling of contaminant fate and transport. For example, models developed to support Total Maximum Daily Load (TMDL) analysis must often consider the contributions of surface and groundwater (both saturated and unsaturated) over a large spatial region. Furthermore, the role of groundwater in Nitrogen cycling is an important open science question (Holland et al., 2005) that will likely be addressed by the development of large-scale heavily-instrumented hydrologic observatories, such as those envisioned by the CUAHSI (Consortium of Universities for the Advancement of Hydrologic Sciences, Incorporated) and CLEANER (Collaborative Large-scale Engineering Assessment Network for Environmental Research) initiatives. As TMDL and nutrient cycling research proceeds, it is anticipated that selection and calibration of the associated complex, large-scale models will be desired. The surrogate-model approach introduced here may be ideally suited for such activity.

7 SUMMARY AND CONCLUSIONS

The objective of the research performed for this dissertation was to advance the state-of-practice of heuristic optimization, as applied to problems involving groundwater management. This chapter summarizes the key contributions of the research.

7.1 Contributions: Heuristic Optimization

The use of heuristic optimization algorithms within the groundwater management community was advanced in several ways:

- A rigorous examination and comparison of alternative heuristic and gradient-based algorithms, as applied to several important groundwater management problems, was performed. For the considered problems, heuristic techniques tended to provide more robust performance, relative to gradient-based approaches. Following a heuristic search with a gradient based polishing step (as in the PSO-regression hybrid considered in Chapter 6) provided additional performance improvement.
- A design-of-experiments technique for objectively tuning algorithm performance was introduced, and the technique was found to be a useful mechanism for performing robust algorithm comparisons. These comparisons of tuned algorithm behavior and performance have led to novel insights into the physico-chemical processes governing the performance of multi-layer sorptive barriers.
- Heuristic algorithms based on swarm intelligence were demonstrated to be readily adaptable to a variety of groundwater management problems,

including reactive transport calibration, multi-layer sorptive barrier design, and pump-and-treat aquifer remediation. Such algorithms were readily parallelized and produced nearly linear speedup, making them suitable for large-scale optimization and/or calibration problems involving many parameters.

- The calibration of reactive transport models containing a complex suite of biogeochemical reactions was examined. Graphical analysis of slices through the calibration design space revealed a high degree of non-linearity, with vast regions of insensitivity punctuated by localized areas of extreme sensitivity and multiple extrema. Somewhat unsurprisingly, the gradient-based Levenberg-Marquardt regression method (a popular choice for calibrating groundwater flow models) had difficulty navigating the aforementioned reactive-transport calibration terrain. Conversely, the PSO heuristic and a PSO-regression hybrid were demonstrated to be effective alternatives.
- When combined with a novel surrogate-model scheme, heuristic algorithms were shown to be capable of simultaneously ranking, selecting and calibrating a suite of candidate reactive transport models. Such an approach was demonstrated to incur significantly less computational expense than traditional techniques, which involve a series of individual model calibrations, followed by model ranking and selection.

7.2 Contributions: Groundwater Management Applications

Because realistic groundwater management problems served as the experimental framework for the aforementioned advancements in heuristic optimization, this research has also made several application-specific contributions:

- Analytic element modeling engines were effectively employed as the underlying flow simulator for pump-and-treat optimization problems. Particular advantages of the AEM approach include the ability to directly represent well coordinates as continuous design variables and the availability of analytically computed head gradient constraints. While these features did not necessarily improve optimization results, they provided additional flexibility with regard to the choice of search algorithm and problem formulation.
- The zone outflux constraint, a new plume containment constraint for pump-and-treat optimization, was introduced. This constraint was shown to be effective and at least as efficient as the considered alternatives (i.e. head gradient and particle tracking constraints). The analytic nature of the 'zone outflux constraint' results in better plume containment, leading to improved reliability and eliminating the need for 'constraint calibration'; a pre-optimization process that involves the determination of the appropriate number and location of particles and/or gradient control pairs.
- Analysis of a set of sorptive landfill liner design problems revealed that barrier performance was sensitive to the order in which barrier layers were

assembled. The precise nature of this sensitivity remains the topic of future research, and is probably related to isotherm modeling conventions. However, the discovery itself is an important contribution that highlights the value of simulation-optimization as a tool for developing insight into groundwater management applications.

- Groundwater management applications commonly involve a variable number of design components (such as the number of wells in a pump-and-treat system or the number of layers in a sorptive barrier system). When optimizing such applications using a simulation-optimization approach, the ability to eliminate unnecessary components was found to be an important criterion for search-algorithm selection.
- A set of hypothetical (but realistic) reactive transport calibration problems were examined. Using carefully formulated and highly complex synthetic reference models, alternative models of varying complexity were developed and subjected to multi-model calibration, ranking and selection procedures. Rankings of the calibrated models indicated a selection preference for models of high and low complexity, and a general disregard for models of intermediate-complexity. Graphical comparisons of calibrated concentration profiles supported such a model hierarchy. While these results are necessarily problem-specific, the counterintuitive nature of the model rankings underscores the usefulness of applying multi-model uncertainty analysis procedures to reactive-transport problems.

APPENDIX A: INITIAL SOFTWARE TESTS

During initial software testing, particular attention was placed on the Levenberg-Marquardt regression algorithm and the calculation of calibration statistics and diagnostic measures, as these deterministic features are readily compared against existing software packages.

A.1 West Valley Calibrations

A series of calibrations were performed to support modeling of competitive cation exchange processes in a permeable reactive barrier (PRB) located at the West Valley Demonstration Project (WVDP) in Western New York (Rabideau et al., 2005b). Data from column experiments served as observations for calibrations in which values for species selectivity coefficients were estimated. A MOUSER (formerly known as TRANS1D) WVDP model was initially calibrated using UCODE (Chang, 2000), and the results served as a useful benchmark for subsequent calibrations utilizing selected OSTRICH algorithms (as shown in Table A.1). In Table A.1, LEV indicates the Levenberg-Marquardt algorithm, RMSE is the root mean squared error, R_y is the correlation between observed and simulated data, R_N^2 is a measure of residuals normality, C_K^{est}, C_{Mg}^{est}, C_{Ca}^{est}, and C_{Sr}^{est} are the calibrated selectivity coefficients for potassium (*K*), magnesium (*Mg*), calcium (*Ca*) and strontium (*Sr*), and the C^{lo} and C^{hi} terms represent upper and lower 95% confidence limits. The data in Table A.1 indicates good agreement between comparable UCODE and OSTRICH features, and also demonstrates that heuristics can be effective at solving calibration problems.

Table A.1: WVDP Calibration: Algorithm Comparisons

Program	UCODE	OSTRICH			
Algorithm	LEV	LEV	GA	PSO	SA
RMSE	12.06	12.12	12.20	12.19	13.10
R_y	0.96	0.96	0.96	0.96	0.96
R_N^2	0.92	0.91	0.91	0.93	0.96
C_K^{est}	28	28	29	27	32
C_K^{lo}–C_K^{hi}	22–35	21–35	22–36	20–33	23–42
C_{Mg}^{est}	306	330	368	277	588
C_{Mg}^{lo}–C_{Mg}^{hi}	173–544	142–518	155–582	119–434	238–938
C_{Ca}^{est}	354	372	393	325	342
C_{Ca}^{lo}–C_{Ca}^{hi}	269–466	269–474	280–505	236–414	244–440
C_{Sr}^{est}	4789	5026	5125	4406	4883
C_{Sr}^{lo}–C_{Sr}^{hi}	3750–6120	3788–6263	3861–6569	3346–5466	3603–6163

A.2 AEM Calibration Paper

Using the Ischua Creek drainage basin in Western New York as a case study site, Lim (2005) compared calibration results obtained using analytic element modeling (Rabideau et al., 2005) with those generated using finite difference flow modeling. AEM-based models were calibrated using OSTRICH, while FD-based models utilized PEST. Allowing for differences between the flow model formulations, the calibration results qualitatively demonstrate good agreement between the PEST and OSTRICH regression algorithm (Levenberg-Marquardt) and related statistical output (e.g. confidence intervals, parameter sensitivities, etc.).

A.3 Sorption Isotherms

Non-linear sorption isotherms, such as the Freundlich and Langmiur isotherms, are typically fit using trial-and-error or spreadsheet utilities, such as the MS Excel Solver add-in. In preparation of Bartelt-Hunt et al. (2005), isotherm fitting of laboratory sorption data was performed using both Solver and ISOFIT, an isotherm fitting code that utilizes OSTRICH. Results of the two isotherm fitting

approaches are given in Table A.2, which demonstrates that ISOFIT, which uses the PSO algorithm, discovers better (in terms of RMSE) Langmuir isotherm fits than the Solver package, which uses a gradient-based algorithm.

Table A.2: Isotherm Fitting: ISOFIT and Solver Comparisons

Sorption Media	Chemical	Isotherm	RMSE	
			Solver	IsoFit
BTEA-Bentonite	Benzene	Langmuir	815	755
	1,2-DCB		380	347
	TCE	Freundlich	1,061	1,060
GAC	Benzene	Langmuir	21,784	20,200
	1,2-DCB		28,615	27,300
	TCE		24,760	22,900
Shale	Benzene	Freundlich	48	48
	1,2-DCB		116	116
	TCE		178	178

A.4 PEST And UCODE Comparisons

The calibration exercise presented in the Visual Bluebird manual (Craig, 2005) was solved using the PEST, UCODE, and OSTRICH implementations of the Levenberg-Marquardt regression algorithm. For the UCODE calibration, the Cook's D and DFBETAS measures of influential observation were computed using the RESAN2K post-processing program (Hill et al., 2000), which uses a file-format that is consistent with UCODE output. Influential observation and linearity measures are not available (n/a) in the present version of PEST. Table A.3 summarizes the results from the various calibration packages, and the agreement between the packages suggests that the calibration and statistical components of OSTRICH are properly implemented. In Table A.3 K is the aquifer conductivity [m/d], N is the recharge [m/d] to a wetland region of the model, M^2 is

Linssen's linearity measure (Linssen, 1975), and the Cook's D and DFBETAS rows identify influential observations and corresponding influence values.

Table A.3: Groundwater Calibration: Program Comparisons

	UCODE	PEST	OSTRICH
RMSE	1.778	1.778	1.778
R_y	0.982	0.982	0.982
R_N^2	0.546	0.542	0.546
K^{est}	2.18	2.19	2.19
K^{lo}–K^{hi}	0.251–18.9	0.250–19.3	0.250–19.2
N^{est}	-0.00482	-0.00486	-0.00484
N^{lo}–N^{hi}	-0.165–0.00689	-0.167–0.00698	-0.166–0.00688
Linearity (M^2)	97	n/a	97
Assessment	non-linear	n/a	non-linear
Cook's D Influential Observations (Cook and Weisberg, 1982)			
obs# (Cook's D)	obs15 (0.268)	n/a	obs15 (0.276)
DFBETAS Influential Observations (Belsley et al., 1980)			
observation #	obs09 (-0.55,0.58)	n/a	obs09 (-0.56,0.60)
($DF\beta_N$, $DF\beta_K$)	obs15 (-0.86,0.88)	n/a	obs15 (-0.87,0.89)

A.5 Spring Problem Comparisons

The problem described in Example 3-3 of Vanderplaats (2001) is an unconstrained optimization problem involving a series of springs and weights. The optimization determines the (*x,y*)-coordinates of the weights such that the potential energy (*PE*) of the spring system is minimized. Vanderplaats (2001) presents solutions obtained via the Fletcher-Reeves (FRV), Steepest-Descent (STP) and Powell (PWL) methods, and Table A.4 compares these solutions to a variety of algorithms implemented in OSTRICH. In Table A.4, X_2 - X_5 and Y_2 - Y_5 are the optimized design variables, *PE* is the optimal objective function (potential energy), and "*Evals**" and "*Total*" are the number of required PE evaluations, which Vanderplaats reports without including the cost of one-dimensional searches. Gradient-based methods utilize a one-dimensional search procedure

at each step of the optimization process, and comparisons among different methods are confounded if different procedures are used.

The data in Table A.4 shows a close match between the Vanderplaats solutions and the equivalent OSTRICH gradient-based algorithms. The table also highlights the inefficiency of heuristic algorithms and underscores the importance of utilizing such methods only when gradient-based methods are found to be inadequate or inappropriate.

Table A.4: Spring-Weight Optimization: Algorithm Comparisons

	Vanderplaats			Ostrich					
	FRV	PWL	STP	FRV	PWL	STP	GA	PSO	SA
X_2	10.4	10.3	10.3	10.4	10.3	10.4	10.0	9.77	9.49
X_3	21.1	21.1	20.7	21.1	20.9	21.0	20.8	20.2	19.7
X_4	31.6	31.7	31.0	31.7	31.5	31.3	31.3	30.8	30.2
X_5	42.0	42.1	41.3	42.1	41.9	41.5	41.5	41.2	40.6
X_6	51.6	51.8	51.1	51.8	51.6	51.6	51.2	51.1	50.9
Y_2	-3.97	-4.28	-2.65	-4.06	-4.35	-2.46	-4.35	-4.83	-5.67
Y_3	-7.78	-7.90	-5.25	-7.79	-7.95	-4.87	-7.51	-8.35	-10.1
Y_4	-10.20	-9.86	-7.35	-9.96	-9.77	-6.90	-9.49	-9.28	-7.98
Y_5	-9.52	-9.40	-7.63	-9.43	-9.15	-7.66	-8.42	-8.12	-6.18
Y_6	-5.79	-6.01	-4.97	-6.03	-5.81	-5.51	-5.16	-4.91	-4.64
PE	-4393	-4416	-3964	-4411	-4410	-3871	-4318	-4212	-3420
Evals*	286	465	587	276	467	577	n/a	n/a	n/a
Total	unk	unk	unk	564	817	892	5,101	5,051	5,202
** : not counting one-dimensional search procedure*									

APPENDIX B: SUPPORTING INFORMATION FOR CHAPTER 4

Appendix B provides more information on the pump-and-treat cost and constraint formulations described in Chapter 4, as well as a list of acronyms. Throughout the appendix, numbers in parentheses following variable definitions correspond to the values used in the study of Chapter 4 and brackets following these numbers define the associated units. In cases where two numbers are provided, the first number applies to the control problem, and the second to the complex problem.

B.1 List Of Acronyms

AEM	analytic element method
APM	additive penalty method
CG	conjugate gradient algorithm
CG/AR	conjugate gradient algorithm, with initial parameters values randomly assigned
CG/EJ	conjugate gradient algorithm, with initial parameter values assigned based on engineering judgment and a limited number of manual trial-and-error runs
C_{OPER}	cost function that considers operational costs only (such as energy, treatment, disposal and labor costs)
C_{OPER+}	cost function that considers operational and capital (well installation and pump) costs
C_{TOTQ}	cost function that uses total pumping rate as a surrogate for cost
EPM	exponential penalty method
FD	finite difference
FD/FE	finite difference and finite element
FE	finite element

GA	genetic algorithm
HGHA	hydraulic gradient plume containment constraint formulation, using a high number of control points, distributed along the plume perimeter and computed analytically
HGHN	hydraulic gradient plume containment constraint formulation, using a high number of control points, distributed along the plume perimeter and computed numerically
HGLA	hydraulic gradient plume containment constraint formulation, using a low number of control points, distributed along the plume perimeter and computed analytically
HGLN	hydraulic gradient plume containment constraint formulation, using a low number of control points, distributed along the plume perimeter and computed numerically
HGMA	hydraulic gradient plume containment constraint formulation, using a medium number of control points, distributed along the plume perimeter and computed analytically
HGMN	hydraulic gradient plume containment constraint formulation, using a medium number of control points, distributed along the plume perimeter and computed numerically
MPI	message passing interface
MPM	multiplicative penalty method
PAT	pump-and-treat
PATO	pump-and-treat optimization
PSO	particle swarm optimization algorithm
PTHB	particle tracking plume containment constraint formulation, using a high number of particles distributed throughout the plume body
PTHP	particle tracking plume containment constraint formulation, using a high number of particles distributed along the plume perimeter
PTLB	particle tracking plume containment constraint formulation, using a low number of particles distributed throughout the plume body

PTLP particle tracking plume containment constraint formulation, using a low number of particles distributed along the plume perimeter

PTMB particle tracking plume containment constraint formulation, using a medium number of particles distributed throughout the plume body

PTMP particle tracking plume containment constraint formulation, using a medium number of particles distributed along the plume perimeter

P_{TOTAL} a penalty function that accounts for the cost of various constraint violations (drawdown, capacity and plume containment)

RND random search algorithm

SA simulated annealing algorithm

ZONE zone outflux plume containment constraint formulation

B.2 System Cost

Three cost functions were considered in this study: i) total pumping rate (C_{TOTQ}), ii) operational costs only (C_{OPER}), and iii) both operational and capital costs (C_{OPER+}). The equations for these costs are derived from the formulations provided in Mayer et al (2002) and RS Means ECHOS (2004).

B.2.1 Total pumping rate

Minimization of the total pumping rate is often used as a surrogate for a rigorous cost minimization objective. For problems in which the system will be operated in the long term, this approximation is often adequate because operational costs (which are largely a function of pumping rate) will dominate capital costs.

$$C_{TOTQ} = \alpha_{ext} \sum_{i=1}^{n_{ext}} \left| Q_{i,ext} \right| + \alpha_{inj} \sum_{i=1}^{n_{inj}} \left| Q_{i,inj} \right| \qquad \text{(B.1)}$$

where C_{TOTQ} is the cost as a function of total pumping rate; α_{ext} is a cost conversion factor for the total extraction rate (10.59, 53.98) [\$-day/m^3]; α_{inj} is a

cost conversion factor for the total injection rate (0.26, 1.59) [$-day/m^3]; n_{ext} is the number of extraction wells; n_{inj} is the number of injection wells; $Q_{i,ext}$ is the rate of extraction of the *i*th extraction well; and $Q_{i,inj}$ is the rate of injection of the *i*th injection well.

B.2.2 Operational costs

Pump-and-treat operational costs reflect the ongoing cost of operating the pump-and-treat system. Like the total pumping rate cost, operational costs do not account for capital costs, making this an appropriate cost function for long-term operations-dominated systems. Unlike the C_{TOTQ} formulation, the operational cost is a non-linear function of pumping rates (due to the additional consideration of lift), and may also be a function of the total number of wells (if maintenance, analytic and/or labor costs are included).

$$C_{OPER} = \left[C_L + C_E + C_A + C_D + C_M\right]T \tag{B.2}$$

where, C_{OPER} is the operational cost, C_L, C_E, C_A, C_D, and C_M are the annual labor, energy, analytic, disposal and maintenance costs, respectively; and T is the remediation time frame (5 and 30 years for the control and complex problems, respectively). To be consistent with the community problems Mayer et al (2002), only energy costs are considered in this paper (i.e. C_L=C_A=C_D=C_M=*0*), and the formulation of C_E is given in Equation B.3.

$$C_E = \beta_0 \sum_{i=1}^{n_{ext}} \left|Q_{i,ext}\right| \left(h_i - Z_{gs,i}\right) + \beta_1 \sum_{i=1}^{n_{inj}} \left|Q_{i,inj}\right| \tag{B.3}$$

where β_0 is the annualized energy cost conversion factor for extraction (0.11) [$-day/year-m4], β_1 is the annualized energy cost conversion factor for injection

(0.05) [$-day/year-m3], h_i is the head at extraction well i, and $Z_{gs,i}$ is the ground surface elevation at the i-th extraction well.

B.2.3 Operational and capital costs

Operational and capital costs account for fixed (one-time) installation costs as well as ongoing operational costs. As such, the formulation of C_{OPER+} adds capital cost terms to the operational cost defined previously.

$$C_{OPER+} = C_{OPER} + \beta_2(NW) + \beta_3(n_{ext}) \tag{B.4}$$

where, β_2 is the per-well drilling cost (15258, 13511) [$/well]; NW is the number of active wells; β_3 is the pump cost, assuming a design pumping rate of 553 m3/day (4028, 3832) [$/pump].

B.3 Constraints

The total constraint violation (P_{TOTAL}) is computed as the sum of the violations of the three types of constraints considered in this study, namely capacity (P_{CPCY}), drawdown (P_{DRAW}) and plume containment (P_{PLUME}).

$$P_{TOTAL} = P_{CPCY} + P_{DRAW} + P_{PLUME} \tag{B.5}$$

B.3.1 Capacity constraints

Capacity constraints reflect a limit on the total pumping rate that can be handled by an existing treatment system.

$$P_{CPCY} = \begin{cases} \beta_{CPCY}\left(Q_{tot} - Q_{\max}\right), & Q_{tot} > Q_{\max} \\ 0, & Q_{tot} \le Q_{\max} \end{cases} \tag{B.6}$$

where β_{CPCY} is the cost-conversion factor (dollars per L^3/T of excess) (100000) [$-day/$m^3$]; Q_{tot} is the net extraction rate (total extraction minus total injection); and Q_{max} is the maximum allowable extraction rate (2765, 3000) [m^3/day].

B.3.2 Drawdown constraints

Drawdown constraints prevent the pump-and-treat system from dewatering the aquifer, and are assessed by examining the head near each well. If the head near a given well is reduced (via pumping) below some minimum allowable head level, a penalty is assessed.

$$P_{DRAW} = \beta_{DRAW} \sum_{i=1}^{NW} \max\left(h_{\min} - h_i, 0\right) \tag{B.7}$$

where β_{DRAW} is the cost-conversion factor (dollars per length of excess) (100000) [$/m]; and h_{min} is the minimum allowable head (10, 1.5) [m].

B.3.3 Plume containment constraints

Plume containment constraints use flow-model output to gauge the effectiveness of a given well-field design at controlling plume migration. Each experiment in this study considered one of three plume containment constraints: hydraulic gradient control, particle tracking, or zone outflux.

$$P_{PLUME} = \beta_{HGRAD} \sum_{i=1}^{m} P_{HGRAD,i} + \beta_{PTRK} \sum_{i=1}^{n} P_{PTRK,i} + \beta_{ZONE} P_{ZONE} \tag{B.8}$$

where, β_{HGRAD}, β_{PTRK}, and β_{ZONE} arecost-conversion factors (100000) [$/m, $/m^2, $-day/m^3]; m is the number of gradient control constraints; n is the number of particle tracking constraints; $P_{HGRAD,i}$ is the penalty of the ith gradient control constraint; $P_{PTRK,i}$ is the penalty of the ith particle tracking constraint; and P_{ZONE} is the zone outflux penalty.

B.3.3.1 *Gradient control constraints*

Gradient control constraints examine the head gradient at a given control location, and assess a penalty if the gradient is oriented away from the plume

interior. For numerical gradient computations, a pair of control points, one outside and one inside the plume is considered, and the constraint requires that the head outside the plume be greater than the head inside the plume, implying flow direction is towards the plume interior.

$$\begin{aligned} P_{HGRAD,i} &= \max\left(0, h_{in,i} - h_{out,i}\right) \quad \text{if numerical} \\ P_{HGRAD,i} &= \max\left(0, dh_i\right) \qquad\qquad \text{if analytic} \end{aligned} \tag{B.9}$$

Where, $h_{in,i}$ and $h_{out,i}$ are the inside and outside head of the ith control pair and dh_i is the analytically computed gradient at the ith control location (a positive value of dh_i indicates flow away from the plume, and results in a constraint violation).

B.3.3.2 *Particle tracking constraints*

Particle tracking constraints advect a given particle from an initial location within the plume body or along the plume perimeter. If the particle is not within the plume boundary or captured by a well at the conclusion of the remediation time frame, then a penalty is assessed.

$$P_{PCAP,i} = \begin{cases} d_i^{\,2}, \text{particle}_\text{i} \text{ outside plume} \\ 0 \quad , \text{particle}_\text{i} \text{ inside plume} \end{cases} \tag{B.10}$$

Where d_i is the distance from the particle to the plume boundary.

B.3.3.3 *Zone outflux constraints*

The zone outflux constraint examines the total outflux (F_{ZFP}^{+} , as defined in Equation 4.3) across the perimeter of the plume and assigns a penalty if this outflux is non-zero.

$$P_{ZONE} = \max\left(F_{ZFP}^{+}, 0\right) \tag{B.11}$$

B.3.4 Objective functions

The functional forms of the additive (F_{APM}), multiplicative (F_{MPM}) and exponential (F_{EPM}) penalty methods, as applied in this study, are given below.

$$F_{APM}\left(NW,\overline{Q},\overline{X},\overline{Y}\right)=Cost+P_{TOTAL} \tag{B.12}$$

$$F_{MPM}\left(NW,\overline{Q},\overline{X},\overline{Y}\right)=\max\left(Cost,P_{TOTAL}\right)\left(1+P_{TOTAL}\right) \tag{B.13}$$

$$F_{EPM}\left(NW,\overline{Q},\overline{X},\overline{Y}\right)=\max\left(Cost,P_{TOTAL}\right)\exp\left(P_{TOTAL}\right) \tag{B.14}$$

where $\overline{Q}=[Q_1,Q_2,...Q_{NW}]^T$ is a vector of pumping rates; $\overline{X}=[x_1,x_2,...x_{NW}]^T$ is a vector of x-coordinates; $\overline{Y}=[y_1,y_2,...y_{NW}]^T$ is a vector of y-coordinates; and *Cost* is one of C_{TOTQ}, C_{OPER} or C_{OPER+}.

B.4 Parameter Bounds

Tables B.1 and B.2 provide parameter bounds used in solving the PATO problems.

Table B.1: Control Problem Parameter Bounds

Parameter	Min value	Max value	Units
Q_i	-553	553	m^3/day
X_i	189	328	m
Y_i	495	769	m
NW	1	5	n/a

Table B.2: Complex Problem Parameter Bounds

Parameter	Min value	Max value	Units
Q_i	0	550	m^3/day
X_i	1112	1624	m
Y_i	1619	2031	m
NW	1	19	n/a

APPENDIX C: SUPPORTING INFORMATION FOR CHAPTER 5

C.1 Multi-Layer Sorptive Landfill Liner Optimization

In general, landfill leachate is composed of one or more contaminants that have a range of sorptive and chemical properties. As shown in Figure C.1, leachate transport is mitigated by a sequence of one or more layers that form the landfill liner. The goal of liner design is to determine the liner configuration that minimizes leachate transport (preventing migration to human and/or animal receptors) at the lowest financial cost. In such problems, design variables include the number, ordering, and material composition of the layers; and in the considered problems, multiple sorptive layer amendments were considered.

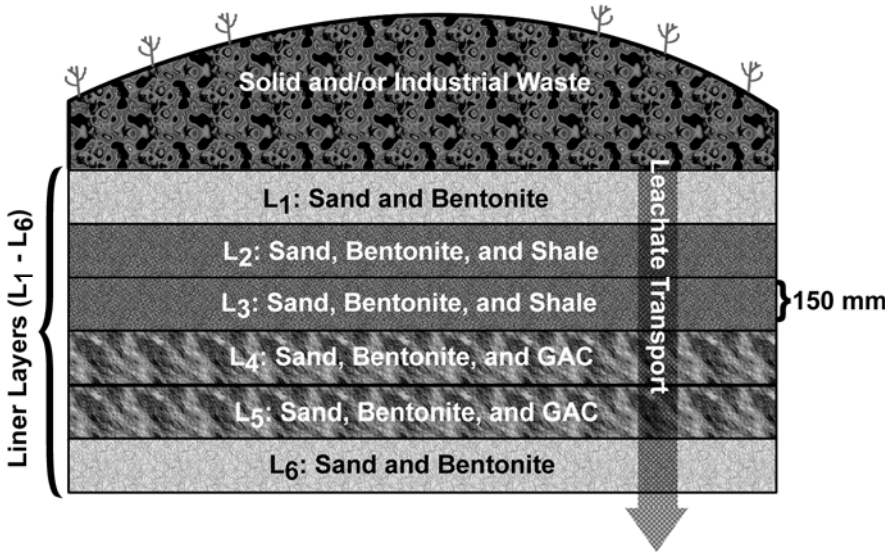

Figure C.1: Example multi-layered sorptive landfill liner design

C.2 Taguchi DOE Method

Figure C.2 contains example factor interaction plots. In Figure C.2a, factors A and B interact and the optimal factor-level settings would be A_2 and B_2, corresponding to the peak point of the four interaction lines. In Figure C.2b, none

of the lines intersect, suggesting that no interaction is occurring. In this case, the optimal factor-level settings for C and E would be assigned using main-effects analysis.

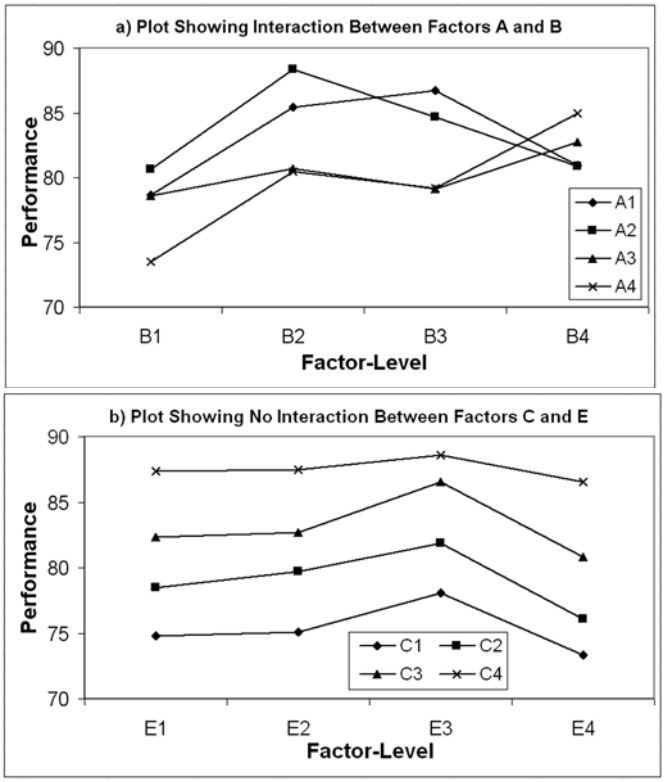

Figure C.2: Illustrative factor interaction plots.
(a) plot showing interaction between Factors A and B,
(b) plot showing no interaction between Factors C and E

C.3 Views of the Design Space

A primary justification for the use of heuristic (global search) algorithms to solve the considered multi-layer sorptive landfill liner problems is the presence of multiple local minima, as illustrated by the one-dimensional slices of design space plotted in Figure C.3.

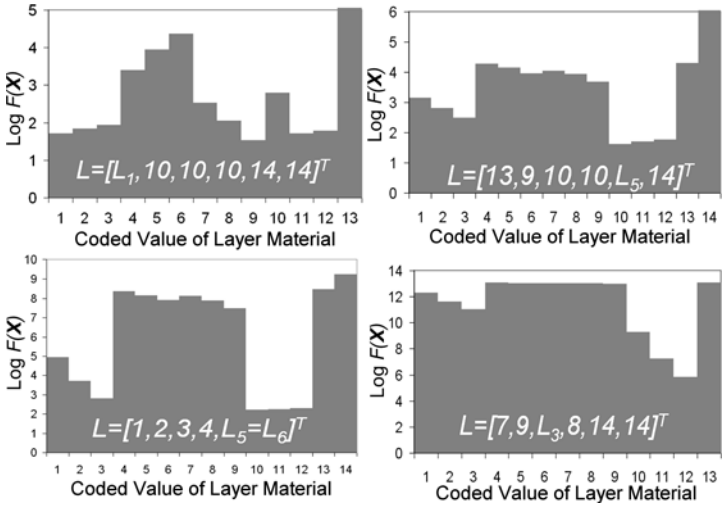

Figure C.3: One dimensional slices of the design space, highlighting the non-linear and discrete-valued nature of the sorptive barrier problem, as formulated in this study.

C.4 Solute Transport Model

The movement of leachate through a multi-layered sorptive landfill liner can be modeled as transient one-dimensional solute transport through low-permeability sorptive material(s). Assuming equilibrium sorption, the governing advective-dispersive-reactive (ADR) equation for transport of a single solute through a single layer is given in Equation C.1.

$$\frac{\partial C}{\partial t} = -v\frac{\partial C}{\partial z} + D\frac{\partial^2 C}{\partial z^2} - \frac{\rho_b}{n}\frac{\partial S}{\partial t} \tag{C.1}$$

where C is the aqueous phase leachate (either TCE, Benzene, or 1,2-DCB, depending on liner problem) concentration [mg/L], t is time [s], z is the distance from the top of the layer [m], v is the fluid velocity [m/s], D is the dispersion coefficient, incorporating both hydrodynamic dispersion and molecular diffusion [m^2/s], ρ_b is the bulk dry density of the layer material [kg/m^3], n is the porosity of the layer material [dimensionless], and S is the sorbed phase leachate concentration [mg/kg]. As written, the ADR equation contains two unknowns

(aqueous and sorbed concentrations) and isotherm expressions describing the partitioning of solute between these two phases are used to close the system. For a given combination of sorptive amendment and solute, isotherm selection (e.g. Langmuir, Freundlich or Linear) and configuration of relevant isotherm parameters is accomplished by regression against experimental data, as reported in Bartelt-Hunt et al. (2005). When multiple layers consisting of different sorptive material compositions are considered, the sorption isotherms and parameters are spatially variable and numerical solution of the ADR equations is required. Therefore, leachate transport was solved numerically using a version of the MOUSER (Rabideau, 2003) software, modified to support multiple layers. The following boundary and initial conditions were applied: the top of the liner was treated as a constant 10 mg/L source of leachate while the concentration just below the liner and the initial concentration within the liner were set to 0 mg/L. Usage of a zero concentration boundary below the liner induces a maximum diffusive gradient, corresponding to a worst-case transport scenario in a diffusion-dominated system, and results in conservative liner designs (Rabideau and Khandelwal, 1998). Due to differences in the material properties of their respective contaminants (benzene, 1,2-DCB or TCE), the three considered problems yielded different optimal liner configurations. Relevant characteristics of these contaminants are: sorption behavior with respect to each sorptive amendment (defined in terms of empirical isotherm parameters), solubility, and liquid diffusion coefficient. Assumed values for these

characteristics were taken from previously published studies (Bartelt-Hunt et al, 2005 and in press).

C.5 Overview of Experimental Setup

Figure C.4 provides an overview of the numerical experiments performed in the study. As shown in the figure, a given heuristic algorithm searched for the optimal liner design by performing repeated executions of a solute transport model. Transport output was forwarded to a constraint-integration step that determined whether the given design violated constraints, in which case the design was considered infeasible and a penalty was assessed to the overall liner cost. Overarching the optimization process was a set of Taguchi DOE tuning experiments, where analysis of algorithm performance provided the optimal configuration of algorithm and penalty parameters. After completing the DOE experiments, tuned algorithms were utilized in a set of confirmation optimizations and these results facilitated a rigorous comparison and evaluation of the various algorithms with respect to each of the three organic solutes.

C.6 Summary of Numerical Experiments

Transport simulation was performed using an explicit finite-difference time-step formulation coupled with an operator splitting technique, and in which each layer is spatially discretized into 10 grid cells. Equilibrium sorption was assumed in all simulations, and a typical simulation of 100 years of leachate transport required 0.8 seconds of computation time and had a mass balance error of less than 5%. All optimizations were performed using OSTRICH (Matott, 2005) and experiment samples were run in parallel on Linux-based computing clusters

maintained by the University at Buffalo Center for Computational Research (CCR). Access to the CCR clusters is via a Portable Batch System (PBS) resource manager and Maui scheduler, and programs are parallelized using the industry standard Message Passing Interface (MPI) specification (Gropp et al, 1999). The utilized clusters consist of 32 1-GHz Intel Pentium III processors with 256-kB cache and 1-GB of 32-bit wide RAM, and 24 3.2-GHz Intel Pentium IV processors with 1-MB cache and 4-GB of 64-bit wide RAM. All processors run version 7.3 of the Red Hat Linux operating system. These parallel clusters were also utilized to perform an exhaustive search of the design space of all three problems, a process that established 'true' optimality for each of the considered problems.

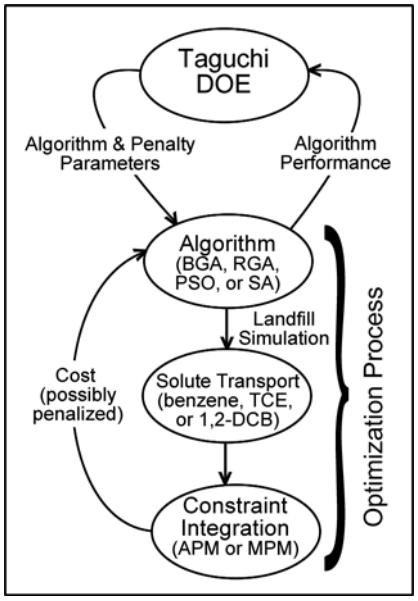

Figure C.4: Overview of the Experimental Setup. (DOE = design of experiments, BGA = binary-coded genetic algorithm, RGA = real-coded genetic algorithm, PSO = particle swarm optimization, SA = simulated annealing, TCE = trichloroethylene, DCB = dichlorobenzene, APM = additive penalty method, MPM = multiplicative penalty method)

C.7 Results

Table C.1 summarizes the optimal parameter settings and corresponding optimal performance for each algorithm and solute type.

Table C.1: Summary of tuned parameter settings

Binary-Coded Genetic Algorithm									
Solute	Penalty Method	Penalty Weight	Pop. Size	Number of Generations	Number of Elites	Mutation Rate	Perform-ance	System Cost ($/m2)	MOUSER Runs
Benzene	MPM	$1/ug	100	100	3	15%	95.00	$34.27	10,100
1,2-DCB	APM	$1/ug	50	20	3	15%	99.38	$16.66	1,050
TCE	APM	$1/ug	50	50	3	15%	98.55	$8.66	2,550
Real-Coded Genetic Algorithm									
Solute	Penalty Method	Penalty Weight	Population Size	Number of Generations	Number of Elites	Mutation Rate	Perform-ance	System Cost	MOUSER Runs
Benzene	MPM	$1/ug	50	50	3	15%	89.68	$41.86	2,550
1,2-DCB	MPM	$1/ug	100	50	3	15%	97.37	$16.66	5,100
TCE	MPM	$1/ug	50	50	3	15%	87.16	$16.26	2,550
Particle Swarm Optimization									
Solute	Penalty Method	Penalty Weight	Swarm Size	Number of Generations	Inertia Weight	Cognitive Weight	Social Weight	Perform-ance	System Cost	MOUSER Runs
Benzene	APM	$1/ug	100	100	2	4	1	90.55	$38.00	10,100
1,2-DCB	MPM	$1/ug	50	20	2	1	4	99.48	$16.66	1,050
TCE	APM	$1/ug	100	50	2	4	4	97.39	$8.66	5,100
Simulated Annealing									
Solute	Penalty Method	Penalty Weight	Equilibration Steps	Temperature Reductions	Melting Trials	Cooling Rate		Perform-ance	System Cost	MOUSER Runs
Benzene	MPM	$10/ug	50	100	20	20%		88.27	$41.98	5,120
1,2-DCB	APM	$10/ug	50	100	20	20%		97.36	$16.66	5,120
TCE	APM	$1/ug	20	100	50	50%		87.36	$16.26	2,150

Table C.2 compares the tuning and main-effects confirmation runs against ANOVA-generated lower confidence limits on predicted performance. Figure C.5 compares the number of feasible designs having 4, 5, and 6 active layers, for each of the landfill liner design problems (distinguished by the type of organic solute).

Table C.2: Comparison of tuning results against lower confidence limit on predicted performance. Y_{main} and Y_{inter} are the confirmation performances of the main-effects and interaction tuning procedures, respectively, and Y_{LCL} is the lower confidence limit of the tuned performance.

Leachate Composition	Algorithm	Penalty Method	Y_{main}	Y_{inter}	Y_{LCL}	$Y_{main} > Y_{LCL}$?	$Y_{inter} > Y_{LCL}$?
Benzene	BGA	APM	90.00	95.00	92.95	no	yes
		MPM	90.00	95.00	90.19	no	yes
	PSO	APM	90.00	90.55	73.53	yes	yes
		MPM	86.09	90.09	82.70	yes	yes
	RGA	APM	81.02	88.73	84.49	no	yes
		MPM	80.77	89.68	83.38	no	yes
	SA	APM	88.42	88.88	93.68	no	no
		MPM	83.99	88.27	81.61	yes	yes
1,2-DCB	BGA	APM	98.66	99.38	83.16	yes	yes
		MPM	97.45	99.18	92.08	yes	yes
	PSO	APM	97.48	98.95	87.73	yes	yes
		MPM	98.68	99.48	89.36	yes	yes
	RGA	APM	94.84	97.27	91.38	yes	yes
		MPM	94.84	97.37	90.95	yes	yes
	SA	APM	97.05	97.36	95.34	yes	yes
		MPM	89.94	97.20	91.53	no	yes
TCE	BGA	APM	97.83	98.55	95.96	yes	yes
		MPM	87.80	99.10	100.68	no	no
	PSO	APM	94.95	97.39	92.12	yes	yes
		MPM	94.65	97.30	83.77	yes	yes
	RGA	APM	85.72	87.16	84.08	yes	yes
		MPM	85.71	87.16	87.01	no	yes
	SA	APM	83.41	87.36	82.75	yes	yes
		MPM	83.37	87.72	82.06	yes	yes
					Total	16	22
					Within	67%	92%

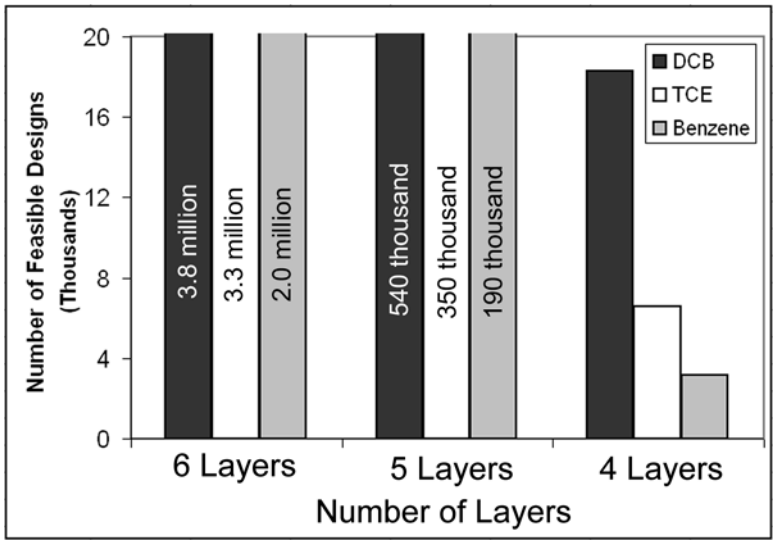

Figure C.5: Feasible solutions as a function of the number of active layers

APPENDIX D: SUPPORTING INFORMATION FOR CHAPTER 6

For the fully-kinetic reaction formulation considered in Chapter 6, the expressions that make up the system of ordinary differential equations take the form given in Equation D.1:

$$\frac{\partial[C_i]}{\partial t} = \sum_{j=1}^{58} (-1)^a b R_j \tag{D.1}$$

where, a is 0 if species C_i is a reactant in reaction R_j, or 1 if C_i is a product in R_j, b is the stoichiometric coefficient of C_i in R_j (or 0 if C_i does not appear in R_j), and R_j corresponds to the rate expression of the j-th reaction, numbered in accordance with the reaction network given in Table 6.1. In Equation D.1, C_i is an element of **C**, a vector of up to 65 rate-dependent species concentrations:

$$\mathbf{C}^{\mathrm{T}} = \begin{bmatrix} [H^+],[OH^-],[Fe^{2+}],[Fe(OH_3)(s)],[Mn^{2+}],[MnO_2(s)],[CO_2], \\ [HCO_3^-],[CO_3^{2-}],[Ca^{2+}],[Cl^-],[K^+],[Mg^{2+}],[Na^+],[CaCO_3], \\ [CaHCO_3^+],[MgCO_3],[MgHCO_3^+],[NaCO_3^-],[NaHCO_3],[O_2], \\ [CH_2O],[CH_2O(ads)],[NH_4^+],[NO_3^-],[HS^-],[SO_4^{2-}],[HSO_4^-], \\ [CaSO_4],[MgSO_4],[NaSO_4^-],[KSO_4^-],[FeOH^+],[FeCO_3], \\ [FeHCO_3^+],[FeSO_4],[MnCl^+],[MnCO_3],[MnHCO_3^+],[MnSO_4], \\ [H_2S],[S^{2-}],[S^0],[NH_3],[N_2],[CaCO_3(s)],[FeCO_3(s)], \\ [MnCO_3(s)],[CaSO_4(H_2O)_2(s)],[FeS(s)],[NaX],[KX], \\ [CaX_2],[MgX_2],[\equiv HFO^sO^-],[\equiv HFO^sOFe^+],[\equiv HFO^sOH], \\ [\equiv HFO^sOH_2^+],[\equiv HFO^sOMn^+],[\equiv HFO^wO^-],[\equiv HFO^wOFe^+], \\ [\equiv HFO^wOFeOH],[\equiv HFO^wOH],[\equiv HFO^wOH_2^+],[\equiv HFO^wOMn^+] \end{bmatrix} \tag{D.2}$$

Note that in the transport model, only the following 12 species were considered: H^+, OH^-, CO_2, HCO_3^-, CO_3^{-2}, DOC, O_2, NO_3^-, N_2, Ca^{+2}, Mg^{+2}, and Cl^-.

D.1 Microbially-mediated Reactions

Rate expressions for the microbially-mediated reactions (R_1 through R_5), depend on the level of model complexity and are of the form:

$$R_j = \phi_j \, k^j_{\max}\left(\frac{[CH_2O]}{k^j_S + [CH_2O]}\right)\left(\frac{[E_j]}{k^j_E + [E_j]}\right), \text{or} \tag{D.3a}$$

$$R_j = \phi_j \, k^{'j}_{\max}\left(\frac{[E_j]}{k^{'j}_E + [E_j]}\right), \text{or} \tag{D.3b}$$

$$R_j = \phi_j \, k_j [E_j], \text{or} \tag{D.3c}$$

$$R_j = \phi_j \, k_{,j} \tag{D.3d}$$

where, R_j is a rate expression for the j-th microbial reaction using a dual-Monod (D.3a), single-Monod (D.3b), first-order (D.3c), or zero-order formulation (D.3d), $[E_j]$ is the electron acceptor concentration, such that $\mathbf{E}^{\mathbf{T}} = \left[[O_2],[NO_3^-],[MnO_2(s)],[Fe(OH)_3(s)],[SO_4^{2-}]\right]$, $k^j_{\max}$, k^j_S, and k^j_E are multiple-Monod parameters, $k^{'j}_{\max}$ and $k^{'j}_E$ are single Monod-parameters, k_j is a first order biodegradation rate, k_j is a zero-order biodegradation rate, and ϕ_j is an inhibition function which enforces a sequential utilization of electron acceptors. The inhibition functions are given below:

$$\phi_2 = \begin{cases} 0, \text{ if } [O_2] \geq 0.5 \text{ mg/L} \\ \phi_1 = 1, \text{otherwise} \end{cases} \tag{D.4}$$

$$\phi_3 = \begin{cases} 0, \text{ if } [NO_3^-] \geq 0.5 \text{ mg/L} \\ \phi_2, \text{otherwise} \end{cases} \tag{D.5}$$

$$\phi_4 = \begin{cases} 0, \text{ if } [MnO_2(s)] \geq 0.5 \text{ ppm} \\ \phi_3, \text{otherwise} \end{cases} \tag{D.6}$$

$$\phi_5 = \begin{cases} 0, \text{ if } [Fe(OH)_3(s)] \geq 0.5 \text{ ppm} \\ \phi_4, \text{otherwise} \end{cases} \quad \text{(D.7)}$$

D.2 Inorganic Redox Reactions

Complex rate expressions for the inorganic redox reactions (R_6 through R_{12}) are of the form given in Equation 6.15 of the manuscript. A full elaboration of the resulting equations is given below:

$$R_6 = k_6[Mn^{2+}][O_2] \quad \text{(D.8)}$$

$$R_7 = k_7[Fe^{2+}][O_2] \quad \text{(D.9)}$$

$$R_8 = k_8[Fe^{2+}][MnO_2(s)] \quad \text{(D.10)}$$

$$R_9 = k_9[O_2][H_2S] \quad \text{(D.11)}$$

$$R_{10} = k_{10}[O_2][FeS(s)] \quad \text{(D.12)}$$

$$R_{11} = k_{11}[H_2S][MnO_2(s)] \quad \text{(D.13)}$$

$$R_{12} = k_{12}[H_2S][Fe(OH)_3(s)] \quad \text{(D.14)}$$

D.3 Aqueous Equilibrium Chemistry

Rate expressions for aqueous equilibrium chemistry (R_{13} through R_{37}), are of the form given in Equation D.15:

$$R_j = k_j^f \prod_{l=1}^{LHS_j} [A_{l,j}]^{c_{l,j}} - k_j^b \prod_{r=1}^{RHS_j} [A_{r,j}]^{c_{r,j}} \quad \text{(D.15)}$$

where, k_j^f and k_j^b are the respective forward and backward rate constants for the j-th reaction, LHS_j and RHS_j are the respective number of species on the left-hand and right-hand sides of reaction j, as written in Table 6.1, $[A_{l,j}]$ is the concentration of the l-th left-hand side species in R_j, which has stoichiometric

coefficient $c_{l,j}$, and $[A_{r,j}]$ is the concentration of the r-th right-hand side species in R_j, which has stoichiometric coefficient $c_{r,j}$.

D.4 Mineral Precipitation and Dissolution

Rate expressions for mineral precipitation and dissolution (R_{38} through R_{42}), are of the form given in Equation D.16:

$$R_j = \phi_j \left(k_j^f - k_j^b \prod_{r=1}^{RHS_j} [A_{r,j}] \right) \tag{D.16}$$

where, k_j^f and k_j^b are the respective forward and backward rate constants for the j-th reaction, RHS_j is the number of dissolution species for reaction j, $[A_{r,j}]$ is the concentration of the r-th dissolution species in R_j, and ϕ_j is an inhibition term that disables the reaction if conditions are unsaturated and the solid phase material of R_j is not present.

D.5 Linear Partitioning

The rate expression for organic carbon partitioning (R_{43}) is given in Equation D.17.

$$R_{43} = k_{43}^f [CH_2O(ads)] - k_{43}^b [CH_2O] \tag{D.17}$$

D.6 Surface Complexation

Rate expressions for surface complexation reactions (R_{44} through R_{52}), are of the form given in Equation D.18:

$$R_j = \frac{k_j^f}{\psi^{(|dz_j|+dz_j)/|2dz_j|}} \prod_{l=1}^{LHS_j} \{A_{l,j}\} - \frac{k_j^b}{\psi^{(|dz_j|-dz_j)/|2dz_j|}} \prod_{r=1}^{RHS_j} \{A_{r,j}\} \tag{D.18}$$

where, k_j^f and k_j^b are the respective forward and backward rate constants for the j-th reaction, ψ is the activity of the surface potential (computed using Equation

D.21), dz_j is the net change in surface charge resulting from reaction *j* as it proceeds from left-to-right, as expressed in Table 6.1, LHS_j and RHS_j are the respective number of species on the left-hand and right-hand sides of reaction *j*, as written in Table 6.1, $\{A_{l,j}\}$ is the activity of the *l*-th left-hand side species in R_j, and $\{A_{r,j}\}$ is the activity of the *r*-th right-hand side species in R_j. If a given $A_{l,j}$ or $A_{r,j}$ is an aqueous-phase constituent, then the activity equals the concentration ($\{A\} = [A]$), otherwise, for surface components, the activity is the mole fraction of the given surface site-type that is occupied (e.g. $[\equiv HFO^wOH]/[TOT \equiv HFO^w]$, $[\equiv HFO^sO^-]/[TOT \equiv HFO^s]$, etc., where expressions for $[TOT \equiv HFO^w]$ and $[TOT \equiv HFO^s]$ are given in Equations D.19 and D.20). Note that the exponents of the ψ terms are such that positive values of *dz* match $1/\psi$ with k_j^f, while negative values match $1/\psi$ with k_j^b.

$$[TOT \equiv HFO^w] = \begin{pmatrix} [\equiv HFO^wOH] + [\equiv HFO^wOH_2^+] + [\equiv HFO^wOFe^+] \\ + [\equiv HFO^wO^-] + [\equiv HFO^wOFeOH] + [\equiv HFO^wOMn^+] \end{pmatrix} \quad \text{(D.19)}$$

$$[TOT \equiv HFO^s] = \begin{pmatrix} [\equiv HFO^sOH] + [\equiv HFO^sOH_2^+] + [\equiv HFO^sOFe^+] \\ + [\equiv HFO^sO^-] + [\equiv HFO^sOMn^+] \end{pmatrix} \quad \text{(D.20)}$$

For surface complexation reactions, the activity of the surface potential (ψ) is computed using Equation D.21 and is a function of solution temperature (*T*, degrees Kelvin), the ionic strength of the solution (*I*), and the charge density of the surface (σ).

$$\psi = \exp\left(2\,\text{arcsinh}\left(\frac{\sigma}{\sqrt{8000 \times e \times e_0 \times R \times T \times I}}\right)\right) \quad \text{(D.21)}$$

where, e is the dielectric constant of water (78.5), e_0 is the permittivity of free space ($8.854\times10_{-12}$ C^2/m-J), R is the gas constant (8.314 J/mol-K), and σ is computed using Equation D.22:

$$\sigma = \frac{F}{SA_{HFO}}\begin{pmatrix}[\equiv HFO^{w}OH_2^+]+[\equiv HFO^{w}OFe^+]-[\equiv HFO^{w}O^-] \\ +[\equiv HFO^{w}OMn^+]+[\equiv HFO^{s}OH_2^+]+[\equiv HFO^{s}OFe^+] \\ -[\equiv HFO^{s}O^-]+[\equiv HFO^{s}OMn^+]\end{pmatrix} \quad \text{(D.22)}$$

where, F is the Faraday constant (96493.5 C/mol), and SA_{HFO} is the surface area of the surface complex material (m^2), and the term in parentheses is the net charge of the surface material, summed over both the weak and strong surface sites.

D.7 Ion Exchange

Rate expressions for ion exchange reactions (R_{52} through R_{58}), are of the form given in Equation D.23:

$$R_j = k_j^f \prod_{l=1}^{LHS_j}\{A_{l,j}\}^{c_{l,j}} - k_j^b \prod_{r=1}^{RHS_j}\{A_{r,j}\}^{c_{r,j}} \quad \text{(D.23)}$$

where, k_j^f and k_j^b are the respective forward and backward rate constants for the j-th reaction, LHS_j and RHS_j are the respective number of species on the left-hand and right-hand sides of reaction j, as written in Table 6.1, $\{A_{l,j}\}$ is the activity of the l-th left-hand side species in R_j, which has stoichiometric coefficient $c_{l,j}$, and $\{A_{r,j}\}$ is the activity of the r-th right-hand side species in R_j, which has stoichiometric coefficient $c_{r,j}$. If a given $A_{l,j}$ or $A_{r,j}$ species is an aqueous-phase constituent, then activity equals concentration ($\{A\} = [A]$), otherwise, for exchange components, activity is the equivalent fraction of the given exchange species

(e.g. $[NaX]/[CEC]$, $[KX]/[CEC]$, $2\times[CaX_2]/[CEC]$, or $2\times[MgX_2]/[CEC]$, where [*CEC*] is computed using Equation D.24.

$$[CEC] = 2[MgX_2] + 2[CaX_2] + [NaX] + [KX] \quad \text{(D.24)}$$

D.8 Equilibrium Reaction Rates

Forward and backward reaction rates (in $\log_{10}$ units) for all equilibrium reactions (R_{13}-R_{58}) are given in Table D.1.

Table D.1: Equilibrium Reaction Rates

Rate	Value ($\log_{10}$)	Rate	Value ($\log_{10}$)	Rate	Value ($\log_{10}$)	Rate	Value ($\log_{10}$)
k_{13}^f	0.000 *	k_{25}^f	3.224	k_{37}^f	9.252	k_{49}^f	2.518
k_{13}^b	14.000 *	k_{25}^b	0.000	k_{37}^b	0.000	k_{49}^b	-4.772
k_{14}^f	10.329 *	k_{26}^f	11.435	k_{38}^f	0.000 *	k_{50}^f	-4.772
k_{14}^b	0.000 *	k_{26}^b	0.000	k_{38}^b	8.480 *	k_{50}^b	4.158
k_{15}^f	6.352 *	k_{27}^f	2.980	k_{39}^f	0.000	k_{51}^f	0.228
k_{15}^b	0.000 *	k_{27}^b	0.000	k_{39}^b	11.130	k_{51}^b	1.178
k_{16}^f	0.000	k_{28}^f	11.399	k_{40}^f	0.000	k_{52}^f	0.228
k_{16}^b	6.994	k_{28}^b	0.000	k_{40}^b	10.890	k_{52}^b	0.628
k_{17}^f	0.000	k_{29}^f	1.270	k_{41}^f	0.000	k_{53}^f	0.700
k_{17}^b	12.918	k_{29}^b	0.000	k_{41}^b	16.833	k_{53}^b	0.000
k_{18}^f	1.988	k_{30}^f	0.250	k_{42}^f	0.000	k_{54}^f	0.800
k_{18}^b	0.000	k_{30}^b	0.000	k_{42}^b	4.580	k_{54}^b	0.000
k_{19}^f	2.300	k_{31}^f	0.000	k_{43}^f	0.000	k_{55}^f	0.600
k_{19}^b	0.000	k_{31}^b	9.500	k_{43}^b	2.019	k_{55}^b	0.000
k_{20}^f	2.370	k_{32}^f	4.380	k_{44}^f	4.120	k_{56}^f	0.600
k_{20}^b	0.000	k_{32}^b	0.000	k_{44}^b	-3.170	k_{56}^b	0.000
k_{21}^f	0.700	k_{33}^f	2.000	k_{45}^f	-2.170	k_{57}^f	0.800
k_{21}^b	0.000	k_{33}^b	0.000	k_{45}^b	0.810	k_{57}^b	0.000
k_{22}^f	0.850	k_{34}^f	0.610	k_{46}^f	-3.170	k_{58}^f	0.200
k_{22}^b	0.000	k_{34}^b	0.000	k_{46}^b	5.760	k_{58}^b	0.000

Rate	Value (log_{10})	Rate	Value (log_{10})	Rate	Value (log_{10})	Rate	Value (log_{10})
k_{23}^{f}	2.250	k_{35}^{f}	4.900	k_{47}^{f}	-3.170		
k_{23}^{b}	0.000	k_{35}^{b}	0.000	k_{47}^{b}	5.400		
k_{24}^{f}	2.250	k_{36}^{f}	1.950	k_{48}^{f}	-3.170		
k_{24}^{b}	0.000	k_{36}^{b}	0.000	k_{48}^{b}	0.330		

Rates were assigned such that K_f/K_b are consistent with Parkhurst and Appelo (1999)
* - reaction and corresponding rate were used in the transport model

D.9 "True" Kinetic Reaction Rates

Reaction rates of the kinetic terms (R_1-R_{12}) that were assigned to the "true" model and utilized to generate synthetic observation data are given in Table D.2.

Table D.2: Kinetic Reaction Rates of the "True" Models (only the first column of rates applies to the transport model)

Rate	Value (log_{10})	Rate	Value (log_{10})	Rate	Value (log_{10})	Rate	Value (log_{10})
$k_{\max}^{1}$	-10.638 [a]	$k_{\max}^{3}$	-10.437 [a]	$k_{\max}^{5}$	-10.823 [b]	k_9	-2.295 [c]
k_S^{1}	-5.000 [a]	k_S^{3}	-5.000 [a]	k_S^{5}	-3.699 [b]	k_{10}	-2.721 [c]
k_E^{1}	-4.801 [a]	k_E^{3}	-6.400 [a]	k_E^{5}	-3.495 [b]	k_{11}	-3.198 [c]
$k_{\max}^{2}$	-10.738 [a]	$k_{\max}^{4}$	-10.437 [a]	k_6	-0.499 [c]	k_{12}	-3.596 [c]
k_S^{2}	-5.000 [a]	k_S^{4}	-5.000 [a]	k_7	-0.499 [c]		
k_E^{2}	-4.801 [a]	k_E^{4}	-4.801 [a]	k_8	-4.499 [c]		

Literature sources
[a] – Abrams and Loague (2000), [b] – Watson et al. (2003) , [c] – Hunter et al. (1998)

REFERENCES

Abrams RH, Loague K. 2000. A compartmentalized solute transport model for redox zones in contaminated aquifers, 2. Field-scale simulations, *Water Resources Research*, vol. 36, no. 8, pg. 2015-2029.

Ahlfeld DP, Page RH, Pinder GF. 1995. Optimal ground-water remediation methods applied to a superfund site: From formulation to implementation. *Ground Water*, vol. 33, no. 1, pg. 58-70.

Ahlfeld DP, Sprong MP. 1998. Presence of Non-Convexity in Groundwater Concentration Response Functions. *Journal of Water Resources Planning and Management*, vol. 124, no. 1, pg. 8-14.

Aly AH, Peralta RC. 1999. Comparison of a genetic algorithm and mathematical programming to the design of groundwater cleanup systems. *Water Resources Research*, vol. 35, no. 8, pg. 2415-2425.

Atwood DF, Gorelick SM. 1985. Hydraulic gradient control for groundwater contaminant removal. *Journal of Hydrology*, vol. 76, pg. 85-106.

Bakker M. 2004. "Tim^{ML}: A Multiaquifer Analytic Element Model, version 2.1", University of Georgia, Athens, GA (available from www.engr.uga.edu/~mbakker/TimML.html).

Balas E. 1968. A note on the branch-and-bound principle. *Operations Research*, vol. 16, pg. 442-444.

Barcelona MJ, Holm TR. 1991. Oxidation-reduction capacities of aquifer solids, *Environmental Science and Technology*, vol. 25, no. 9, pg. 565-1572.

Barry DA, Prommer H, Miller CT, Engesgaard P, Brun A, Zheng C. 2002. Modelling the fate of oxidisable organic contaminants in groundwater. *Advances in Water Resources*, vol. 25, pg. 945-983.

Bartelt-Hunt SL, Culver TB, Smith JA, Matott LS, Rabideau AJ. in press. Optimal Design of a Compacted Soil Liner Containing Sorptive Amendments. *Journal of Environmental Engineering.*

Bartelt-Hunt SL, Smith JA, Burns SE, Rabideau AR. 2005. Evaluation of granular activated carbon, shale and two organoclays for use as sorptive amendments in clay landfill liners. *Journal of Geotechnical and Geoenvironmental Engineering*, DOI:10.1061/(ASCE)1090-0241(2005)131:7(848).

Barth G, Hill MC. 2005. Numerical methods for improviing sensitivity analysis and parameter estimation of virus transport simulated using sorptive-reactive processes. *Journal of Contaminant Hydrology*, vol. 76, pg. 251-277.

Bates DM, Watts DG. 1980. Relative curvature measures of nonlinearity. *Journal of the Royal Statistical Society, Series B*, vol. 42, no. 1, pg. 1-25.

Baveye P, Volocchi A. 1989. An evaluation of mathematical models of the transport of biologically reacting solutes in saturated soils and aquifers, *Water Resources Research*, vol. 25, no. 6, pg. 1413-1421.

Beielstein T, Parsopoulos KE, Vrahatis MN. 2002. "Tuning PSO parameters through sensitivity analysis". Technical Report, Reihe Computational Intelligence CI 124\/02. Collaborative Research Center, Department of Computer Science, University of Dortmund.

Bell LS, Binning PJ. 2004. A split operator approach to reactive transpot with the forward particle tracking Eulerian Lagrangian localized adjoint method. *Advances in Water Resources*, vol. 27, pg. 323-334.

Bell LS, Binning PJ, Kuczera G, Kau PM. 2002. Rigorous uncertainty assessment in contaminant transport inverse modeling: a case study of fluoride diffusion through clay liners. *Journal of Contaminant Hydrology*, vol. 57, nos. 1-2, pg. 1-20.

Belsley D, Kuh E, Welsch R. 1980. *Regression Diagnostics: Identifying Influential Data and Sources of Colinearity*. John Wiley & Sons, Inc., New York, NY.

Booker AJ, Dennis JE, Frank PD, Serafini DB, Torczon V, Trosset MW. 1999. A rigorous framework for optimization of expensive functions by surrogates. *Structural Optimization*, vol. 17, pg. 1-13.

Brun A, Engesgaard P. 2002. Modelling of transport and biogeochemical processes in pollution plumes: literature review and model development. *Journal of Hydrology*, vol. 256, pg. 211-227.

Chan Hilton AB, Culver TB. 2005. Groundwater remediation design under uncertainty using genetic algorithms. *Journal of Water Resources Planning and Management*, vol. 131, no. 1, pg. 25-34.

Chan Hilton AB, Culver TB. 2000. Constraint handling for genetic algorithms in optimal remediation design. *Journal of Water Resources Planning and Management*, vol. 126, no. 3, pg. 128-137.

Chang HJ. 2000. Modeling of Strontium Transport in Groundwater Influenced by Competetitive Ion Exchange: Application to Zeolite Barriers. M. Eng. thesis,

Department of Civil, Structural, and Environmental Engineering, University at Buffalo, Buffalo, NY.

Chang LC, Shoemaker CA, Liu PL. 1992. Optimal time-varying pumping rates for groundwater remediation: application of a constrained optimal control algorithm. *Water Resources Research*, vol. 28, no. 12, pg. 3157-3173.

Charbeneau RJ. 2000. *Groundwater Hydraulics and Pollutant Transport.* Prentice-Hall, Upper Saddle River, NJ.

Christensen S, Cooley RL. 1999. Evaluation of confidence intervals for a steady-state leaky aquifer model. *Advances in Water Resources*, vol. 22, no. 8, pg. 807-817.

Clerc, M., TRIBES - an example of optimization by particulate swarm without parameters of control. Paper presented at *Optimization by Particulate Swarm (OEP 2003)*, Paris, France, 2003.

Coelho JP, Oliveira PM, Cunha JB. 2002. Greenhouse air temperature control using the particle swarm optimisation algorithm. In *Proceedings of 15th Triennial World Congress of the International Federation of Automatic Control (IFAC 2002)*, Barcelona, Spain.

Cook R, Weisberg S. 1982. Residuals and Influence in Regression. *Monographs of Statistics and Applied Probability, vol. 18*, Chapman and Hall, New York, NY.

Cooley RL, Naff RL. 1990. Regression modeling of ground-water flow. *U.S. Geological Survey Techniques of Water Resources Investigations, Book 3, Chapter B4*, Denver, CO.

Coy SP, Golden BL, Runger GC, Wasil EA. 2001. Using experimental design to find effective parameter settings for heuristics. *Journal of Heuristics*, vol. 7, no. 1, pg. 77-97.

Craig JR. 2005. Reactive Contaminant Transport Modeling Using Analytic Element Flow Solutions, Ph.D. thesis, Department of Civil, Structural, and Environmental Engineering, University at Buffalo, Buffalo, NY.

Craig JR, Matott LS. 2005. “Visual Bluebird User’s Manual: Version 2.0,” Department of Civil, Structural, and Environmental Engineering, University at Buffalo, Buffalo, NY, (available from www.groundwater.buffalo.edu).

Craig JR, Rabideau AJ. 2006. Contaminant Transport Modeling using Analytic Element Flow Solutions: Finite Difference Methods. *Advances in Water Resources*, vol. 29, no. 7, pg. 1075-1087.

Craig JR, Rabideau AJ. 2004. Discretization of analytic element flow solutions for transport modeling. In: *Proceedings of the XV International Conference on Computational Methods in Water Resources*. Chapel Hill, NC, Elsevier, pg. 381-391.

Culver TB, Shenk GW. 1998. Dynamic optimal ground water remediation by granular activated carbon. *Journal of Water Resources Planning and Management*, vol. 124, no. 1, pg. 59-64.

Culver TB, Shoemaker CA. 1997. Dynamic optimal ground-water reclamation with treatment capital costs. *Journal of Water Resources Planning and Management* , vol. 123, no. 1, pg. 23-29.

Culver TB, Shoemaker CA. 1993. Optimal control for groundwater remediation by differential dynamic programming with quasi-Newton approximations. *Water Resources Research*, vol. 29, no. 4, pg. 823-831.

Culver TB, Shoemaker CA. 1992. Dynamic optimal control for groundwater remediation with flexible management periods. *Water Resources Research*, vol. 28, no. 3, pg. 629-641.

Dai Z, Samper J. 2004. Inverse problem of multicomponent reactive chemical transport in porous media: Formulation and applications. *Water Resources Research*, vol. 40, W07407, doi:10.1029/2004WR003248.

Deitsch JJ, Smith JA, Arnold MB, Bolus J.1998. Sorption and Desorption Rates of Carbon Tetrachloride and 1,2-Dichlorobenzene to Three Organobentonites and a Natural Peat Soil. *Environmental Science and Technology,* vol. 32, pg. 3169-3177.

Doherty J. 2004. *PEST: Model-independent parameter estimation, User Manual, 5th edition*. Watermark Numerical Computing.

Dorigo M, Stutzle T. 2004. Ant Colony Optimization. MIT Press, Cambridge, MA.

Doussan C, Poitevin G, Ledoux E, Detay M. 1997. River bank filtration: modelling of the changes in water chemistry with emphasis on nitrogen species. *Journal of Contaminant Hydrology*, vol. 25, pg. 129-156.

Dougherty DE, Marryott RA, Stollar RL. 1991. Optimal groundwater management, 2, Application of simulated annealing to a field-scale contamination site. *Water Resources Research*, vol. 29, no. 4, pg. 847-860.

Draper N, Smith H. 1998. *Applied Regression Analysis: Third Edition*. John Wiley & Sons, Inc., New York, NY.

Duran MA, Grossman IE. 1986. An outer-approximation algorithm for a class of mixed-integer nonlinear programs. *Mathematical Programming*, vol. 36, pg. 307-339.

Dzombak DA, Morel FMM. 1990. *Surface complexation modeling--Hydrous ferric oxide*. John Wiley, New York, NY, 393 pp.

Edil TB. 2003. A review of aqueous-phase VOC transport in modern landfill liners. *Waste Management*, vol. 23, pg. 561–571.

Engesgaard P, Kipp KL. 1992. A geochemical transport model for redox-controlled movement of mineral fronts in groundwater flow systems: A case of nitrate removal by oxidation of pyrite. *Water Resources Research*, vol. 28, no. 10, pg. 2829-2843.

Environmental Protection Agency. 1999. Protocol for Developing Nutrient TMDLs. *EPA 841-B-99-007*, Office of Water, Environmental Protection Agency, Washington, D.C., 135 pp.

Environmental Protection Agency. 2002. The twenty needs report: how research can improve the TMDL program. *EPA 841-B-02-002*, Office of Water, Environmental Protection Agency, Washington, D.C., 43 pp.

Environmental Security Technology Certification Program (ESTCP). 2004. Cost and performance report: Application of flow and transport optimization codes to groundwater pump-and-treat systems. U.S. Department of Defense, *ESTCP Report CU-0010*, (available from www.estcp.org/documents/techdocs/CU-0010.pdf).

Erol OK, Eksin I. 2006. A new optimization method: Big Bang-Big Crunch. *Advances in Engineering Software*, vol. 37, pg. 106-111.

Essaid HI, Cozzarelli IM, Eganhouse RP, Herkelrath WN, Bekins BA, Delin GN. 2003. Inverse modeling of BTEX dissolution and biodegradation at the Bemidji, MN crude-oil spill site. *Journal of Contaminant Hydrology*, vol. 67, no. 1, pg. 269-299.

Fang Y, Yeh GT, Burgos WD. 2003. A general paradigm to model reaction-based biogeochemical processes in batch systems. *Water Resources Research*, vol. 39, no. 4, pg. 1083, doi:10.1029/2002WR001694.

Fletcher R, Reeves C. 1964. Function minimization by conjugate gradients. *The Computer Journal*, vol. 7, pg. 149-154.

Foster I. 1995. *Designing and Building Parallel Programs: Concepts and Tools for Parallel Software Engineering*. Addison-Wesley, Boston, MA.

Fowler KR, Kelley CT, Kees CE, Miller CT. 2004a. A Hydraulic capture application for optimal remediation design, In: *Proceedings of the XV International Conference on Computational Methods in Water Resources*. Chapel Hill, NC, Elsevier, pg. 1149-1157.

Fowler KR, Kelley CT, Miller CT, Kees CE, Darwin RW, Reese JP, Farthing MW, Reed MSC. 2004b. Solution of a well-field design problem with implicit filtering. *Optimization and Engineering*, vol. 5, pg. 207 – 234.

Gaines GL, Thomas HC. 1953. Adsorption studies on clay minerals. II. A formulation of the thermodynamics of exchange adsorption. *Journal of Chemical Physics*, vol. 21, pg. 714-718.

Gies D, Rahmat-Samii Y. 2003. Particle swarm optimization for reconfigurable phase-differentiated array design. *Microwave and Optical Technology Letters*, vol. 38, no. 3, pg. 168-175.

Gilmore P, Kelley CT. 1995. An implicit filtering algorithm for optimization of functions with many local minima. *SIAM Journal of Optimization*, vol. 5, pg. 269-285.

Glover F. 1986. Future paths for integer programming and links to artificial intelligence. *Computers and Operations Research*, vol. 5, pg. 533-549.

Goldberg DE. 1989. *Genetic Algorithms in Search, Optimization and Machine Learning*. Addison-Wesley, Reading, MA.

Govindaraju RS, Rao AR. (eds). 2000. *Artificial Neural Networks in Hydrology*. Kluwer Academic Publishers, Amsterdam, Netherlands.

Gropp W, Lusk W, Skjellum A. 1999. *Using MPI: Portable Parallel Programming with the Message Passing Interface, second edition*. MIT Press, Cambridge, MA.

Grubb S. 1993. Analytical model for estimation of steady-state capture zones of pumping in confined and unconfined aquifers. *Ground Water*, vol. 31, no. 1, pg. 27-32.

Guan J, Aral MM. 2004. Optimal design of groundwater remediation systems using fuzzy set theory. *Water Resources Research*, vol. 33, no. 5, pg. 1001-1012.

Gullick RW. 1998. Effects of sorbent addition on the transport of inorganic and organic chemicals in soil-bentonite cutoff wall containment barriers. Dissertation. University of Michigan, Ann Arbor, MI.

Gullick RW, Weber WJ. 2001. Evaluation of Shale and Organoclays as Sorbent Additives for Low-Permeability Soil Containment Barriers. *Environmental Science and Technology,* vol. 35, pg. 1523-1530.

Haitjema H. 1995. *Analytic Element modeling of ground water flow*, Academic Press, San Diego, CA.

Hannan EJ, Quinn BG. 1979. The determination of the order of an autoregression. *Journal of the Royal Statistical Society Series B*, vol. 41, no. 1, pg. 190–195.

Haws NW, Bouwer EJ, Ball WP. 2006. The influence of biogeochemical conditions and level of model complexity when simulating cometabolic biodegradation in sorbent-water systems. *Advances in Water Resources*, vol. 29, no. 4, pg. 571-589.

Hem JD. 1985. "Study and Interpretation of the Chemical Characteristics of Natural Water, 3rd Edition", *USGS Water-Supply Paper 2254*, 263 pp.

Hill MC. 1998. Methods and guidelines for effective model calibration. *U.S. Geological Survey Water Resources Investigation Report 98-4005*, Denver, CO.

Hill MC, Banta ER, Harbaugh AW, Anderman ER. 2000. Modflow-2000, The U.S. Geological Survey Modular Ground-Water Model -- User guide to the Observation, Sensitivity, and Parameter-Estimation Process and three postprocessing programs. *U.S. Geological Survey Open-File Report 00-184*, Denver, CO.

Hindmarsh AC, Brown PN, Grant KE, Lee SL, Serban R, Shumaker DE, Woodward CS. 2005. SUNDIALS: Suite of nonlinear and differential/algebraic equation solvers. *ACM Transactions on Mathematical Software*, vol. 31, no. 3, pg. 363-396.

Hindmarsh AC, Serban R. 2006. User documentation for CVODE v2.4.0. *LLNL technical report UCRL-SM-208108*, Lawrence Livermore National Laboratory, Livermore, CA.

Hinterding R, Zbigniew M, Eiben AE. 1997. Adaptation in Evolutionary Computation: a Survey. *Proceedings of the fourth IEEE International Conference on Evolutionary Computation*, pg. 65-69.

Holland EA, Bertman SB, Carroll MA, Guenther AB, Shepson PB, Sparks JP, Lee-Taylor. 2005. U.S. Nitrogen Science Plan Focuses Collaborative Efforts. *Eos, Transactions of the American Geophysical Union*, vol. 86, no. 27, pg. 253 and 256.

Huang C, Mayer AS. 1997. Pump-and-treat optimization using well location and pumping rates as decision variables. *Water Resources Research*, vol. 33, no. 5, pg. 1001-1012.

Hunter KS, Wang Y, Van Capellen P. 1998. Kinetic modeling of microbially-driven redox chemistry of subsurface environments: coupling transport, microbial metabolism and geochemistry. *Journal of Hydrology*, vol. 209, pg. 53-80.

Hurvich CM, Tsai C-L. 1994. Autoregressive model selection in small samples using a bias-corrected version of AIC. In *Engineering and Scientific Applications*, vol. 3, ed. Bozdogan, H. pg. 137–157. Proceedings of the First U.S./Japan Conference on the Frontiers of Statistical Modeling: An Informational Approach. Dordrecht, Netherlands: Kluwer Academic Publishers.

Jankovic I. 2005. "SPLIT: Win32 computer program for analytic-based modeling of single-layer groundwater flow in heterogeneous aquifers with particle tracking, capture zone delineation, and parameter estimation," Department of Civil, Structural, and Environmental Engineering, University at Buffalo, Buffalo, NY, (available from www.groundwater.buffalo.edu)

Jankovic I. 1997. High-order analytic elements in modeling groundwater flow, Ph.D. thesis, University of Minnesota, Minneapolis, MN.

Jankovic I, Barnes R. 1999. High order line elements in modeling two-dimensional ground water flow. *Journal of Hydrology*, vol. 226, pg. 211 – 223.

Javandel I, Tsang C. 1986. Capture-zone type curves: A tool for aquifer cleanup. *Ground Water*, vol. 24, no. 5, pg. 616-625.

Johnson RL, Cherry JA, Pankow JF. 1989. Diffusive Contaminant Transport in Natural Clay: A Field Example and Implications for Clay-Lined Waste Disposal Sites. *Environmental Science and Technology,* vol. 23, pg. 340-349.

Kansa EJ. 1990. Multiquadrics -- A scattered data approximation scheme with applications to computational fluid-dynamics -- I. surface approximations and partial derivative estimates. *Computers & Mathematics with Applications*, vol. 19, no. 8-9, pg. 127-145.

Kashyap RL. 1982. Optimal choice of AR and MA parts in autoregressive moving average models. *IEEE Transactions on Pattern Analysis and Machine Intelligence*, vol. 4, no. 2, pg. 99–104.

Keating EH, Bahr JM. 1998. Reactive transport modeling of redox geochemistry: Approaches to chemical disequilibrium and reaction rate estimation at a site in

northern Wisconsin. *Water Resources Research*, vol. 34, no. 12, pg. 3573-3584.

Kennedy J, Eberhart RC. 1995. Particle swarm optimization. In: *Proceedings of IEEE International Conference on Neural Networks*, Piscataway, NJ, pg. 1942-1948.

Khandelwal A, Rabideau AJ, Shen P. 1998. Analysis of Diffusion and Sorption of Organic Solutes in Soil-Bentonite Barrier Materials. *Environmental Science and Technology,* vol. 32, pg.1333-1339.

Killingstad MW, Widdowson MA, Smith RL. 2002. Modeling enhanced in situ denitrification in groundwater. *Journal of Environmental Engineering*, vol. 128, no. 6, pg. 491-504.

Kinzelbach W, Schafer W. 1991. Numerical modeling of natural and enhanced denitrification processes in aquifers. *Water Resources Research*, vol. 27, no. 6, pg. 1123-1135.

Kirkpatrick S, Gelatt JC, Vecchi M. 1983. Optimization by simulated annealing. *Science*, vol. 220, pg. 671-680.

Kivijarvi J, Franti P, Olli N. 2003. Self-Adaptive Genetic Algorithm for Clustering. *Journal of Heuristics*, vol. 9, no. 2, pg. 113-129.

Knapp EP Herman JS, Hornberger GM, Mills AL. 1998. The effect of distribution of iron-oxyhydroxide grain coatings on the transport of bacterial cells in porous media. *Environmental Geology*, vol. 33, no. 4, pg. 243-248.

Koerner RM. 1994. *Designing with Geosynthetics, Third Edition*, Prentice Hall, Englewood Cliffs, NJ.

Lee S-I, Kitanidis PK. 1991. Optimal estimation and scheduling in aquifer remediation with incomplete information. *Water Resources Research*, vol. 27, no. 9, pg. 2203-2217.

Lensing H, Vogt M, Herrling B. 1994. Modeling of biologically mediated redox processes in the subsurface. *Journal of Hydrology*, vol. 159, pg. 125-143.

Levenberg K. 1944. A Method for the Solution of Certain Problems in Least Squares. *Quarterly of Applied Mathematics*, vol. 2, pg. 164-168.

Lim M. 2005. Comparison of automated calibrations of finite difference and analytic element groundwater flow models. M. Eng. thesis, Department of Civil, Structural, and Environmental Engineering, University at Buffalo, Buffalo, NY.

Linssen HN. 1975. Nonlinearity measures: A case study. *Statistica Neerlandica*, vol. 29, pg. 93-99.

MacQuarrie KT, Sudicky EA. 2001. Multicomponent simulation of wastewater-derived nitrogen and carbon in shallow unconfined aquifers I. Model formulation and performance. *Journal of Contaminant Hydrology*, vol. 47, pg. 53-84.

MacQuarrie KT, Sudicky EA, Robertson WD. 2001. Multicomponent simulation of wastewater-derived nitrogen and carbon in shallow unconfined aquifers II. Model application to a field site. *Journal of Contaminant Hydrology*, vol. *47*, pg. 85-104.

Marquardt D. 1963. An Algorithm for Least-Squares Estimation of Nonlinear Parameters. *SIAM Journal of Applied Mathematics*, vol. 11, pg. 431-441.

Maskey S, Jonoski A, Solomatine DP. 2002. Groundwater Remediation Strategy Using Global Optimization Algorithms. *Journal of Water Resources Planning and Management*, vol. 128, no. 6, pg. 431-440.

Matott LS. 2004. "Ostrich: an Optimization Software Tool, Documentation and User's Guide, Version 1.4," Department of Civil, Structural, and Environmental Engineering, University at Buffalo, Buffalo, NY (available from www.groundwater.buffalo.edu).

Matott LS. 2005. “Ostrich: an Optimization Software Tool, Documentation and User’s Guide, Version 1.6”, Department of Civil, Structural, and Environmental Engineering, University at Buffalo, Buffalo, NY. (available from www.groundwater.buffalo.edu)

Matott LS. 2006. “Ostrich: an Optimization Software Tool, Documentation and User’s Guide, Version 1.8”, Department of Civil, Structural, and Environmental Engineering, University at Buffalo, Buffalo, NY, (available from www.groundwater.buffalo.edu)

Matott LS, Bartelt-Hunt SL, Rabideau AJ, Fowler KR. 2006. Application of Heuristic Optimization Techniques and Algorithm Tuning to Multi-layered Sorptive Barrier Design. *Environmental Science and Technology,* in press.

Matott LS, Rabideau AJ, Craig JR. 2006. Pump-and-treat optimization using analytic element method flow models. *Advances in Water Resources, vol. 29*, pg. 760–775.

Mayer AS, Kelley CT, Miller CT. 2002. Optimal design for problems involving flow and transport phenomena in subsurface systems. *Advances in Water Resources*, vol. 25, pg. 1233-1256.

Mayer KU, Benner SG, Frind EO, Thornton SF, Lerner DN. 2001. Reactive transport modeling of processes controlling the distribution and natural attenuation of phenolic compounds in a deep sandstone aquifer. *Journal of Contaminant Hydrology*, vol. 53, no. 3-4, pg. 341-368.

McKinney DC, Lin M. 1996. Pump-and-treat ground-water remediation system optimization. *Journal of Water Resources Planning and Management*, vol. 122, no. 2, pg. 128-136.

McNab WW, Narasimhan TN. 1994. Modeling reactive transport of organic compounds in groundwater using a partial redox disequilibrium approach. *Water Resources Research*, vol. 30, no. 9, pg. 2619-2635.

Metropolis N, Rosenbluth AW, Rosenbluth MN, Teller AH, Teller E. 1953. Equations of state calculations by fast computing machines. *Journal of Chemical Physics*, vol. 21, pg. 1087-1091.

Mugunthan P, Shoemaker CA. 2005. An Efficient Method for Assessing Uncertainty in Forecast of Computationally Intensive Groundwater Models. *ASCE Conference Proceedings,* vol. 173, pg. 366, doi:10.1061/40792(173)366.

Mulligan AE, Ahlfeld DP. 2001. Optimal plume capture design in unconfined aquifers, J. Smith and S. Burns, eds., *Physicochemical groundwater remediation*, Kluwer Academic, pg. 23-44.

Mulligan AE, Ahlfeld DP. 1999. Advective control of groundwater contaminant plumes: Model development and comparison to hydraulic control. *Water Resources Research*, vol. 35, no. 8, pg. 2285-2294.

National Research Council. 1994. *Alternatives for Groundwater Cleanup*, National Academy Press, Washington, DC.

Parkhurst DL, Appelo CAJ. 1999. User's guide to PHREEQC (version 2) – a computer program for speciation, batch-reaction, one-dimensional transport, and inverse geochemical calculations. US Geological Survey, *Water Resources Investigations Report 99-4259*, 312 pp.

Parsons R, Johnson M. 1997. A case study in experimental design applied to genetic algorithms with applications to DNA sequence assembly. *American Journal of Mathematical and Management Sciences*, vol. 17, nos. 3-4, pg. 369-396.

Poeter E, Anderson D. 2005. Multimodel ranking and inference in ground water modeling. *Ground Water*, vol. 43, no. 4, pg. 597 – 605.

Poeter EP, Hill MC. 1998. Documentation of UCODE: A computer code for universal inverse modeling. *U.S. Geological Survey, Water Resources Investigation Report 98-4080*.

Postma D, Boesen C, Kristiansen H, Larsen F.1991. Nitrate reduction in an unconfined sandy aquifer: Water chemistry, reduction processes, and geochemical modeling. *Water Resources Research*, vol. 27,no. 8, pg. 2027-2045.

Press WH, Teukolsky SA, Vetterling WT, Flannery BP. 1995. *Numerical Recipes in C, Second Edition*, Cambridge University Press, New York, NY.

Prommer HD, Barry A, Davis GB. 1999. A one-dimensional reactive multi-component transport model for biodegradation of petroleum hydrocarbons in groundwater. *Environmental Modelling & Software*, vol. 14, pg. 213-223.

Rabideau AJ. 2003. "MOUSER Version 1: Moderately User-friendly Reactive Transport Model", Department of Civil, Structural, and Environmental Engineering, University at Buffalo, Buffalo, NY. (available from www.groundwater.buffalo.edu)

Rabideau AJ, Khandelwal A. 1998. Boundary Conditions for Modeling Contaminant Transport in Vertical Barriers. *Journal of Environmental Engineering,* vol. 124, pg. 1135-1141.

Rabideau AJ, Matott LS, Jankovic I, Craig JR, Becker MW. 2005. Influence of numerical precision on the calibration of AEM ground water models. *Environmental Geology*, vol. 48, no. 1, pg. 57-67.

Rabideau AJ, Van Benschoten J, Patel A, Bandilla K. 2005b. Performance assessment of a zeolite treatment wall for removing Sr-90 from groundwater. *Journal of Contaminant Hydrology*. vol. 79, no. 1-2, pg. 1-24.

Rardin RL, Uzsoy R. 2001. Experimental Evaluation of Heuristic Optimization Algorithms: a Tutorial. *Journal of Heuristics*, vol. 7, pg. 261-304.

Regis RG, Shoemaker CA. 2004. Local function approximation in evolutionary algorithms for the optimization of costly functions. *IEEE Transactions on Evolutionary Computation*, vol. 8, no. 5, pg. 490-505.

Rogers LL, Dowla FU. 1994. Optimization of groundwater remediation using artificial neural networks with parallel solute transport modeling. *Water Resources Research*, vol. 30, no. 2, pg. 457-481.

RS Means ECHOS. 2004. *Environmental Remediation Cost Data Assemblies,* R.S. Means Company, Kingston, MA.

Roy RK. 2001. *Design of Experiments Using the Taguchi Approach*. John Wiley & Sons, New York, NY.

Sawyer CS, Ahlfeld DP, King AJ. 1995. Groundwater remediation design using a three-dimensional simulation model and mixed-integer programming. *Water Resources Research*, vol. 31, no. 5, pg. 1373-1385.

Schafer D, Schafer W, Kinzelbach W. 1998. Simulation of reactive processes related to biodegradation in aquifers, 1. Structure of the three-dimensional reactive transport model. *Journal of Contaminant Hydrology*, vol. 31, pg. 167-186.

Schafer W, Therrien R. 1995. Simulating transport and removal of xylene during remediation of a sandy aquifer. *Journal of Contaminant Hydrology*, vol. 19, pg. 205-236.

Schwarz G. 1978. Estimating the dimension of a model. *Annals of Statistics*, vol. 6, no. 2, pg. 461–464.

Smalley JB, Minsker BS, Goldberg DE. 2000. Risk-based in situ bioremediation design using a noisy genetic algorithm. *Water Resources Research*, vol. 36, no. 20, pg. 3043-3052.

Solomatine DP, Dibiki YB, Kukuric N. 1999. Automatic calibration of groundwater models using global optimization techniques. *Journal of the Hydrological Sciences*, vol. 44, no. 6, pg. 879-894.

Spruill TB, Tesoriero HE, Mew HE, Farrell KM, Harden SL, Colosimo AB, Kraemer SR. 2005. “Geochemistry and Characteristics of Nitrogen Transport at a Confined Animal Feeding Operation in a Coastal Plain Agricultural Watershed, and Implications for Nutrient Loading in the Neuse River Basin, North Carolina, 1999-2002”, *U.S. Geological Survey Scientific Investigations Report 2004-5283*, pp. 57.

Steefel CI, MacQuarrie KTB. 1996. Approaches to modeling of reactive transport in porous media, In: Lichtner PC, Steefel CI, Oelkers EH (eds), *Reactive Transport in Porous Media*, Reviews in Mineralogy Series vol. 34. Mineralogical Society of America, pg. 83-129.

Strack ODL. 1989. *Ground Water Mechanics*, Prentice-Hall, Englewood Cliffs, NJ.

Strack ODL, Jankovic I. 1999. A multi-quadric area-sink for analytic element modeling of groundwater flow. *Journal of Hydrology*, vol. 226, no. 3-4, pg. 188–196.

Talbi EG. 2002. A Taxonomy of Hybrid Metaheuristics. *Journal of Heuristics*, vol. 8, no. 5, pg. 561-564.

Tucker RM. 1999. Clay Minerals: Their Importance and Function in Soils. *Soil Fertility Note 13*, North Carolina Department of Agriculture and Consumer Services, Agronomic Division, Raleigh, NC. (available online at www.ncagr.com/agronomi/sfn13.htm)

U.S. EPA. 1999. Protocol for Developing Nutrient TMDLs. *EPA 841-B-99-007*, U.S. Environmental Protection Agency Office of Water, Washington, DC, 135 pg.

U.S. EPA. 2002. The Twenty Needs Report: How Research Can Improve the TMDL Program. *EPA 841-B-02-002*, U.S. Environmental Protection Agency Office of Water, Washington, DC, 43 pg.

van Breuklen BM, Appelo CA, Olsthoorn TN. 1998. Hydrogeochemical transport modeling of 24 years of Rhine water infiltration in the dunes of the Amsterdam water supply. *Journal of Hydrology*, vol. 209, pg. 281-296.

Vanderbilt D, Louie SG. 1984. A Monte Carlo Simulated Annealing Approach to Optimization over Continuous Variables. *Journal of Computational Physics*, vol. 56, pg. 259-271.

Vanderplaats GN. 2001. *Numerical Optimization Techniques for Engineering Design*. Vanderplaats Research & Development, Colorado Springs, CO.

Wang W, Ahlfeld DP. 1994. Optimal groundwater remediation with well location as a decision variable; Model development. *Water Resources Research*, vol. 30, no. 5, pg. 1605-1618.

Watson IA, Oswald SE, Mayer KU, Wu Y, Banwart SA. 2003. Modeling kinetic processes controlling hydrogen and acetate concentrations in an aquifer-derived microcosm. *Environmental Science and Technology*, vol. 37, no. 17, pg. 3910–3919.

Widdowson MA, Molz FJ, Benefield LD. 1988. A numerical transport model for oxygen- and nitrate-bassed respiration linked to substrate and nutrient availability in porous media. *Water Resources Research*, vol. 24, no. 9, pg. 1553-1565.

Yager R. 1998. Detecting influential observations in nonlinear regression modeling of groundwater flow. *Water Resources Research*, vol. 34, no. 7, pg. 1623-1633.

Yoon J-H, Shoemaker CA. 2001. Improved Real-Coded GA for Groundwater Bioremediation. *Journal of Computing in Civil Engineering*, vol. 15, no. 3, pg. 224-231.

Yoon J-H, Shoemaker CA. 1999. Comparison of optimization methods for ground-water bioremediation. *Journal of Water Resources Planning and Management*, vol. 125, no. 1, pg. 54-63.

Zheng C, Bennett GD. 2002. *Applied Contaminant Transport Modeling*, 2nd Edition, John Wiley and Sons, New York, NY.

Zheng C, Wang PP. 2003. *MGO: A Modular Groundwater Optimizer Incorporating MODFLOW and MT3DMS; Documentation and User's Guide*, University of Alabama and Groundwater Systems Research Ltd.